Title
“Process-based similarity” revealed by discharge-dependent relative submergence dynamics of thousands of large bed elements

Journal
Earth Surface Processes and Landforms, 48(5)

ISSN
0197-9337

Authors
Wiener, Jason
Pasternack, Gregory

Publication Date
2023-04-01

DOI
10.1002/esp.5524

‘Process-based similarity’ revealed by discharge-dependent relative submergence dynamics of thousands of large bed elements

Accepted manuscript

Keywords:

Relative submergence, large bed elements, macroroughness, flow resistance, mountain rivers, 2D hydraulic modeling, boulders

Cite as: Wiener, J. S., Pasternack, G. B. 2022. ‘Process-based similarity’ revealed by discharge-dependent relative submergence dynamics of thousands of large bed elements. Earth Surface Process and Landforms. DOI: 10.1002/esp.5524.

Abstract

Relative submergence of macroroughness elements such as boulders and bedrock outcrops, or large bed elements (LBEs), collectively, is a primary control on hydraulics and morphodynamics in steep, coarse-bedded rivers. However, in practice, the property is typically represented by singular, often reach- or cross-section-averaged values that mask bed-surface heterogeneity and joint distributions of local flow depths. By coupling sub-meter resolution 2D hydrodynamic modeling with spatially explicit mapping of LBEs from a 13.2 km segment of a boulder-bedded mountain river, we present complete distributions of LBE relative submergences at multiple spatial scales and explore their dynamism across discharges. Through distribution fitting and statistical analysis of resultant discharge-dependent LBE relative submergence datasets, it was confirmed that segment- and reach-scale datasets exhibited similar statistical properties and were able to be drawn from the same type of distribution. Further, the rate at which statistical and parametric properties changed between discharge-dependent datasets were statistically equivalent between spatial domains, which we term 'process-based similarity'. Commonality in distribution type and the uniform between-discharge scaling relationships suggest mutual self-organizing processes associated with the size-frequency

distribution, spatial arrangement, and submergence of LBEs were present between most domains.

Main Text:

1 Introduction

River morphology may be defined as the baseline landform topography combined with the overlying structural elements, bedforms, and/or bed features (e.g. Venditti et al., 2017). In relative high-gradient (≥1.5% channel slope), coarse-bedded (D_{50} ≥ 5 mm) rivers, morphology typically includes large, predominantly immobile features such as boulders and bedrock outcrops. Generally occupying 2-50% of the bed surface area (Wittenberg & Newson, 2005; Wiener & Pasternack, 2022), these large bed elements (LBEs) protrude from the bed-surface into the flow-field, often extending above the water surface over a range of discharges. Among the totality of surficial "bed roughness" features on the riverbed, LBEs function as "macroroughness" features in a fashion similar to individual sediment grains of diverse shapes and smaller sizes, even if the former are integrated features in the terrain instead of being individual, detached particles sitting on top of it. Protrusions of LBEs into the flow exert resistance on the fluid (Robert, 1990), reduce energy available for sediment transport (Yager et al., 2007; Monsalve & Yager, 2017), influence the temporal and spatial structure of mean and turbulent flow characteristics (Lacey & Roy, 2008; Cooper et al., 2013; Groom & Friedrich, 2019), and influence the mosaic of physical habitat conditions (Kondolf et al., 1996; Crowder & Diplas, 2006).

The manner in which LBEs effect hydraulic and morphodynamic properties is strongly related to the degree of LBE relative submergence (h/D_c), where h is local flow depth and D_c is the "characteristic diameter" of the bed roughness element of interest, typically normal to an arbitrary datum representing the mean bed surface (see definition in Papanicolaou & Tsakiris, 2017). Standard practice when addressing an alluvial river is to quantify relative submergence using singular, often reach- or cross-section-averaged h and a single characteristic grain size (D_i), where the subscript i is the percent of grains finer (e.g. D_{50} and D_{84}) (Nitsche et al., 2011; Schneider et al., 2015; Ferguson et al., 2017). However, in rivers with particle clusters, non-alluvial bed elements, and bedforms of various sorts, the standard approach has been to measure the height that the LBE sticks out above the bed (e.g., average cluster height of Strom and Papanicolaou, 2006; bedform amplitude of Wohl and Merritt, 2008; maximum large bed element height of Judd and Peterson, 1969) and use that as D_c. Owing to limited availability of continuous and comprehensive segment-scale LBE datasets (Benda, 1990;

Resop et al., 2012; Shobe et al., 2016) that are rarely if ever coupled with measurements of local flow depths, few if any studies document statistical distributions of relative submergences for complete sets of LBEs present in natural rivers or how such distributions change with discharge. However, heterogeneity of LBE sizes and configurations present along the bed and banks of coarse-grained rivers means a variety of h/D_c values are likely present at any given discharge (Q). Accounting for sub-reach-scale h/D_c heterogeneity is very important to hydraulics (Abu-Aly et al., 2014; Groom & Friedrich, 2019), sediment transport and morphodynamics (Brown & Pasternack, 2014; Monsalve & Yager, 2017; Golpira et al., 2020), and ecological functions (e.g. Roni et al., 2006; Branco et al., 2013).

The purpose of this study was to theorize on the nature of discharge-dependent distributions of h/D_c in a confined mountain river with abundant LBEs and then use a testbed river to document such distributions at reach and segment scales to answer three specific, tractable scientific questions. First, what are the discharge-dependent distributions of h/D_c in different spatial domains (i.e. segment and river reaches) in a confined mountain river with abundant LBEs? In addressing this question, based on studies documenting roughness height distributions of water-worked coarse-grained surfaces (natural or experimental) to be positively skewed and leptokurtic

(Robert, 1990; Gomez, 1993; Hodge et al., 2009), it was hypothesized that h/D_c distributions would have these same properties (hypothesis 1). Second, what h/D_c distribution statistical properties change most prominently as stage increases? It was hypothesized that the combination of depth changes at previously wetted and partly-to-fully submerged LBEs along with new LBEs becoming wetted along expanding channel margins would cause h/D_c distribution variance to increase and central tendency measures such as mean and mode to remain relatively constant and/or increase (Aberle et al., 2010; Yochum et al., 2014; Wiener & Pasternack, 2022) (hypothesis 2). Third, which hypothesized Style of changes in h/D_c distributions with Q is evident in the testbed river, which may be indicative of this type of mountain river setting? It was hypothesized that either Style 2 or Style 4 of section 2 would match the data best, because while they represent different behaviors both are consistent with the trends posited in hypothesis 2 (hypothesis 3). Documenting spatially explicit h/D_c dynamics offers a novel approach for representing bed-surface heterogeneity with implications to the study of channel hydraulics and geomorphology, and is in alignment with other studies to understand the complexities of a river's "bed state" (e.g. Adams & Zampiron, 2020). Throughout this article, references to "Text S", "Table S", and “Figure S” followed by a number refer to locations in the supplementary materials file where that item can be located.

1.1 Bed roughness, flow resistance, and relative submergence

In coarse-grained natural rivers, bed roughness as a topographic property of the riverbed has predominately been quantified using four classes of methods: (i) characteristic particle-size approaches (Bunte & Abt, 2001); (ii) random-field approaches (Nikora et al., 1998; Aberle et al., 2010); (iii) statistical representations such as the standard deviation, skewness, or kurtosis of detrended bed-surface elevations within a sub-meter convolution kernel (Aberle & Smart, 2003; Yochum et al., 2012); and (iv) hybrid approaches combining aspects of the aforementioned approaches with additional metrics representing the size and/or spatial arrangement of roughness elements (Schlichting, 1936; Nitsche et al., 2012). Each class has strengths and weaknesses, so bed roughness estimation remains debatable (Hodge & Hoey, 2016). Regardless, applying any method typically yields a single bed-roughness length-scale coefficient (Δ) applied to scales from grain patches to river reaches.

Flow resistance is the sum of all forces within and acting on the flow to resist motion and is a measure of the energy loss caused by bed roughness

(Yen, 2002). There are diverse methods for representing resistance as a coefficient in flow resistance equations. Singular Δ values are practical for use with spatially averaged resistance equations (Powell, 2014), among other uses. However, they are composite approximations that mask significant heterogeneity of natural channel sediments (Furbish, 1987; Robert, 1990). Figuring out how to quantify multiple roughness length scales (e.g. Adams & Zampiron, 2020) or otherwise better represent spatially explicit topographic variability could stimulate the development of new methods for more accurate predictions of resistance and/or velocity (Smith, 2014; Ferguson et al., 2019).

Once determined, it is common practice for Δ values to be held constant in flow resistance equations, irrespective of stage (e.g. Nitsche et al., 2011; Yochum et al., 2012; Ferguson et al., 2017; see Aberle et al. [2010] and Abu-Aly et al. [2014] as exceptions). The Δ value for a fixed individual riverbed feature is stage-independent (i.e. the object is fixed and unchanging, so its properties are too). Similarly, for any non-mobile constant wetted area or channel width, a composite Δ value for that area must also be constant, as the bed itself is unchanging. However, as Q and stage increase, width and inundated area increase. As a result, more bed features are inundated, so the composite Δ value for the spatial domain of relevance for the flow resistance equation (typically a cross-section) also changes. Thus, the composite *Δ* value can be discharge-dependent; holding a composite *Δ* value constant ignores the discharge-dependent topographic variability of the portion of the bed in contact with the flow, which has implications for landscape evolution modeling, resistance estimates, and other applications (Ferguson et al., 2017).

Separate from bed roughness metrics, there also exist dedicated flow resistance coefficients (e.g., Manning's *n* or the Darcy-Weisbach friction factor *f*). Theoretical and empirical correspondence between *R/Δ*, where R is hydraulic radius and *Δ* is parameterized from one of the methods described above (e.g., D_{50}, D_{84}, σ_z [standard deviation of detrended bed elevations], etc.) and common resistance coefficients has resulted in scaled relative submergence variables of this form being ubiquitous in hydraulic resistance equations (i.e. $\frac{1}{n} \propto \frac{1}{\sqrt{f}} \propto \frac{R}{\Delta}$). The most common functional relationships of these equations being of logarithmic or power-law forms (e.g. Powell, 2014). Notably, the assumption that *h~R*, which has minimal errors only for large width-to-depth ratios (>20), is regularly applied (Bathurst, 1985).

On the basis of such resistance equations, many workers document that total resistance values decrease monotonically as flow and depth increase (i.e. as relative submergence increases) (Powell, 2014).

Universality of this norm remains debated, especially in boulder-bedded and bedrock-alluvial channels, and findings based on constant Δ contribute added uncertainty (Abu-Aly et al., 2014; Hodge & Hoey, 2016; Cassan et al., 2017; Ferguson et al., 2017; Wiener & Pasternack, 2022). For instance, if Δ is constant, discharge-dependent resistance estimates of many resistance equations simply reduce to being a function of local h versus Q relationships. The underlying assumption is then that there exists a 1:1 correspondence between h and resistance for all systems with common Δ values. These factors, amongst others (e.g. Comiti et al., 2009; Yochum et al., 2012), contribute to scatter when comparing h/Δ versus hydraulic resistance observations (Rickenmann & Recking, 2011) and why no single resistance equation is universally accepted for steep rivers with abundant LBEs and low relative submergence flows (Nitsche et al., 2012). By addressing discharge-dependent h/D_c distributions, this study provides new inference into the efficacy of fixing Δ and an approach that better represents bed-surface heterogeneity compared to singular Δ values. It remains for hydraulic engineers and geomorphologists to determine how to best use this new information in future theories and tools.

1.2 LBE submergence effects

Flow structures and sediment-transport patterns are influenced by LBE submergence. Locally, LBEs induce pressure gradients that drive flow acceleration over and around elements followed by downstream deceleration and flow separation. These changes in momentum generate turbulence and large amounts of turbulent kinetic energy (Groom & Friedrich, 2019). The size and structure of LBE driven wakes and vortex structures are variable and difficult to predict. However, under idealized conditions, flows around isolated LBEs include a horseshoe vortex region extending ~0.5-1·D_c upstream and a downstream dual wake (primary and far wake) system extending up to ~7·D_c downstream (Shamloo et al., 2001; Tan & Curran, 2012). These structures result in characteristic patterns of scour and deposition that differ depending on submergence and can facilitate development of stable sediment patches (Shamloo et al., 2001; Monsalve & Yager, 2017).

A threshold value of 3.5 has been associated with shifts in depositional tendencies, wherein under high relative-submergence (HRS) conditions (h/D_c > 3.5), mobile particles preferentially deposit in wakes downstream of LBEs, and under low relative-submergence (LRS) conditions (h/D_c < 3.5) the probability of upstream deposition is heightened (Papanicolaou & Tsakiris, 2017). Threshold values for h/D_c have also been used to classify regimes where different resistance types (e.g. grain, form, spill) are believed to dominate (Bathurst, 1985) and to define scales for separating vertical velocity profiles into distinct layers with unique properties and governing functional equations (e.g. Shamloo et al., 2001; Cooper et al., 2013). With these associations in mind, mapping spatially explicit LBE configurations and flow properties such as h/D_c can enable more detailed, localized, geomorphic and hydraulic analysis than permitted by spatially averaged values, though new methods may be needed to take advantage of this new information.

2 Styles of LBE relative submergence response to discharge

The first step in understanding nature at a higher level of detail and with more dynamism considered than in the past is to theorize the full range of how a phenomenon might function. The evolution of river channel h/D_c distributions from one Q to another involves two main processes: (i) h changes at previously wetted, partly-to-fully submerged LBEs result in a new distribution of h/D_c values at just these LBEs; and (ii) new LBEs become wetted along the expanding channel margin and their distribution is convolved with the new distribution of previously wetted LBEs. For each change in *Q*, these two processes occur in tandem to form unique sets of discharged-dependent h/D_c values.

In confined river canyons, several workers have documented higher LBE concentrations occurring along hillslope margins outside of valley bottom baseflow and/or bankfull channels (Benda, 1990; Sklar et al., 2020; Wiener & Pasternack, 2022). While the mechanisms for such configurations remain unclear, these circumstances provide conditions to initially hypothesize that h/D_c distributions in a given spatial domain (e.g. river reach) would remain nearly constant across a range of *Q* as newly encountered, low submergence LBEs compensate for valley bottom LBEs that become increasingly submerged (Figure 1a). This type of statistical self-similarity (Style 1), defined by statistical equivalency of discharge-dependent h/D_c distribution properties, such as distribution type and statistical moments, between one or more *Q's* has been posited as an emergent property of dynamical systems with many interacting elements and extended spatial degrees of freedom, whereby internal dynamics and feedbacks result in system properties evolving toward a critical equilibrium state with self-similar distributions (Sornette, 2000). In fluvial geomorphology, statistical self-similarity has been related to the geometric properties of river networks and the size and spacing of aeolian, fluvial, glacial, and submarine landforms, but remains a controversial topic (Furbish, 1987; Baas, 2002; Ely et al., 2018).

Style 1 contrasts somewhat with the expectations stated in the study's second hypothesis. Increased depths at previously wetted LBEs mean some degree of increase in the number of highly submerged LBEs and an increase in the right-tail of h/D_c distributions is unavoidable. Therefore, five other conceptual discharge-dependent h/D_c distribution evolution Styles for partly-confined to confined rivers were theorized drawing on concepts of self-similarity and self-organized criticality (Sapozhnikov & Foufoula-Georgiou, 1999; Baas, 2002) (Figure 1).

Figure 1b depicts the case where h/D_c distributions in a given domain have similar central tendencies across *Q's*, but differ in shape as variance increases (Style 2). This trajectory follows from slight imbalances between how depth increases at previously wetted LBEs relative to the number of newly wetted, presumably low submergence, LBEs that contribute to heavier tails but maintain overall central tendency (Figure S1a). This style is consistent with the study's second hypotheses and could emerge in a river channel with several laterally nested floodplain-like alluvial surfaces hosting abundant LBEs, provided low-flow channel LBEs rapidly submerged simultaneous with the incremental shallow submergence of floodplain LBEs at successively greater discharges. This style reflects processes of increasing entropy, and divergence toward greater hydrogeomorphic diversity around a steady attractor state (Chin & Phillips, 2007).

Figure 1d shows the case where distribution shape and variance in a given domain remain constant but central tendency increases with Q (Style 3). Mathematically, this occurs if depth increases uniformly at all previously wetted LBEs and no new LBEs are encountered as Q increases. This could be physically plausible for highly concave cross-sections (e.g. incised or canyon-confined channels) with LBEs relegated to the low-flow portions of the valley bottom, though the prospect of spatially uniform increases in depth is questionable in most rivers. In the context of rivers with hierarchically nested LBE non-uniformity (Pasternack et al., 2021; Wiener & Pasternack, 2022), conditions to achieve Style 3 generally require depths at previously wetted LBEs to increase at relatively uniform rates with magnitudes nearly equal to the shifts in central tendency (e.g. depth increases are normally distributed with low variance and means close to shift magnitudes), and depths at newly wetted LBEs to increase rapidly such that submergences are similar to the shifted distributions (Figure S1b). This Style is comparable to simple stabilization of landscape patterns whereby self-organizing processes drive stability in pattern wavelengths, the pattern here being the shape and variance of discharge-dependent h/D_c distributions (Ely et al., 2018).

Figure 1f reflects the case where central tendency and variance are not conserved between discharge-dependent h/D_c distributions in a given domain, but distributions evolve such that rates at which parametric and certain statistical properties increase (i.e. slopes of property-discharge relationships) are equivalent between domains (Style 4). Unlike the within-domain conservation mechanisms of Style 1, this style involves statistical similarity across domains in the combined effects how depths change at each domain-specific set of previously wetted LBEs, and in the h/D_c values of newly wetted LBEs, and is referred to as 'process-based similarity'. This style reflects a mutualistic nature to how h/D_c distributions change across spatial domains similar to the phenomena of dynamic self-similarity (Sapozhnikov & Foufoula-Georgiou, 1999) and is indicative of universal autogenic dynamics (Ely et al., 2018). This style is also consistent with the study's second hypothesis.

Styles 2-4 above all involve continuous, though not necessarily linear, changes in h/D_c distribution properties between Q's. Thresholds are a ubiquitous paradigm in fluvial geomorphology with utility for revealing activity of morphodynamic processes (Phillips, 2006; Pasternack et al., 2021), therefore it is valuable to consider these same Styles in the form of threshold type behaviors. Threshold Styles mimic the continuous Styles but involve small, gradual changes in h/D_c distribution properties over a narrow range of geomorphically-related *Q's* followed by dramatic shifts in distribution properties due to changes in inundated channel morphology. Figure 1(c,e) depict threshold type h/D_c evolution for Styles 2 and 3, referred as 2(b) and 3(b), respectively. Style 2(b), which involves stepped increases in variance, could occur in a valley with a triangular main channel cross-section and one or more side channels with variable LBE configurations. If LBE configurations in the main channel were laterally uniform, h/D_c distributions would remain relatively constant to the point where flows begin to inundate side channels. Rapid addition of the newly wetted LBEs with variable h/D_c values to the increasingly inundated main channel LBEs would drive the hypothetical stepped response. Style 3(b), which involves similar variances and stepped increases in central tendency, could occur in a confined valley with an inset, triangular, main channel with laterally uniform LBEs but few LBEs outside the main channel. Here, the threshold changes in h/D_c central tendency would be driven by non-linearity of the compound channel's stage-discharge relationship when stage exceeds the inset channel and flows onto the floodplain. These processes may repeat if multiple threshold are present.

The Styles described in this section cover a range of h/D_c behaviors pertinent to partly-confined to confined rivers, but are not all-inclusive. Notably, as Q increases the central tendency and variance of all h/D_c distributions are portrayed to increase or remain static, but are never theorized to decrease. For a river with a broad, well-defined floodplain having LBEs outnumbering those in the main channel, transition to out-of-bank flow could result in a decrease in h/D_c distribution central tendency. Certainly this and other Styles not included here are possible considering the diversity of global river morphology.

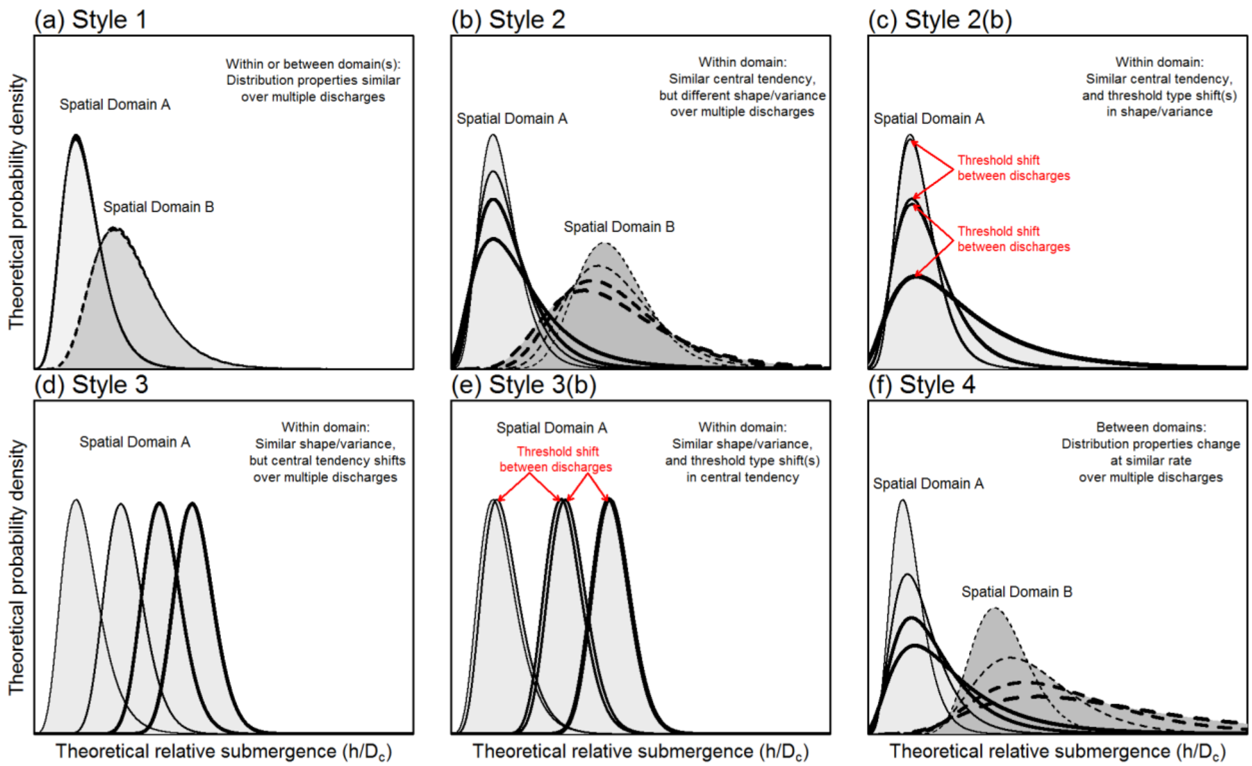

Figure 1. Conceptual representations of discharge-dependent h/D_c distribution dynamism. (a) Style 1 where distributions exhibit statistical self-similarity. (b) Style 2 wherein central tendency remains constant but variance increase with *Q*. Two examples are provided where spatial domain A has constant modal values between *Q's*, and spatial domain B has constant means. (c) Style 2(b) which is similar to Style 2 but has h/D_c distributions that are nearly identical (represented by lines with considerable overlap) followed by distributions with threshold shifts in variance. (d) Style 3 wherein shape and variance are constant but central tendencies increase with *Q*. (e) Style 3(b) which is similar to Style 3 but has threshold shifts in central tendency. (f) Style 4 wherein the rate of change of parametric and statistical properties are equivalent between domains. In each panel, increasing *Q* is represented by increased line thicknesses. Different line styles represent h/D_c distributions for different domains. The number of discharge-dependent h/D_c distributions (lines) and domains shown are illustrative and differ between panels.

3 Study river segment

A 13.2-km segment of the mountainous Yuba River (Northern California) draining 1853 km^2 of the western Sierra Nevada range was used to test concepts (Figure 2). The study segment is comprised of a low-sinuosity, boulder-bedded, 5^{th}-order mountain river confined within a steep-walled bedrock and forested hillside canyon. The mean bed slope is 2%, but there are significant, high amplitude bed and width undulations at multiple frequencies (Pasternack et al., 2021), including shorter intervals of 10 – 100 m (10^0 – 10^1 channel widths) having slopes > 10%. The river segment was delineated into six parsimonious reaches (slopes of 0.8-2.6%) based on major channel-bed slope breaks (Figure S2). Slope breaks were vetted using expert judgement and sensitivity analysis considering several factors reported in the supplementary materials file (Text S3).

Based on limited sedimentological data, bed substrates alternate between bedrock and alluvial sections with estimates of larger boulders (> 512 mm) or bedrock covering over 60% of the channel (YCWA, 2013). Alluvial substrate, where present, is a heterogeneous mixture of materials dominated by coarse fractions (medium gravel/cobbles and larger). The presence of large bounders and the heterogeneity of sizes makes manual grain-size quantification difficult and labor intensive, if attempted. That said, Wolman (1954) pebble counts by YCWA (2013) consisting of sampling of a minimum of 100 pebbles along channel cross-sections within very limited portions of the study segment found average D_{50} values of 193 and 106 mm in the upstream and downstream most portions of the site, respectively, and a D_{84} value of 512 mm in both portions of the site. Fluvial landforms present comprise a diverse suite of individual morphological units (Wiener & Pasternack, 2019) including cascades, step-pools, and riffle-pools, as well as forced and intermediate morphologies (Thompson et al., 2006).

Like many bedrock-confined rivers, the study segment lacks a contiguous floodplain having only localized areas supporting accumulation of alluvium at major tributary junctions, meander bends, or other areas of local valley widening. Remaining channel margins are comprised of coarse colluvium/alluvium and bedrock. Hydrodynamic modeling (section 4.2) found the limited number of alluvial surfaces (e.g. bars) to become inundated over a range of *Q's*. This non-uniformity corroborates evidence that bankfull discharge in mountain rivers be thought of as a range of recurring discharges (Radecki-Pawlik, 2002). Despite this ambiguity, it remains helpful for dimensional and comparative purposes to identify a single bankfull flow. A previously reported morphologically determined bankfull discharge of 10.73 m^3/s (YCWA, 2013) was used for this purpose. The associated segment-averaged bankfull wetted width and depth, estimated on the basis of hydraulic modeling, were 26 and 1.34 m, respectively.

Previous scientific studies have used this river segment. Geomorphic covariance structure analysis of width and bed undulations by Pasternack et al. (2021) revealed a threshold stage of ~161 m^3/s above which landform structure was found to be organized and freely self-maintaining via flow convergence routing morphodynamics. Wiener and Pasternack (2022) introduced a novel LBE mapping method and identified complex multi-scalar LBE organizational patterns often corresponding with Morris's (1959) wake interference regime that theoretically maximizes flow resistance for the channel. Concentrations of LBEs located along channel margins continuously increased laterally away from the channel.

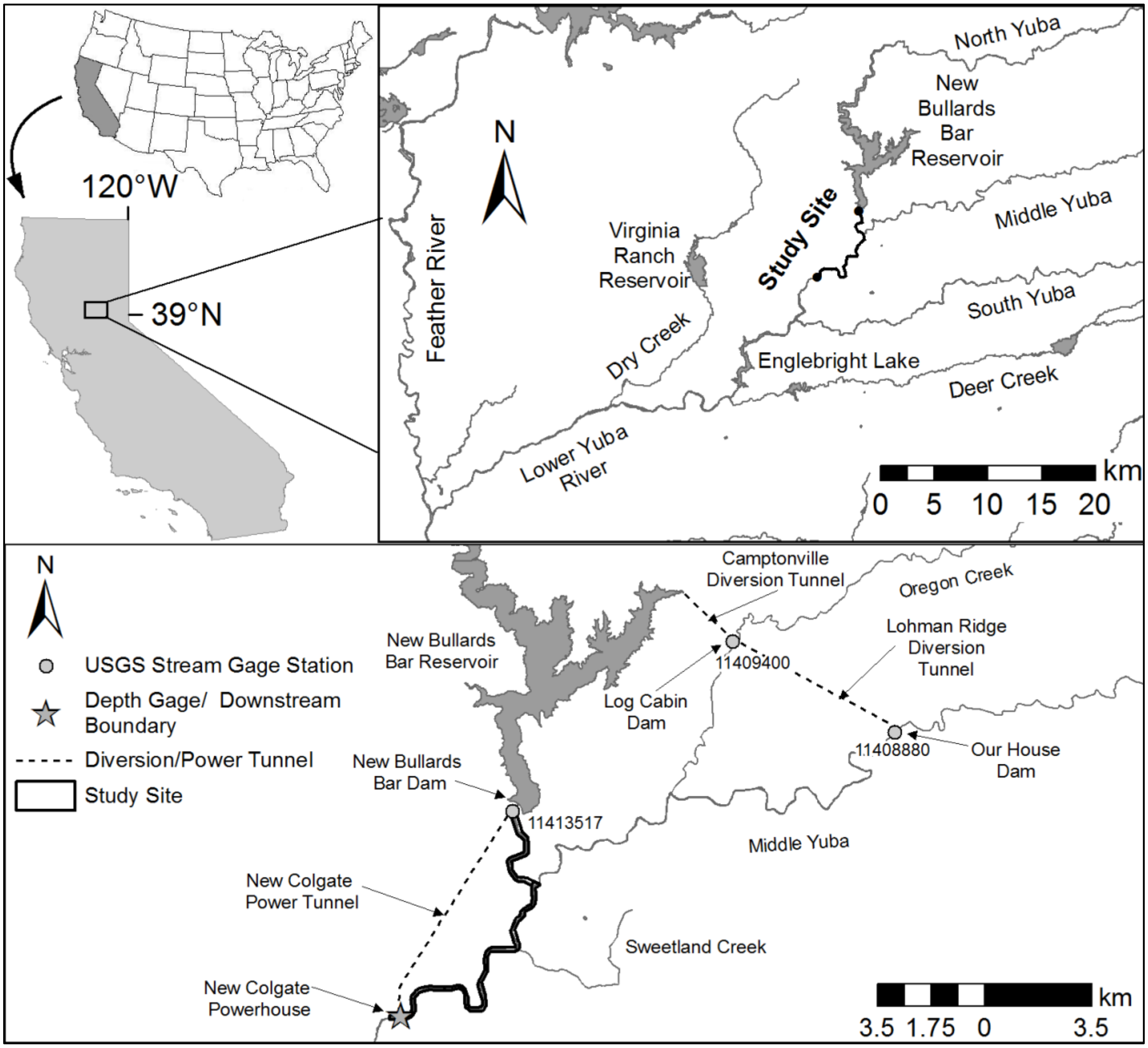

Figure 2. Map of study segment, tributaries, gages, and infrastructure facilities, Yuba River, CA.

4 Methods

The study's experimental design included a combination of field work, remote sensing, numerical modeling, geospatial analysis, and statistical analysis to make h/D_c statistical distributions in support of rigorous hypothesis testing (Figure 3). Depths at LBEs were predicted with a two-dimensional (2D) hydrodynamic model. LBE heights were estimated using a novel LBE map for 13.2 km of a confined, boulder-bedded river (i.e. $D_{50} \geq$ 64 mm [*sensu* Bathurst, 1982]). Discharges ranged widely from a representative baseflow condition to a valley-filling flood stage with an estimated 13.7-year recurrence interval; dynamics at larger floods were investigated by extrapolating statistical models.

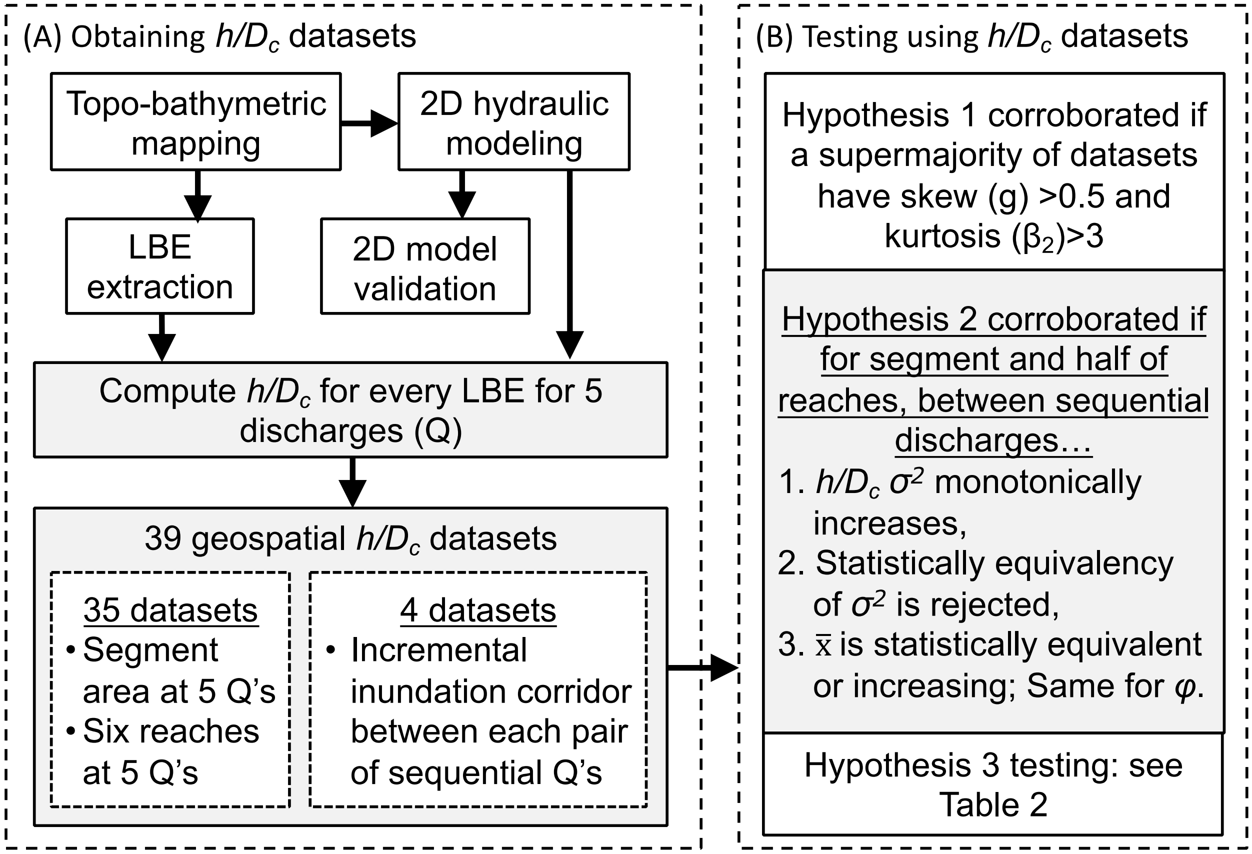

Figure 3. Study experimental design. σ^2, $\bar{x}$, and φ, are standard deviation, mean, and mode, respectively.

4.1 Topo-bathymetric and LBE mapping

An extremely detailed (> 21 million points; ~ 16 pts/m^2) and accurate topographic point dataset was made from terrestrial and bathymetric Airborne Light Detection and Ranging (LiDAR), boat-based echosounding, imagery-derived depth estimation (*sensu* Legleiter et al., 2004), and expert-based point augmentation (Valle & Pasternack, 2006). Points were vetted, vertically aligned and merged. A triangulated irregular network was used to interpolate elevations to a 0.46-m resolution digital terrain model (DTM) raster (bare Earth DTM).

Spatially explicit mapping of 42,176 LBEs (e.g., Figure 4) was done by Wiener and Pasternack (2022) using a novel procedure. First, a ground classification algorithm applied to the bare Earth point cloud separated landform points from those of overlying features to create a ‘smoothed’ DTM raster. The smoothed DTM raster was differenced from the bare Earth DTM to generate a roughness surface model (RSM) raster. A marker-controlled watershed segmentation algorithm was used to extract LBEs from the RSM. Minimum LBE size was a single raster cell (0.46 m x 0.46 m).

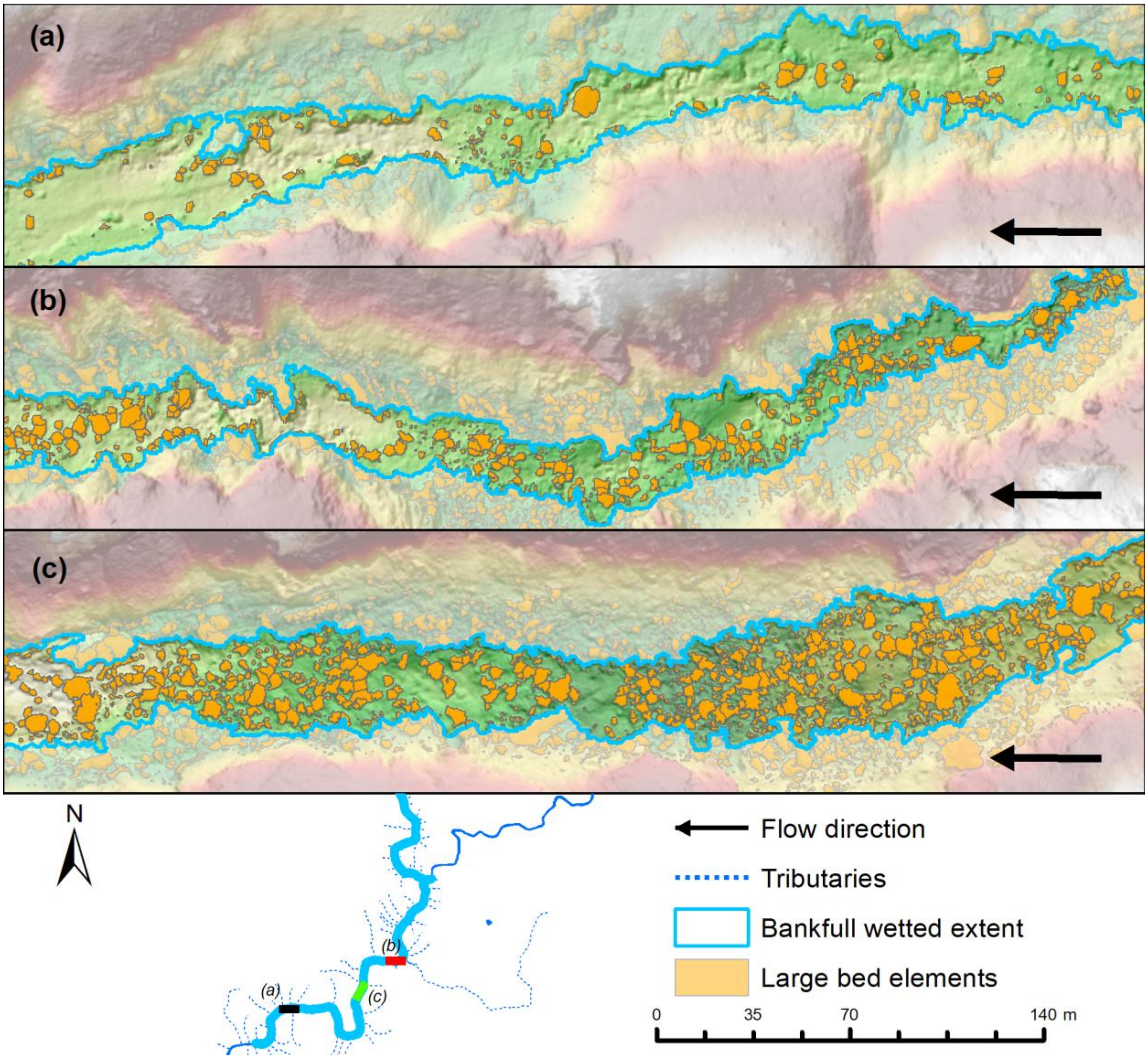

Figure 4. Typical configurations of LBEs within the study segment's bankfull channel overlain on shaded relief that include: (a) low concentration isolated and clustered LBEs, (b) moderate LBE concentrations with transverse and step structures, and (c) high LBE concentrations with mixtures of steps, transverse structures and possible reticulate formations. LBEs outside the bankfull channel are partially transparent. Polygon boundaries define individually mapped LBEs but may include clustered boulders as noted in text.

4.2 Two-dimensional hydrodynamic modeling

Steady-state, two-dimensional (2D) hydrodynamics were simulated with Sedimentation and River Hydraulics—Two-Dimensional model (SRH-2D) v. 2.2 (Lai, 2008), which is capable of simulating complex hydraulic conditions in mountain rivers (Brown & Pasternack, 2014; Strom et al., 2016). To meet the study's need for precise delineation of wetted areas and flow-depth prediction aggregated at 10^0-10^2 m^2 scales, a resolution of ~ 1-m was used. Simulations were run for five geomorphically or otherwise relevant discharges (1.54, 10.73, 82.12, 343.6, and 1184.6 m^3/s) (Table 1). Wiener and Pasternack (2022) details model development, parameterization, and performance assessment.

Depth prediction performance was important to this study given the need to accurately estimate relative submergence (analysis methods and additional performance results in supplementary materials [Text S4.2]). The majority (53%) of absolute deviations were less than the independently reported 0.117 m vertical accuracy uncertainty of the bathymetric LiDAR, which aligns with the expectation that 2D model WSE deviations should not exceed uncertainty in the topographic data (Pasternack, 2011; Brown & Pasternack, 2012). Mean absolute deviation between rod-measured and model-predicted depths was 0.092 m. The coefficient of determination (R^2)

for predicted versus observed depths was 0.80 ($p<0.001$) and the linear regression slope was 0.87 ($p<0.001$). These values are considered very good amongst 2D models (Brown & Pasternack, 2012) and exceed recommended minimum norms for model performance (Pasternack, 2011).

Table 1. Simulated discharges.

Simulated discharge (m^3/s)	Approximate annual recurrence interval (years)	Segment averaged Froude number	Number of wetted LBEs	Description
1.54	-	0.11	13976	Representative baseflow taken as average of daily dry season (July 1 - September 30) flows at downstream boundary from 1930-2015.
10.73	1.06	0.18	17792	YCWA (2013) morphologically estimated bankfull flow.
82.12	1.59	0.28	24249	Flow observed to inundate several alluvial channel margins and with ~1.59-year recurrence, which nearly corresponds to most probable annual flood (Langbein, 1949).
343.6	3.46	0.35	31314	Maximum flow for which 2014-2015 boundary conditions were available
1184.6	13.7	0.39	39319	Boundary condition opportunistically collected for January 9, 2017 flood.

4.3 Relative submergence calculations

Relative submergence was calculated for each LBE at each simulated Q. For an individual roughness element, h/D_c is typically defined as the ratio of the approach flow depth (h) to particle height (D_c) (Papanicolaou & Tsakiris, 2017). In this study, each LBE's D_c value was set as the max RSM within each polygon. RSM values represent the extent that elevations extend above a smooth but variable bed surface, thus max RSM values are a proxy for true D_c values.

For each Q, h was calculated as the arithmetic mean of model predicted h added to RSM heights in all raster cells occupied by each LBE as well as cells within a one-cell buffer around the feature:

$$h = \frac{1}{q+r}\sum_{i=1}^{q}\sum_{j=1}^{r}\left((h_i + RSM_i) + (h_j + RSM_j)\right) \in \left\{h_i \middle| h_i > 0 \text{ and } h_j \middle| h_j > 0\right\} \qquad \text{(EQ.1)}$$

where i is an index for cells where the LBE is present, j is an index for cells located within a one-cell buffer of the LBE, q is the number of LBE cells, and r is the number of buffer cells (Figure 5). To explore h/D_c uncertainty, one alternative method for calculating h as well as an alternative for calculating D_c at each LBE were implemented (Text S3.4).

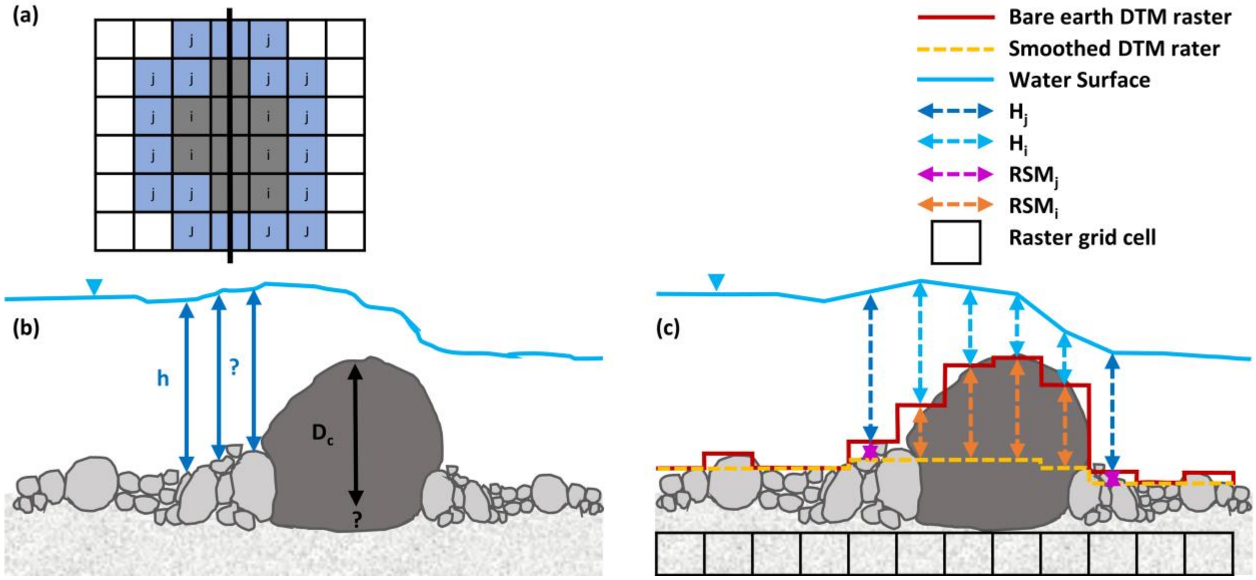

Figure 5. Conceptual illustration showing (a) plan-view of hypothetical LBE in gray with one-cell buffer region in blue and profile views along dark line in (a) of (b) natural conditions and (c) how natural conditions are represented in this study along with measurements needed for LBE relative submergence calculation. Note, question marks in (b) indicate uncertainty in how h and D_c should be measured under natural conditions.

4.4 LBE relative submergence hypothesis testing

Answering study questions required obtaining 39 h/D_c distributions corresponding to the wetted area of each of the five *Q's* for each of the seven spatial domains (entire river segment plus the six reaches) as well as for four discharge-dependent river margins (aka incremental inundation corridors, Figure 6) ('discharge-dependent datasets'). Hypothesis testing metrics, which included the mean ($\bar{x}$), standard deviation (σ), mode (φ), coefficient of skewness (*g*), and kurtosis (β_2) were calculated for all 39 h/D_c datasets (Text S4.4). Corroboration of hypothesis 1 required a supermajority of datasets in each spatial domain (i.e., 4 of 6 datasets in the segment and in each reach and 3 of 4 incremental inundation corridor datasets) to be positively skewed ($g>0.5$) and leptokurtic ($\beta_2>3$).

Corroboration of hypothesis 2 for each dataset was based on three criteria. First, variance (σ^2) had to monotonically increase between discharge-dependent datasets. Second, σ^2 statistically equivalency between datasets had to be rejected. Third, central tendencies ($\bar{x}$ and φ) had to be either statistically equivalent or increase between discharge-dependent datasets.

Statistical equivalency was based on metrics being indistinguishable at a 95% confidence level according to standard non-parametric (e.g. Mann-Whitney U and Levene's tests) or appropriate parametric tests (e.g. Welch's t-test and F-test). Because modal values were derived from h/D_c histograms, if values between subsequent datasets were within one bin-width they were considered equivalent (Text S4.4; Table S1). If these criteria were not all met the test was rejected for that dataset. Overall, hypothesis 2 was accepted if positive tests were confirmed for the study segment as a whole and half the reaches.

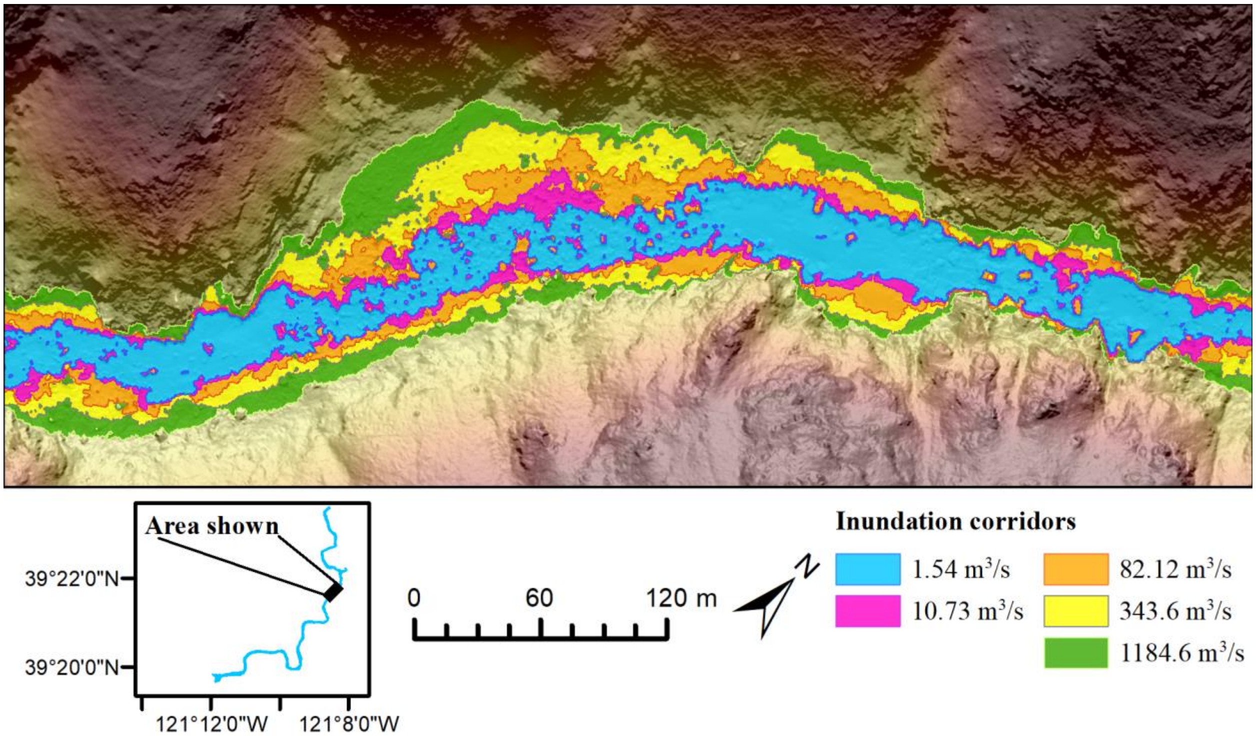

Figure 6. A section of the baseflow wetted area (blue) and the subsequent incremental inundation corridors occurring as strips between successive higher discharges. For example, pink is the incremental inundation corridor between 1.54 and 10.73 m^3/s. Flow is from right to left.

4.5 LBE discharge-dependent style hypothesis testing

A series of statistical tests and acceptance criteria were used on segment- and reach-scale h/D_c datasets to address the study's third question regarding which Style or Styles best explained observed discharge-dependent h/D_c behavior (Table 2, see Text S4.5 for detailed explanations). The study did consider the possibility that no Styles may fit the data or multiple Styles could fit. Incremental inundation corridor h/D_c datasets, which served to isolate sets of LBEs along channel margins, were only analyzed for statistical self-similarity (i.e. Style 1 criteria), but were also used to help ascertain the factors responsible for the results of hypothesis testing (section 5.4).

An initial requirement of all Styles was that h/D_c distributions were from the same distribution type. Thus, h/D_c distributions were fit with Normal, Log-normal, Weibull, Exponential, and Gamma parametric distributions and evaluated on the basis of whether they were best fit by the same type of distribution within (i.e. between discharge-dependent datasets in the same domain) and between spatial domains. If this criteria was met, then distribution fitting parameters and relevant statistical properties of raw h/D_c data (e.g. $\bar{x}$, σ, φ, g, and β_2) were compared either qualitatively or statistically between all discharge-dependent h/D_c datasets (i.e. 10 tests per parameter per domain) using the tests listed in Table 2 and interpreted in accordance with acceptance criteria for each Style.

Tests for threshold Styles 2(b), 3(b), and 4(b) involved a combination of the tests for Styles 1-4 and two additional acceptance criteria. The first criteria was equivalency of all dataset properties between at least one set of successive *Q's* (i.e. same criteria as Style 1). This would show that over a range of *Q's*, no threshold was crossed. Secondly, was that these data be preceded or followed by a dataset with a dramatic difference in relevant parameters (i.e. variance for Style 2(b) and central tendency for Style 3(b)), hence indicative of crossing a threshold.

Given the stringency of Style 1 testing, acceptance of the first criteria was loosened such that datasets could have small, gradual changes in h/D_c distributions between *Q's*. Specifically, if the percent change in all h/D_c dataset properties were less than 5% between *Q's*, the set of *Q's* were considered similar and thus acceptable with this component of threshold Style behavior. In characterizing magnitudes of threshold shifts in distribution properties a separate set of non-dimensional metrics was developed by normalizing the percent change in h/D_c dataset properties between *Q's* by the percent change in averaged depth for the same spatial domain according to the general formulation:

$$\Phi^*_\Delta = \frac{\frac{\Phi_{k+1} - \Phi_k}{\Phi_k}}{\frac{\bar{h}_{k+1} - \bar{h}_k}{\bar{h}_k}};\ \Phi = \{\bar{x}, \sigma, \varphi\} \qquad \text{(EQ.2)}$$

where k is an index for discharge, $\bar{h}$ is domain averaged model predicted flow depth, and Φ^*_Δ is a generic non-dimensional metric for a h/D_c dataset property (Φ). Small (<1) or zero Φ^*_Δ values indicate cases of little or no change between discharges relative to changes in flow depth, whereas larger relative changes occur as Φ^*_Δ values exceed unity. Values above unity indicate that distribution properties increase faster than depth increased. A value of 1.2 was used as a conservative threshold indicating dramatic shifts (*sensu* Wyrick and Pasternack, 2014).

Visually, relationships between h/D_c dataset parametric and statistical properties versus Q appeared to follow power-laws. To explore this further, data in each domain were modeled by fitting linear models to log-transformed discharges and the values for each of the seven h/D_c distribution properties (i.e. $\bar{x}$, σ, φ, g, β_2, and fitted distribution parameters [all datasets were best fit or reasonably fit by 2-parameter Gamma distribution]), with the caveat that only five data points were available per model, one per Q. With seven spatial domains and seven statistical properties, this analysis yielded 49 models. Model fitting by ordinary least squares regression was coded in R.

Table 2. Testing details for hypothesis 3 regarding styles of LBE relative submergence response to discharge.

Style	Description	Domain(s) compared	Acceptance criteria†	Example tests for statistical equivalency‡
1	Statistical self-similarity	within or between	Fitting parameters and statistical properties equivalent between all datasets.	likelihood-ratio test (Held & Bove, 2014) Welch's t-test F-test
2	Constant central tendency shifting variance	within	Central tendency equivalent between all datasets and rejection of equivalency of variance between all datasets.	Welch's t-test (central tendency) Mann-Whitney U test (central tendency) F-test (variance) Levene's test (variance)
2(b)	Constant central tendency threshold type shifting variance	within	Central tendency equivalent between all datasets. Statistical self-similarity between at least two successive datasets. Rejection of equivalency of variance in dataset preceding or following self-similar data accompanied by dramatic shift in σ_{Δ}^{*}.	
3	Constant variance shifting central tendency	within	Variance equivalent between all datasets and rejection of equivalency of central tendency between all datasets.	
3(b)	Constant variance threshold type shifting central tendency	within	Variance equivalent between all datasets. Statistical self-similarity between at least two successive datasets. Rejection of equivalency of central tendency in dataset preceding or following self-similar data accompanied by dramatic shift in $\bar{x}_{\Delta}^{*}$ or φ_{Δ}^{*}.	

4	Process-based similarity	between	Rejection of Styles 1, 2, 2(b), 3, and 3(b). Slope of discharge-dependent $\bar{x}$, σ, and distribution parameters equivalent between domains.	
4(b)	Threshold type process-based similarity	between	Rejection of Styles 1, 2, 2(b), 3, 3(b), and 4. Statistical self-similarity of at least two successive datasets in two or more domains for the same set of discharge-dependent data. Slope of discharge-dependent $\bar{x}$, σ, and distribution parameters equivalent for remaining non self-similar data between same domains.	Equality of regression coefficients test (Paternoster et al., 1998)

†Style rejected if any acceptance criteria not met.
‡Statistical equivalency based on all parameters/properties being indistinguishable at a 95% confidence level.

5 Results

5.1 Hypothesis 1 and 2 results

Distributions of h/D_c values in 38 of 39 segment, reach, and incremental inundation corridor spatial domains were leptokurtic (β_2>3) and had moderate-to-high positive skewness (g>0.5), thus hypothesis 1 was accepted (Figures 7-9; Tables S2 and S3). Only the dataset in Reach 6 associated with the largest Q (1184.6 m^3/s) was platykurtic (β_2<3) and had moderate positive skewness (0<g<0.5). These similarities may partly reflect the underlying trend for discharge-dependent distributions of D_c values to exhibit these same statistical properties (Section 5.5; Figure S9; Figure S10).

Despite these basic similarities, datasets showed clear differences with regard to distribution shape and other statistical properties. Across all spatial domains, higher *Q's* corresponded with monotonic increases in h/D_c dataset means and standard deviations, and decreases in skewness, kurtosis, and fitted Gamma distribution parameters (i.e. shape [α] and rate [β]) values (Table S2). Thus, the dominant trajectory in each domain was toward less peaked, wider, and less positively skewed h/D_c distributions (Figure 7 and Figure 8). One explanation for these observations is depth increases at previously wetted and partly-to-fully submerged LBEs playing a more prominent role in h/D_c distribution changes compared to the contributions of newly wetted LBEs located along the expanding channel margin (see Section 5.5 for additional results on this topic).

Metrics for the distributional changes with *Q* met the criteria to corroborate hypothesis 2. Specifically, all statistical comparisons of h/D_c dataset means (Mann-Whiney U test) and variances (Levene's test) between subsequent discharge-dependent datasets found that these metrics were not equivalent ($p \ll 0.05$). Changes in modal values on the other hand were more variable. While modes tended to increase slightly between *Q's*, decreases occurred on five occasions (Table S2). Decreases were all within one bin-width of the preceding value, so trends in modal values were considered to either increase or remain relatively constant. While the modal decreases leave room for speculation, this fulfilled the final criteria for accepting hypothesis 2.

Notably, the magnitude that h/D_c properties changed with Q varied within and between domains, and especially across *Q's*. Visual inspection revealed greater similarity in data associated with the same Q between domains (e.g. Reach 4, 1.54 m^3/s LBE data compared to Reach 5, 1.54 m^3/s LBE data) compared to similarity that occurred in the sequences of h/D_c values within any given domain. That said, the way distribution shapes changed over the series of discharge-dependent datasets appeared comparable between spatial domains.

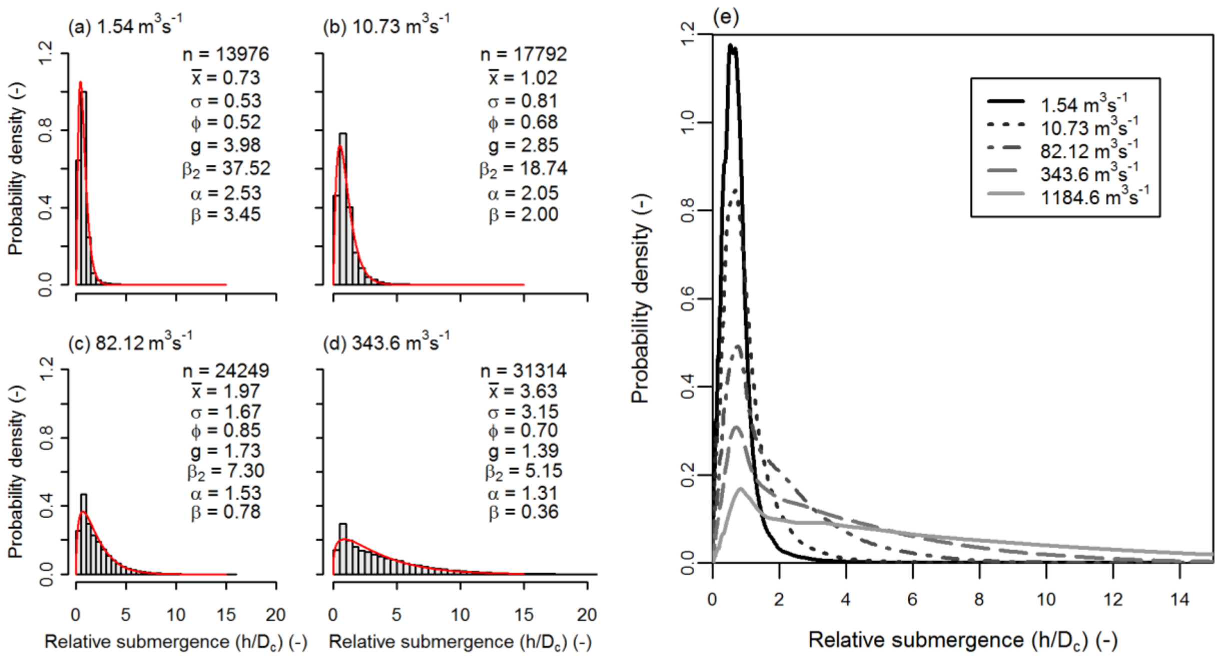

Figure 7. Histograms of (a-d) segment-scale h/D_c probability densities (bars) overlain with fitted gamma distribution (red lines) for discharge-dependent LBE datasets associated with 1.54, 10.73, 82.12, and 343.6 m^3/s and (e) kernel density of all segment-scale h/D_c probability densities overlain together. For panels a-d the count (n), mean ($\bar{x}$), standard deviation (σ), mode (φ), skewness (g), and kurtosis (β2) of each dataset is shown as well as the shape (α) and rate (β) parameters from fitted gamma distributions.

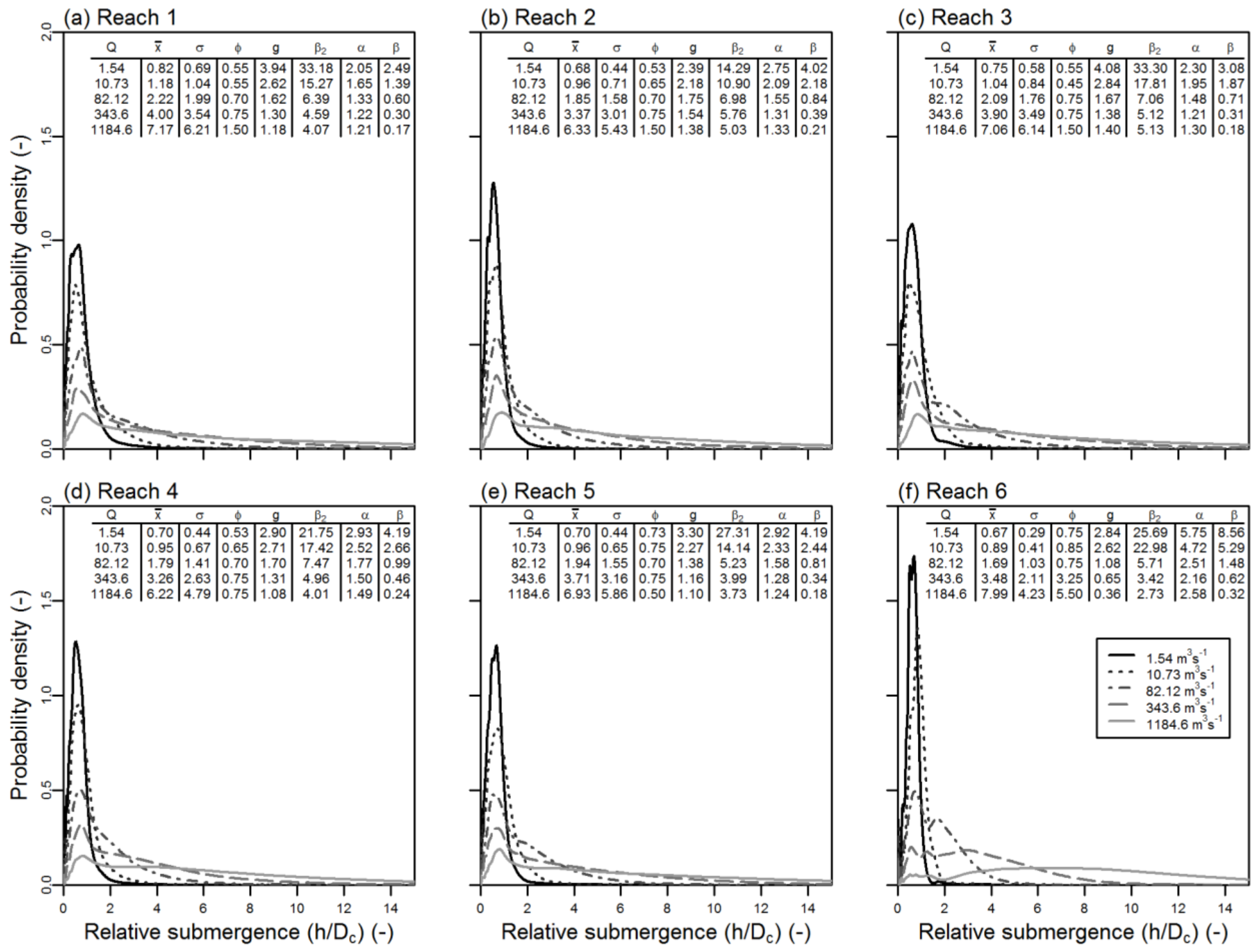

Figure 8. Overlain kernel densities of *h/D_c* probability densities for the five discharge-dependent LBE datasets within each geomorphic reach (a-f). Summary statistics and fitted gamma distribution parameters shown.

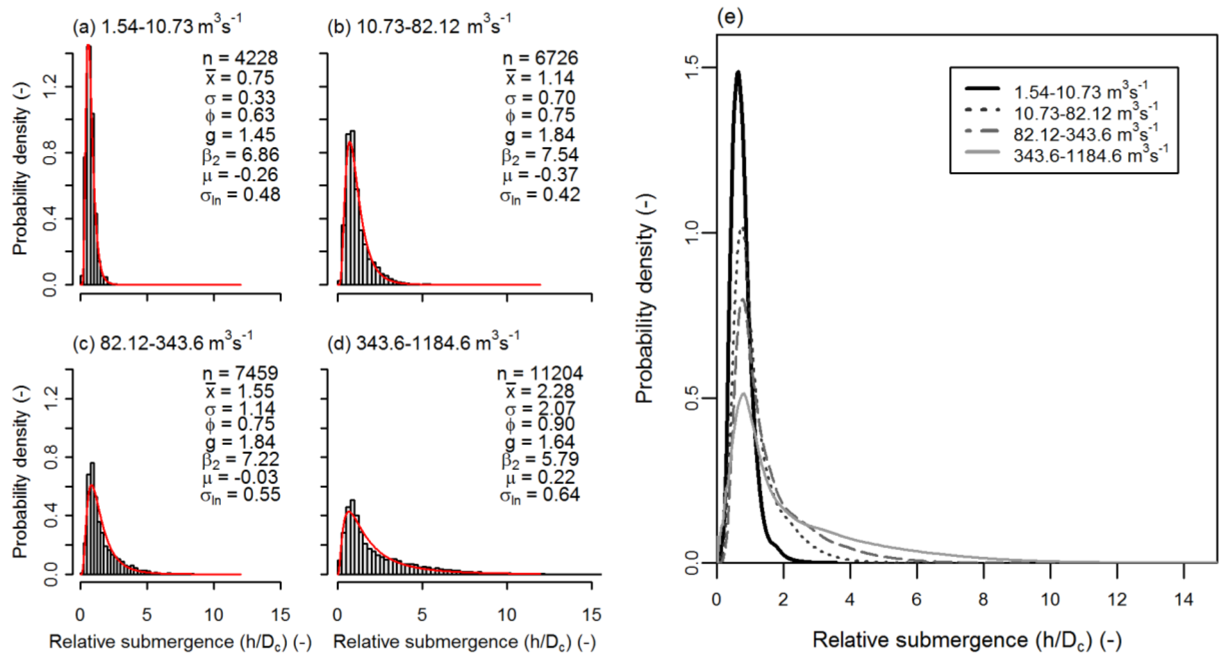

Figure 9. Histograms of (a-d) each incremental inundation corridor's h/D_c probability density (bars) overlain with fitted log-normal distribution (red lines) and (e) kernel density of all incremental inundation corridor probability densities overlain together. Summary statistics and fitted log-normal distributions parameters (μ and σ_{ln}) shown.

5.2 Hypothesis 3 results

Acceptance criteria for all Styles required h/D_c datasets to be from the same distribution type. Distribution fitting and goodness-of-fit testing found four of five segment-scale h/D_c datasets to be best fit by two-parameter Gamma distributions, and one best fit by a Weibull distribution (LBEs associated with the 1184.6 m^3/s wetted area) (Figure 7). At the reach scale, 24 of 30 datasets were best fit by two-parameter Gamma distributions, and six were best fit by Weibull distributions (i.e. Reach 1, 4, and 5 LBEs associated with 1184.6 m^3/s wetted area; Reach 6 LBEs associated with 82.12, 343.6, and 1184.6 m^3/s wetted areas) (Figure S3). However, goodness-of-fit testing found that it was not possible to reject that all segment- and reach-scale datasets could be drawn from Gamma distributions at the 95% confidence level (Text S4.5).

Given nearly all segment- and reach-scale h/D_c datasets were best fit by or could reasonably be drawn from Gamma distributions, fitted parameters, α and β, were evaluated for statistical equivalency through pair-wise comparison of all unique dataset combinations using the likelihood-ratio-test of Krishnamoorthy et al. (2015). Within domain testing required rejecting that parameters were equal above a 95% confidence level for all comparisons. This required rejection of the Style 1 hypothesis (Table 2). Percent change results provided additional support for rejecting Style 1, which unlike statistical metrics were not dominated by the effect of large LBE sample sizes.

Results also rejected that the river exhibited any of the three threshold Styles (Table 2). With the exceptions of comparison of three φ values, percent changes in h/D_c distribution metrics ($\bar{x}$, σ, g, β_2, α, and β) between *Q's* exceeded the 5% test limit for all comparisons (Table S2). The absence of small, gradual changes between h/D_c datasets necessitated rejection of threshold Styles 2(b), 3(b), and 4(b) for the set of tested *Q's*.

Non-dimensional metrics further demonstrated changes in h/D_c dataset properties were more continuous and involved dramatic changes between *Q's* (Figure 10). All segment and reach scale $\bar{x}^*_\Delta$ and σ^*_Δ values exceeded 1.2, indicating dramatic shifts. In contrast, modal change values (φ^*_Δ) were predominantly below 1.2 and included both negative and zero values. Notably, simultaneous exceedances of both $\bar{x}^*_\Delta$ and σ^*_Δ above the shift threshold at each *Q's* also conflicted with acceptance criteria of Styles 2(b) of 3(b) that were based on shifts occurring for only one property at a time (Table 2).

As previously reported in Section 5.1, statistical equivalency of central tendency and variance were rejected above a 95% confidence level (p <<0.05) for all within domain tests, thus requiring rejection of Styles 2 and 3. Though not explicitly part of the testing criteria, the relatively large percent changes in $\bar{x}$ and σ values and magnitude of $\bar{x}^*_\Delta$ and σ^*_Δ values described above further supported rejecting these Styles.

Comparison of between segment- and reach-scale domain h/D_c dataset properties for the purpose of determining if statistical self-similarity existed across multiple domains found the vast majority of dataset properties were not statistically equivalent, indicating h/D_c statistical self-similarity did not exist between spatial domains (Text S5.2). Of the datasets with roughly equivalent h/D_c distribution properties, the vast majority were for LBEs associated with the same Q. Therefore, greater similarity in h/D_c datasets existed between domains at the same Q compared to similarity that occurred within any given domain over the range of tested *Q's*.

Results presented thus far demonstrate discharge-dependent dynamism inconsistent with several Styles in favor of more mutualistic changes aligning with Style 4. Covariation between the mean and standard deviation of geometry properties of Earth surface landforms have been previously reported for drumlins by Ely et al. (2018) and fine-grained aquatic bedforms by Van der Mark et al. (2008). Evaluating bivariate trends of h/D_c dataset properties identified several covarying relationships. For example, decreases in segment-scale α and β were marked by strong linear correlation with Q (R^2 = 0.994, p = 0.003). In other words, there was a mutualistic and predictable nature to how h/D_c dataset properties changed between Q's (Table S4, Figure S6). These results support that changes in parametric and statistical properties between domains were consistent, such as envisioned by Style 4.

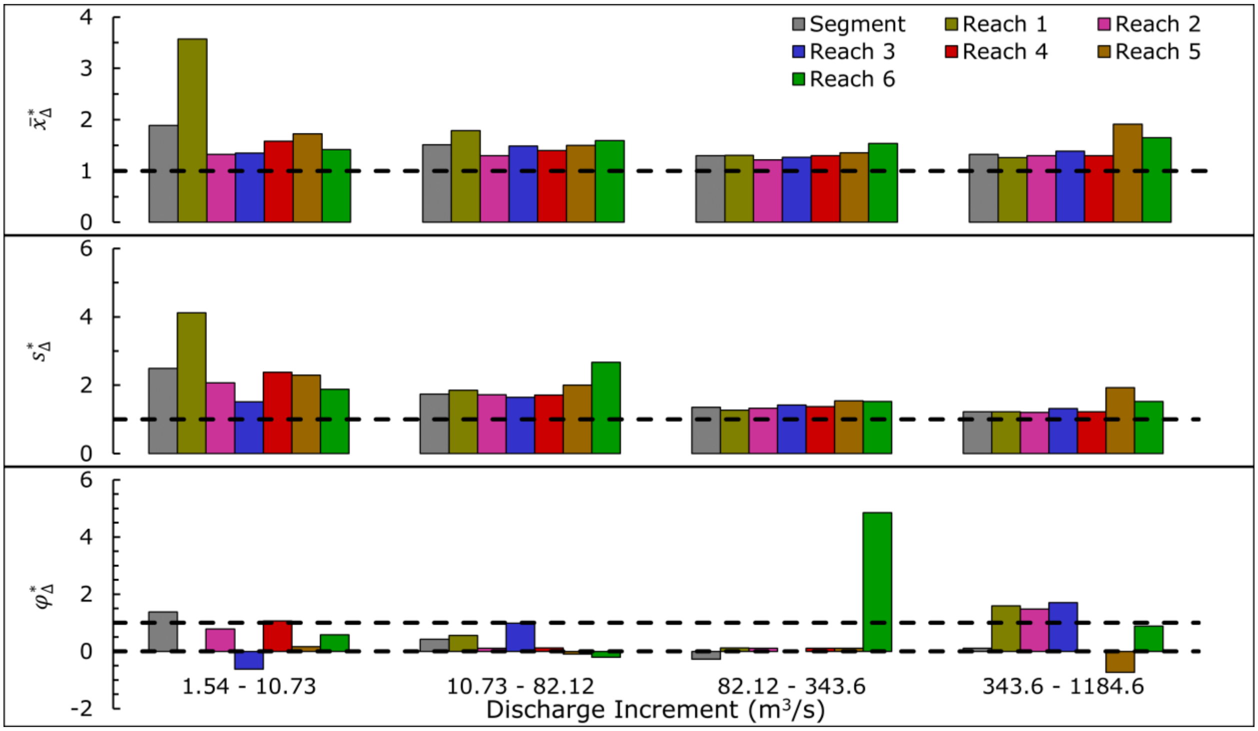

Figure 10. Segment- and reach-scale non-dimensional $\boldsymbol{\bar{x}^*_\Delta}$, $\boldsymbol{s^*_\Delta}$, and $\boldsymbol{\varphi^*_\Delta}$ values illustrating relative magnitudes of change in h/D_c distribution properties between datasets. Smaller values indicate less change between datasets. The horizontal dashed lines at 1.2 represent a threshold for dramatic shifts between datasets.

5.3 Between domain process-based similarity

Results have required rejection of Styles 1, 2, 2(b), 3, and 3(b), but could not reject Style 4 (Figure 1). Style 4 was further tested by considering the slope of power-law regressions for the seven distribution properties versus Q (see Text S4.5). Power-law regressions yielded adjusted-R^2 between 0.776 and 0.989 for all models (Figure S7), except φ, whose values were 0.183 and 0.858. Further, with the exception of six of the seven models for φ, all slope coefficients were statistically significant (F-test, $p < 0.05$) (Table S4). Thus, models were reasonably accurate and Q explained a large majority of property variance, so further testing of Style 4 with this method was justified.

Model slopes (i.e. power-law exponents) of each response metric were compared between all unique domains pairs using EQ. S2. Of the 84 relevant slope comparisons (21 per metric for $\bar{x}$, σ, α, and β), only the Segment and Reach 6 α-slope comparison was rejected for equivalency above a 95% confidence level ($|Z| \geq 2.776$). This meant that all other α slopes, and all $\bar{x}$, σ, and β slopes were considered equivalent between all pairs, consistent with the Style 4 acceptance criteria (Table 2). Of the additional 63 comparisons between φ, g, and β_2 slopes, 23 were rejected (Text S5.3). This meant 20 of 21 unique domain pairs had roughly equivalent $\bar{x}$, σ, α, and β slopes and 7 of the 21 domain pairs had roughly equivalent slopes for all variables. Collectively, these results indicate that Style 4 is both reasonable and the most representative Style for h/D_c distribution behavior in the study segment.

5.4 Incremental inundation corridor relative submergence

All four incremental inundation corridor h/D_c datasets (Table S3) were best fit by log-normal distributions, which was supported at the 95% confidence level by the corrected Anderson-Darling test (Figure 9). As a result, central tendencies were compared with Welch's t-test and variances were compared using F-tests (R Core Team, 2021). Despite slightly stronger visual resemblances between datasets than those present when comparing datasets in other domains (Figure 7, Figure 8, and Figure 9), all tests were rejected above a 95% confidence level ($p <<0.05$) suggesting h/D_c values of LBEs along the incrementally wetted channel margins were each statistically unique.

Isolating the independent sets of h and D_c values in each corridor found distributions of D_c values to exhibit greater similarly across the four corridors (Figure S8). This was confirmed using the non-parametric overlapping index (Pastore & Calcagni, 2019), which found comparison of all possible sets of D_c values to have index values between 0.88-0.94 versus index values between 0.31-0.67 for h comparisons. The index varies from 0-1 for end-member conditions of no distribution overlap and perfect distribution overlap, respectively. This means variations in flow depths along channel margins played a larger role in differences between incremental inundation corridor h/D_c datasets than diversity in LBE heights.

5.5 Submergence trends

Many processes influence h/D_c distribution changes with Q, but especially addition of new peripheral LBEs (indicated by each incremental inundation corridor's LBE count and LBE h/D_c values) and drowning of already-inundated LBEs (indicated by depth change at previously wetted LBEs). Results found that the latter process drastically overshadowed the former and drove trends to less positively skewed h/D_c distributions with higher mean h/D_c values (Text S5.5, Figure S9a-d). This was quantitatively supported by independently calculating the difference in the mean of each h/D_c dataset resulting solely from the addition of newly wetted LBEs ($\Delta\bar{x}_n$) versus the mean difference due to depth changes at previously wetted LBEs ($\Delta\bar{x}_p$), which confirmed the latter always exceeded the former. Though not depicted, the same results were found at the reach-scale.

More minor trends, such as isolated decreases in modal values, were also partly explained by variability in the relative magnitude of the independent dataset components depicted in Figure S9 (a-d). For instance, addition of a large number of newly wetted, very low submergence LBEs between 82.12-343.6 m^3/s, simultaneous with only moderate depth increases at previously wetted LBEs were assumed responsible for the observed decrease in modal values between the two datasets (Figure 7).

A final observation regarding the influence of changing flow depths versus LBE configurations on h/D_c results was that the distribution of segment-scale D_c values remained relatively constant across *Q's* even with the addition of new LBEs, whereas flow depths at LBEs were, unsurprisingly more dynamic (Figure S9e-n). Overlap indexes comparing all possible segment-scale D_c datasets varied between 0.81-0.96 versus between 0.13-0.70 for h comparisons. The same pattern was true for all reach-scale datasets (Text S5.5). This result corroborates the relative significance of the two processes compared in this section.

Amidst near universal trends for increasing h/D_c values at higher *Q's* it is relevant to highlight that a substantial portion of LBEs remained emergent ($h/D_c<1$), below the LRS regime threshold ($h/D_c<3.5$), or below other thresholds used to differentiate bed morphology effects on hydraulic and sedimentological processes across *Q's* (Table 3). For instance, even at the highest simulated *Q*, 10.5% of LBEs would be emergent and 40.2% would still influence hydraulics at the water surface (e.g. $h/D_c<3$, Cooper et al., 2013). It is also important to recall that conditions at LBEs within laterally nested, discharge-dependent portions of the river corridor did not change equally between *Q's*. For example, considering LBEs within the baseflow channel, only 1.4% of these features remained emergent across all *Q's*. A complete accounting of the percent of LBEs intersecting each wetted area that exceeded relevant h/D_c thresholds at each higher *Q* are included in Table S5.

Table 3. Percentage of segment-scale h/D_c values exceeding certain thresholds at each discharge.

Simulated Discharge (m^3/s)	Threshold†					
	1	2	3	3.5	4	10
1.54	17.7	2.5	0.8	0.5	0.3	0.0
10.73	37.7	9.3	3.0	1.7	1.0	0.0
82.12	63.8	37.6	20.9	15.5	11.5	0.2
343.6	78.1	60.1	46.7	40.9	35.7	4.9
1184.6	89.5	77.9	68.7	64.1	59.8	24.2

†Thresholds correspond to following: 1 – Emergent vs submerged conditions; 2 – *h* at double LBE height; 3 – Approximate threshold flow depth where form-induced sublayer always extends to water surface (Cooper et al., 2013); 3.5 – Transition from LRS to HRS regime (Papanicolaou & Tsakiris, 2017); 4 – Transition from intermediate to small-scale roughness (Bathurst, 1985) and surface effects are negligible (Shamloo et al., 2001); and 10 – Threshold for applicability of canonical hydraulically rough boundary-layer theory (Katul et al., 2002).

6 Discussion

This study may be especially impactful, because it not only laid out a new theoretical framework for describing the discharge-dependent dynamism of relative submergence in a confined mountain river strewn with boulders, but it also carried out thorough hypothesis testing with a large (13.2-km river segment), detailed (42,176 LBEs), and accurate dataset. Hopefully future studies will build on this foundation by applying the methods to the global diversity of river types to find out if other settings yield different outcomes. The sections below explore the results, with substantial additional details and additional discussion topics addressed in the supplementary materials file.

6.1 LBE h/D_c distributions and styles

In light of the questions and hypotheses posed by this study two initial takeaways were that results largely corroborated hypotheses 1 and 2. Specifically, h/D_c distributions across multiple discharge-dependent spatial domains were leptokurtic and positively skewed (Figures 7-9). Also, changes between h/D_c distributions over a series of Q's were primary as predicted by hypothesis 2.

In considering how h/D_c values would evolve, an initial hypothesis was that distributions would remain constant in any given spatial domain across *Q's* (Style 1). Despite segment- and reach-scale datasets being reasonably Gamma distributed, visual and statistical differences confirmed h/D_c distributions were not conserved. Thus, the Style 1 hypothesis was rejected. Statistical comparison within and between domains also required rejection of Styles 2 and 3, and conditionally rejecting threshold Styles 2(b), 3(b), and 4(b). Complete rejection of threshold style behavior was limited by the number of flow simulations, as processes associated with these Styles could have been hidden between simulated *Q's*. However, recognizing that the mountain river was confined and there was no dramatic change in LBE patterns along the canyon's fringe, then it is not surprising that the propensity for continuous changes in h/D_c distribution properties did not favor these styles being present in the study segment. Ultimately, what did emerge was strong evidence for process-based similarity (Style 4) being the most appropriate behavioral model to explain h/D_c dynamics in the study segment, as stated in hypothesis 3.

The observation that reach-scale h/D_c distributions evolved in essentially the same manner between *Q's*, has theoretical and practical relevance. One broad interpretation of the consistent scaling and fact that

h/D_c distributions were consistently well-fit by Gamma distributions is that common self-organizing processes associated with the size-frequency distribution, spatial arrangement, and submergence of LBEs were present between domains (Sapozhnikov & Foufoula-Georgiou, 1999; Hillier et al., 2016). Each of these properties involves complex feedbacks in the fluvial-hillslope system that are difficult to disentangle. Thus such inference is tentative, as multiple generative processes cannot be ignored as a means for arriving at a common set of distributions (Sornette, 2000). However, if D_c is taken to represent the bed-roughness length-scale coefficient (Δ), and the set of h/D_c data are proportional to reach-averaged flow resistance, as is widely accepted (Powell, 2014), study results indicate that while individual reach-scale resistance magnitudes might differ, the rate of change in resistance with Q between reaches was roughly equal.

Interpreted in the empirical context of regime theory and extremal hypotheses, this suggests a degree of mutual reach-scale channel adjustment and implies attraction to a common critical state (Eaton & Church, 2009; Adams, 2020). In laterally confined rivers, modification of bed state (e.g. roughness element sizes and configurations) is both the most rapid and often only independent degree of channel adjustment available (Adams, 2020). Where bed state is dominated by LBEs, physical experiments, theory, and field measurements provide evidence that LBE configurations self-organize toward conditions that maximize flow resistance as this promotes channel stability (Church et al., 1998; Eaton & Church, 2009; Adams, 2020). Consistent with these studies, previous analysis found 21 of 24 discharge-dependent reach-scale LBE datasets in the study segment had LBE concentrations, a metric quantifying LBE density in a given spatial area, corresponded to Morris's (1959) wake interference regime, which serves as a hydrodynamic process-based mechanism for maximizing resistance (Wiener & Pasternack, 2022). Recent experiments by Carollo & Ferro (2021) and boundary layer theory analysis of Cassan et al. (2017) applicable to rough bedded rivers indicate that for a given bed condition, resistance is at a global maximimum when relative submergences are in the range ~0.55-1. If taken as a target, keeping the bulk of h/D_c values in this range as stage/discharge increases requires new low submergence LBEs be added in numbers that account for depth increases at previously wetted LBEs. This evolution is consistent with hypothesis 2 and aligns better with Styles 1, 2, and 4 compared to Style 3. Looking at study segment mean and modal h/D_c values, only at the lowest discharges were mean values in the 0.55-1 range. On the other hand, with the exception of Reach 6 nearly all modal values were in this range. Since the Carollo & Ferro (2021) and

Cassan et al. (2017) maximum resistance criteria identifies when flow resistance is at a global maximum for a given spatial domain, it is logical that it would only be achieved over a limited range of Q's. This differs from the concept that there exists bed roughness conditions that maximize possible resistance (local maxima) at any given flow (Morris, 1959; Bathurst, 1985; Church et al., 1998; Eaton & Church, 2009). Thus, our interpretation of h/D_c process-based similarity in the study segment is that it represents a dynamic equilibrium in channel adjustment toward a critical state that minimizes the variance of how resistance changes with discharge between reaches (Wohl & Merritt, 2008). Lateral confinement, observed LBE configurations, and modal h/D_c value support that the critical state toward which reaches adjust coincides with one that maximizes flow resistance. Though further analysis is required, h/D_c process-based similarity and deviation therefrom could serve as a quantitative metric to assess the degree that a series of connected river reaches are in equilibrium (Sapozhnikov & Foufoula-Georgiou, 1999), or may simply indicate if such reaches differ in their primary mode of channel adjustability.

Contrary to h/D_c process-based similarity at the segment- and reach-scale, greater statistical self-similarity was observed between incremental inundation corridor h/D_c distributions. While these data bore greater visual resemblance to the Style 2 conceptualization (Figure 9), statistical testing did not confirm this or any other Style (i.e. central tendencies and variances were considered not statistically equivalent). Nonetheless, results indicated that independent sets of h and D_c values in each corridor were more constant between *Q's* than these same metrics were when considered for the entire river corridor (Figure S8; Figure S9). Factors driving this similarity, especially the uniformity of D_c values along channel margins require additional exploration that is outside the scope of this effort (e.g. Sklar et al., 2020). However, it is logical to expect that the set of depths along incremental channel margins in a confined river canyon would be relatively shallow. Shallow depths together with near constant LBE D_c values explain the comparatively lower variance and lower overall magnitudes of h/D_c values in the incremental inundation corridors.

Lastly, of the reach-scale h/D_c datasets, the wider and lower gradient Reach 6 stood out in its Style. At the highest simulated Q (1184.6 m^3/s) h/D_c values in this reach had near zero skewness and followed a more bell-to-uniform shaped distribution compared to the positively skewed, unimodal distributions in the five upstream reaches (Figure 8; Table S2). This more uniform h/D_c distribution resulted from relatively low numbers of newly wetted LBEs being encountered simultaneous with large relative increases in depth at both previously wetted and newly wetted LBEs. These changes align with the canonical power-law form of channel width and depth hydraulic geometry relationships for an inundated U-shaped valley, whereby rates of channel width increase are low compared to rates of depth increase (Gonzalez & Pasternack, 2015). Convergence toward a uniform h/D_c distribution may be a common limiting state for confined river canyons at high *Q's* when the valley bottom is inundated and few new LBEs are encountered. Indeed, h/D_c distributions of the study's other reaches also appeared to evolve toward this limiting state. Presence of more V-shaped valley geometries with greater abundances of LBEs in these other domains may partly explain the slower trajectory toward uniform h/D_c distributions that could still occur at *Q's* higher than those simulated.

6.2 Evolution toward a relative submergence limiting-state

Evolution of h/D_c values toward uniform distributions may help explain field and experimental observations from bedrock-alluvial channels of reach-averaged flow resistance being stable at high *Q's* (Richardson & Carling, 2006; Hodge & Hoey, 2016; Ferguson et al., 2019). These observations contrast with other empirical data, most resistance equations, and the general idea that resistance should continuously decrease as increasing stage drowns-out bed roughness (e.g. Powell, 2014). Mechanisms driving the decoupling of flow resistance from Q have been previously attributed to increasing sidewall roughness driving lateral and turbulent flow mixing and due to spatial variability of the flow-field being separated into a central core of high-velocity flow surrounded by marginal slack-water zones (Richardson & Carling, 2006; Hodge & Hoey, 2016). Boundary layer theory also supports that hydraulic roughness is independent of depth for $h/D_c>10$, which under certain simplifying assumptions (e.g. uniform flow) would lead to constant resistance (Katul et al., 2002; Cassan et al., 2017). If resistance is considered proportional to the set of h/D_c data, and resistance contributed by LBEs with $h/D_c<10$ vastly exceeds resistance contributed by LBEs with $h/D_c>10$, then evolution toward uniform h/D_c distributions with a constant lower h/D_c bound and finite upper h/D_c bound above 10 would result in resistance being constant. Notably, such conditions do not explicitly conflict with the idea that uniform resistance values are at a local resistance maxima for the physical conditions present at those flows (e.g. width, depth, bed roughness characteristics, friction slope, and erosion threshold). As discussed in Section 6.1, LBE spatial structure, represented by metrics such as LBE concentration that have proven, strong correspondence with channel resistance, are good indicators for such local maxima.

To address the emergent question of whether the study segment's h/D_c distribution approaches a uniform distribution, study results were used to statistically model h/D_c distributions for flows higher than those initially tested. In doing so, the segment-scale, power-law relationship between Q and β (Figure 11a) was used to initially calculate simulated β values for a range of *Q's* (see section 5.3; β-Q model was selected over α-Q model based on slightly better accuracy [R^2 = 0.988 versus 0.959]). Next, α values were predicted using the previously modeled β-α relationship (Figure S6a). Figure 11b shows the resulting series of simulated h/D_c gamma distributions using predicted parameters for discharges ranging between 1.1-4500 m^3/s, the upper bound of which has an ~500-year recurrence level. Although the simulated discharges are larger, Wiener and Pasternack (2022) found study segment LBE concentrations were associated with conditions that maximize resistance up to 343.6 m^3/s, the maximum discharge in their study. Granted, even with the large size of LBEs and alluvium in this river, it is likely that the river would undergo significant morphodynamics at flows of > 50-yr recurrence interval, so this is just a thought exercise.

The simulated data spotlight the transition from high frequencies of relatively low h/D_c values at low flows to more uniformly distributed values at higher flows, which match observations in the study segment. Technically, if α approaches unity and β approaches zero the Gamma probability density function equals zero for all values. For segment- and reach-scale h/D_c distributions, the study found both conditions to be true as *Q* increased (Figure S9). However, if it is assumed that β is asymptotic to zero, as indicated in the β-*Q* relationship (Figure 11a), and α can be estimated using the statistical relationship Figure S9a, then simulated h/D_c values for increasingly larger *Q's* always approach a uniform distribution with probabilities approximately equal to the increasingly smaller β values. Physically, this would suggest that at very high *Q's* there are few, but always nearly equal numbers of, low submergence LBEs along the channel margins and highly submerged LBEs in topographic lows, with a mix of h/D_c values between these extremes. As discussed above, the nearly uniform distribution of h/D_c values provides a preliminary theoretical means for resistance to become constant at higher *Q's*. Such theoretical stochastics require further investigation, but at present could be useful in guiding design of synthetic river channels, numerical simulations, or physical experiments with LBEs.

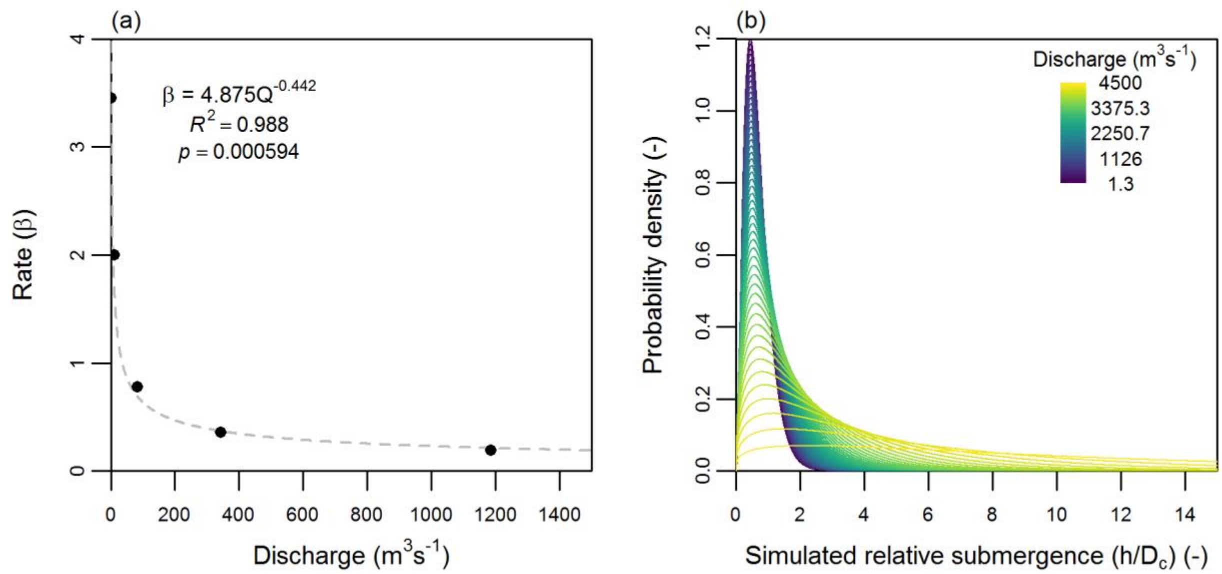

Figure 11. (a) Fitted Gamma distribution rate (β) parameters versus discharge (m^3/s) for segment-scale discharge-dependent h/D_c data and (b) simulated h/D_c distributions for discharges ranging between 1.3-4500 m^3/s.

6.3 Resistance trends and fixed roughness coefficients

Separate analysis in the study segment by Wiener and Pasternack (2022) found LBE concentrations increased with stage. Together with results from this study this has ramifications toward two conventions in engineering hydraulics: (i) that reach-average resistance decreases as Q increases; and (ii) that Δ remain constant in a given domain regardless of Q. To the first point, across all study domains, higher *Q's* corresponded with increased mean h/D_c values and less positively skewed h/D_c distributions as the drowning-out of LBEs in the channel center outweighed addition of low submergence LBEs along channel margins. This translated into monotonic decreases in reach-scale resistance based on the common equations referenced in section Text S6.4 (Figure S12b). These decreases are partly a result of the underlying assumptions of these equations, which may be ill-specified for very low submergence conditions ($h/D_c<1$). For instance, at low stages, river flows diverge around emergent LBEs forming multiple flow paths (Reid & Hickman, 2008). Drag forces from LBEs are also drastically reduced when $h/D_c<0.5$ due to slower flow velocities and reduced frontal-area exposure (Lamb & Brun, 2017). As stage increases and LBEs become fully submerged, drag forces increase and momentum is extracted throughout the flow depth. The hydraulic efficiency and reduced momentum loss from LBEs at low stage support theory that resistance may initially increase as LBEs become fully submerged (Reid & Hickman, 2008; Cassan et al., 2017). As stage continues to rises and LBEs become further submerged, drag forces tend to stay relatively constant, but the portion of the velocity profile influenced by LBEs shrinks (Lamb & Brun, 2017). Thus, while drag forces may be large, the effect on mean velocity and total Q often becomes negligible and a decrease or leveling off of resistance occurs (Lamb & Brun, 2017). This leveling off of resistance in main channel may be partly offset by new emergent LBEs along channel margins.

Study segment hydrodynamic simulation found an increasingly prominent and longitudinally connected central-core of high velocity flow became established at high discharges. This core was surrounded by regions with lower velocities often forming recirculating zones along the channel periphery. The separation of the flow-field in this manner mirrors expected changes in resistance described above based on observed h/D_c conditions (Table 3; Table S5). Namely, that as main channel LBEs became deeply submerged their resistance contribution became less impactful to velocities in the channel center, simultaneous with the central portion of the channel becoming progressively decoupled from resistance contributed from LBEs along channel margins. Though not depicted the relative submergence data could be useful in identifying locations where this hydraulic tendency would occur and potentially locations with very large roughness elements where it would not occur. Ultimately, the manner in which variable conditions at LBEs distributed throughout a channel interact to influence average resistance remains a challenge and findings of this study illustrate the importance of considering spatial variability in channel morphology and hydraulics (Hodge & Hoey, 2016).

On the second point regarding fixed Δ values, while changes in discharge-dependent D_c values were subtle (Figures S6, S7, and S9), they would be ignored by a constant *Δ*, suggesting scrutiny of this common practice is required (Ferguson et al., 2019). Aberle et al. (2010) also found statistical moments of bed elevations (i.e., standard deviation, skewness and kurtosis) to depend on *Q* in a low-gradient, sand-bedded river and Yochum et al. (2104) confirmed the same in several high-gradient coarse-bedded rivers. Using mean D_c values or another representative D_c percentile appears to be the simplest alternative for specifying discharge-dependent variable roughness. Isolating distributions of D_c values in incremental inundation corridors (Figure S8) may also provide a sensible method for parameterizing spatially variable roughness lengths scales along different portions of the channel margins such as proposed by Ferguson et al. (2019). Interestingly, mean D_c values decreased slightly at higher *Q's* in all study domains, which could be an indication of reduced roughness. However, we posit that higher LBE concentrations along channel margins along with unaccounted sources of roughness and resistance provide the means for spatially averaged resistance to increase, remain constant, or only minimally decrease with *Q*, a topic that remains the focus of continued study (Abu-Aly et al., 2014; Cassan et al., 2017; Ferguson et al., 2019).

7 Conclusions

To our knowledge this is the first time complete distributions of h/D_c values have been presented and studied for a natural boulder-bedded river. In doing so we were able to document discharge-dependent h/D_c distributions at multiple spatial scale, address hypotheses regarding h/D_c behavior, and discuss the hydraulic and geomorphic implications of study results and accounting for h/D_c distributions more generally. Through fitting and statistical analysis of discharge-dependent h/D_c datasets we confirmed segment- and reach-scale data exhibited similar general statistical properties (i.e. positive skewness), were able to be drawn from the same type of distribution, but also varied between spatial domains and across discharges. LBE height distributions were also all found to be positively skewed, highlighting the non-Gaussian nature of this property which has implications for how bed roughness is characterized. Dynamism of LBE heights, albeit only slight across discharges calls into question the practice of holding roughness coefficients constant, and highlights the need to uniquely represent this property across discharge conditions. Comparing solutions of four common hydraulic resistance equations found resistance estimates incorporating complete h/D_c distributions had higher resistance than those based on more standard singular h/D_{84} estimates, the latter of which has often been criticized for issues of underestimation. While untested, greater accounting in resistance equations of discharge-dependent relative submergence over larger portions of the riverbed could be relevant toward improved resistance estimation and help collapse scatter in existing h/Δ-channel resistance relationships (Schneider et al., 2015; Monsalve & Yager, 2017).

A key aspect of this study was analyzing the evolution of h/D_c between discharges. Results confirmed changes in study segment h/D_c distributions were predominately as hypothesized, such that in each domain variance in h/D_c values increased and central tendencies either increased or remained relatively constant over the series of tested discharges. Further analysis of these changes against six plausible evolutional Styles revealed statistical and parametric properties of study segment h/D_c distributions evolved consistently between discharges, between spatial domains, thus exhibiting what we term process-based similarity (Style 4). Applying study results to simulate h/D_c values at discharges beyond those tested showed continued evolution toward uniform conditions, which supported previous findings of resistance becoming constant at high discharges. While the universality of relative-submergence stochastics presented requires further testing, the unique distributions and discharge-dependent relationships can serve as an immediate reference for studies wishing to better understand effects of h/D_c diversity on boulder-bedded rivers.

8 References

Aberle, J., Nikora, V., Henning, M., Ettmer, B., and Hentschel, B. (2010) Statistical characterization of bed roughness due to bed forms: A field study in the Elbe River at Aken, Germany. *Water Resources Research, 46*(3), W03521, doi:https://doi.org/10.1029/2008WR007406

Aberle, J., and Smart, G. M. (2003) The influence of roughness structure on flow resistance on steep slopes. *Journal of Hydraulic Research, 41*(3), 259-269. doi:10.1080/00221680309499971

Abu-Aly, T. R., Pasternack, G. B., Wyrick, J. R., Barker, R., Massa, D., and Johnson, T. (2014) Effects of LiDAR-derived, spatially distributed vegetation roughness on two-dimensional hydraulics in a gravel-cobble river at flows of 0.2 to 20 times bankfull. *Geomorphology, 206*(Supplement C), 468-482. doi:https://doi.org/10.1016/j.geomorph.2013.10.017

Adams, D. L. (2020) Toward bed state morphodynamics in gravel-bed rivers. *Progress in Physical Geography: Earth and Environment,* 44(5):700-726. doi:10.1177/0309133320900924

Adams, D. L., and Zampiron, A. (2020) Multiscalar roughness length decomposition in fluvial systems using a transform-roughness correlation (TRC) approach. *Earth Surface Dynamics*, 8(4), 1039-1051. doi: /10.5194/esurf-8-1039-2020

Baas, A. C. W. (2002) Chaos, fractals and self-organization in coastal geomorphology: simulating dune landscapes in vegetated environments. *Geomorphology, 48*(1), 309-328. doi:https://doi.org/10.1016/S0169-555X(02)00187-3

Bathurst, J.C., (1982) Flow resistance in boulder-bed streams. In: Hey, R.D., Bathurst, J.C., Thorne, C.R. (Eds.), Gravel-bed Rivers, Wiley, Chichester, pp. 443–462.

Bathurst, J. C. (1985) Flow Resistance Estimation in Mountain Rivers. *Journal of Hydraulic Engineering, 111*(4), 625-643. doi:doi:10.1061/(ASCE)0733-9429(1985)111:4(625)

Benda, L. (1990) The influence of debris flows on channels and valley floors in the Oregon Coast Range, U.S.A. *Earth Surface Processes and Landforms, 15*(5), 457-466. doi:10.1002/esp.3290150508

Branco, P., Boavida, I., Santos, J. M., Pinheiro, A., & Ferreira, M. T. (2013). Boulders as building blocks: improving habitat and river connectivity for stream fish. Ecohydrology, 6(4), 627-634. doi: 10.1002/eco.1290

Brown, R.A., and Pasternack, G. B. (2012) *Monitoring and assessment of the 2010-2011 gravel/cobble augmentation in the Englebright Dam Reach of the lower Yuba River, CA. Prepared for the U.S. Army Corps of Engineers, Sacramento District.* Retrieved from University of California at Davis, Davis, CA.: http://pasternack.ucdavis.edu/files/5313/7692/9028/EDRreport_20121215_FINAL.pdf

Brown, R. A., and Pasternack, G. B. (2014) Hydrologic and topographic variability modulate channel change in mountain rivers. *Journal of Hydrology, 510*(Supplement C), 551-564. doi:https://doi.org/10.1016/j.jhydrol.2013.12.048

Bunte, K., and Abt, S.R., (2001) Sampling surface and subsurface particle-size distributions in wadable gravel-and cobble-bed streams for analyses in sediment transport, hydraulics, and streambed monitoring. Gen. Tech. Rep. RMRS-GTR-74. Fort Collins,CO: U.S. Department of Agriculture, Forest Service, Rocky Mountain Research Station. 428 p.

Carollo, F.G., and Ferro, V. (2021) Experimental study of boulder concentration effect on flow resistance in gravel bed channels. *Catena*, 205. https://doi.org/10.1016/j.catena.2021.105458.

Cassan, L., Roux, H., and Garambois, P.A. (2017) A Semi-Analytical Model for the Hydraulic Resistance Due to Macro-Roughnesses of Varying Shapes and Densities. *Water, 9*(9), 637.

Chin, A., and Phillips, J. D. (2007) The self-organization of step-pools in mountain streams. *Geomorphology, 83*(3), 346-358. doi:https://doi.org/10.1016/j.geomorph.2006.02.021

Church, M., Hassan, M. A., and Wolcott, J. F. (1998) Stabilizing self-organized structures in gravel-bed stream channels: Field and experimental observations. *Water Resources Research, 34*(11), 3169-3179. doi:10.1029/98wr00484

Comiti, F., Cadol, D., and Wohl, E. (2009) Flow regimes, bed morphology, and flow resistance in self-formed step-pool channels. *Water Resources Research, 45*(4), W04424, doi:https://doi.org/10.1029/2008WR007259

Cooper, J. R., Aberle, J., Koll, K., and Tait, S. J. (2013) Influence of relative submergence on spatial variance and form-induced stress of gravel-bed flows. *Water Resources Research, 49*(9), 5765-5777. doi:https://doi.org/10.1002/wrcr.20464

Crowder, D. W., and Diplas, P. (2006) Applying spatial hydraulic principles to quantify stream habitat. *River Research and Applications, 22*(1), 79-89. doi:10.1002/rra.893

Eaton, B. C., and Church, M. (2009) Channel stability in bed load–dominated streams with nonerodible banks: Inferences from experiments in a sinuous flume, *J. Geophys. Res*., 114, F01024, doi:10.1029/2007JF000902.

Ely, J. C., Clark, C. D., Spagnolo, M., Hughes, A. L. C., and Stokes, C. R. (2018) Using the size and position of drumlins to understand how they grow, interact and evolve. *Earth Surface Processes and Landforms, 43*(5), 1073-1087. doi:10.1002/esp.4241

Ferguson, R. I., Hardy, R. J., and Hodge, R. A. (2019) Flow resistance and hydraulic geometry in bedrock rivers with multiple roughness length scales. *Earth Surface Processes and Landforms, 44*(12), 2437-2449. doi:10.1002/esp.4673

Ferguson, R. I., Sharma, B. P., Hardy, R. J., Hodge, R. A., and Warburton, J. (2017) Flow resistance and hydraulic geometry in contrasting reaches of a bedrock channel. *Water Resources Research, 53*(3), 2278-2293. doi:10.1002/2016WR020233

Furbish, D. J. (1987) Conditions for geometric similarity of coarse stream-bed roughness. *Mathematical Geology, 19*(4), 291-307. doi:10.1007/BF00897840

Golpira, A., Huang, F., and Baki, A. B. (2020) The Effect of Habitat Structure Boulder Spacing on Near-Bed Shear Stress and Turbulent Events in a Gravel Bed Channel. *Water*, 12(5), 1423.

Gomez, B. (1993) Roughness of stable, armored gravel beds. *Water Resources Research, 29*(11), 3631-3642. doi:10.1029/93wr01490

Gonzalez, R. L., and Pasternack, G. B. (2015) Reenvisioning cross-sectional at-a-station hydraulic geometry as spatially explicit hydraulic topography. *Geomorphology, 246*, 394-406. doi:https://doi.org/10.1016/j.geomorph.2015.06.024

Groom, J., and Friedrich, H. (2019) Spatial structure of near-bed flow properties at the grain scale. *Geomorphology, 327*, 14-27. doi:https://doi.org/10.1016/j.geomorph.2018.10.013

Held L., and Bové D. S. (2014) Frequentist Properties of the Likelihood. In: Applied Statistical Inference. Springer, Berlin, Heidelberg. https://doi.org/10.1007/978-3-642-37887-4_4

Hillier, J. K., Kougioumtzoglou, I. A., Stokes, C. R., Smith, M. J., Clark, C. D., and Spagnolo, M. S. (2016) Exploring Explanations of Subglacial

Bedform Sizes Using Statistical Models. *PLOS ONE, 11*(7), e0159489. doi:10.1371/journal.pone.0159489

Hodge, R., Brasington, J., and Richards, K. (2009) Analysing laser-scanned digital terrain models of gravel bed surfaces: linking morphology to sediment transport processes and hydraulics. *Sedimentology, 56*(7), 2024-2043. doi:10.1111/j.1365-3091.2009.01068.x

Hodge, R. A., and Hoey, T. B. (2016) A Froude-scaled model of a bedrock-alluvial channel reach: 1. Hydraulics. *Journal of Geophysical Research: Earth Surface, 121*(9), 1578-1596. doi:https://doi.org/10.1002/2015JF003706

Judd, H. E., and Peterson, D. F. (1969) Hydraulics of large bed element channels. Utah Water Research Laboratory Reports, Paper 285. https://digitalcommons.usu.edu/water_rep/285

Katul, G., Wiberg, P., Albertson, J., and Hornberger, G. (2002) A mixing layer theory for flow resistance in shallow streams. *Water Resources Research, 38*(11), 32-31-32-38. doi:https://doi.org/10.1029/2001WR000817

Kondolf, G. M., Vick, J. C., and Ramirez, T. M. (1996) Salmon Spawning Habitat Rehabilitation on the Merced River, California: An Evaluation of Project Planning and Performance. *Transactions of the American*

Fisheries Society, 125(6), 899-912. doi:10.1577/1548-8659(1996)125<0899:SSHROT>2.3.CO;2

Krishnamoorthy, K., Lee, M., and Xiao, W. (2015) Likelihood ratio tests for comparing several gamma distributions. *Environmetrics, 26*(8), 571-583. doi:10.1002/env.2357

Lacey, R. W. J., and Roy, A. G. (2008) The spatial characterization of turbulence around large roughness elements in a gravel-bed river. *Geomorphology, 102*(3), 542-553. doi:https://doi.org/10.1016/j.geomorph.2008.05.045

Lai, Y. G. (2008) *"SRH-2D version 2: Theory and User's Manual Sedimentation and River Hydraulics – Two-Dimensional River Flow Modeling".* Retrieved from U.S. Department of the Interior, Bureau of Reclamation, Technical Service Center, Sedimentation and River Hydraulics Group. Denver, Colorado.: https://www.usbr.gov/tsc/techreferences/computer%20software/models/srh2d/index.html

Lamb, M. P., and Brun, F. (2017) Direct measurements of lift and drag on shallowly submerged cobbles in steep streams: Implications for flow resistance and sediment transport, *Water Resour. Res.*, 53, 7607–7629, doi:10.1002/2017WR020883.

Langbein, W. B. (1949) Annual floods and the partial-duration flood series. *Eos, Transactions American Geophysical Union, 30*(6), 879-881. doi:https://doi.org/10.1029/TR030i006p00879

Legleiter, C. J., Roberts, D. A., Marcus, W. A., and Fonstad, M. A. (2004) Passive optical remote sensing of river channel morphology and in-stream habitat; physical basis and feasibility. *Remote Sensing of Environment, 93*(4), 493-510. doi:http://dx.doi.org/10.1016/j.rse.2004.07.019

Monsalve, A., and Yager, E. M. (2017) Bed Surface Adjustments to Spatially Variable Flow in Low Relative Submergence Regimes. *Water Resources Research, 53*(11), 9350-9367. doi:https://doi.org/10.1002/2017WR020845

Morris, H. (1959) Design methods for flow in rough channels. Proc. ASCE, Journal of Hydraulics Division, 85((HY7)), 43-62.

Nikora, V. I., Goring, D. G., and Biggs, B. J. F. (1998) On gravel-bed roughness characterization. *Water Resources Research, 34*(3), 517-527. doi:10.1029/97wr02886

Nitsche, M., Rickenmann, D., Kirchner, J. W., Turowski, J. M., and Badoux, A. (2012) Macroroughness and variations in reach-averaged flow resistance in steep mountain streams. *Water Resources Research, 48*(12), W12518, doi:10.1029/2012WR012091

Nitsche, M., Rickenmann, D., Turowski, J. M., Badoux, A., and Kirchner, J. W. (2011) Evaluation of bedload transport predictions using flow resistance equations to account for macro-roughness in steep mountain streams. *Water Resources Research, 47*(8), W08513, doi:10.1029/2011wr010645

Papanicolaou, A. N., and Tsakiris, A. G. (2017) Boulder Effects on Turbulence and Bedload Transport. In D. T. a. J. B. Laronne (Ed.), *Gravel-Bed Rivers*.

Pasternack, G. B. (2011) *2D Modeling and Ecohydraulic Analysis*. Seatle, WA: Createspace.

Pasternack, G. B., Gore, J., Wiener, J. (2021) Geomorphic covariance structure of a confined mountain river reveals landform organization stage threshold. *Earth Surface Processes and Landforms*. https://doi.org/10.1002/esp.5195.

Pastore, M., and Calcagnì, A. (2019) Measuring Distribution Similarities Between Samples: A Distribution-Free Overlapping Index. *Front. Psychol*. 10:1089. doi: 10.3389/fpsyg.2019.01089

Paternoster, R. Brame, R. Mazerolle, P., and Piquero A. (1998) Using the correct statistical test for the equality of regression coefficients. *Criminology, 36*(4), 859-866. doi:https://doi.org/10.1111/j.1745-9125.1998.tb01268.x

Phillips, J. D. (2006) Evolutionary geomorphology: thresholds and nonlinearity in landform response to environmental change, *Hydrol. Earth Syst. Sci.*, 10, 731–742, https://doi.org/10.5194/hess-10-731-2006.

Powell, D. M. (2014) Flow resistance in gravel-bed rivers: Progress in research. *Earth-Science Reviews, 136*, 301-338. doi:https://doi.org/10.1016/j.earscirev.2014.06.001

R Core Team (2021) R: A language and environment for statistical computing. R Foundation for Statistical Computing, Vienna, Austria. URL https://www.R-project.org/.

Radecki-Pawlik, A. (2002) Bankfull discharge in mountain streams: theory and practice. *Earth Surface Processes and Landforms, 27*(2), 115-123. doi:10.1002/esp.259

Reid, D.E., and Hickin, E.J. (2008) Flow resistance in steep mountain streams. *Earth Surface Processes and Landforms*, 33: 2211-2240. https://doi.org/10.1002/esp.1682

Resop, J. P., Kozarek, J. L., and Hession, W. C. (2012) Terrestrial Laser Scanning for Delineating In-stream Boulders and Quantifying Habitat Complexity Measures. *Photogrammetric Engineering and Remote Sensing, 78*(4), 363-371.

Richardson, K., and Carling., P.A. (2006) The hydraulics of a straight bedrock channel: Insights from solute dispersion studies, *Geomorphology*, 82(1–2), 98–125, doi:10.1016/j.geomorph.2005.09.022.

Rickenmann, D., and Recking, A. (2011) Evaluation of flow resistance in gravel-bed rivers through a large field data set. *Water Resources Research, 47*(7), W07538, doi:10.1029/2010wr009793

Robert, A. (1990) Boundary roughness in coarse-grained channels. *Progress in Physical Geography: Earth and Environment, 14*(1), 42-70. doi:10.1177/030913339001400103

Roni, P., Bennett, T., Morley, S., Pess, G. R., Hanson, K., Slyke, D. V., and Olmstead, P. (2006) Rehabilitation of bedrock stream channels: the effects of boulder weir placement on aquatic habitat and biota. *River Research and Applications*, *22*(9), 967-980. doi:10.1002/rra.954

Sapozhnikov, V. B., and Foufoula-Georgiou, E. (1999) Horizontal and vertical self-organization of braided rivers toward a critical state. *Water*

Resources Research, 35(3), 843-851. doi:https://doi.org/10.1029/98WR02744

Schlichting, H. (1936) Experimentelle Untersuchungen zum Rauhigkeitsproblem. *Ingenieur-Archiv, 7*(1), 1-34. doi:10.1007/BF02084166

Schneider, J. M., Rickenmann, D., Turowski, J. M., and Kirchner, J. W. (2015) Self-adjustment of stream bed roughness and flow velocity in a steep mountain channel. *Water Resources Research, 51*(10), 7838-7859. doi:10.1002/2015wr016934

Shamloo, H., Rajaratnam, N., and Katopodis, C. (2001) Hydraulics of simple habitat structures. *Journal of Hydraulic Research, 39*(4), 351-366. doi:10.1080/00221680109499840

Shobe, C. M., Tucker, G. E., and Anderson, R. S. (2016) Hillslope-derived blocks retard river incision. *Geophysical Research Letters, 43*(10), 5070-5078. doi:10.1002/2016gl069262

Sklar, L. S., Riebe, C. S., Genetti, J., Leclere, S., and Lukens, C. E. (2020) Downvalley fining of hillslope sediment in an alpine catchment: implications for downstream fining of sediment flux in mountain rivers. *Earth Surface Processes and Landforms, 45*(8), 1828-1845. doi:10.1002/esp.4849

Smith, M. W. (2014) Roughness in the Earth Sciences. *Earth-Science Reviews, 136*, 202-225. doi:https://doi.org/10.1016/j.earscirev.2014.05.016

Sornette, D. (2000) *Critical Phenomena in Natural Sciences: Chaos, Fractals, Selforganization and Disorder: Concepts and Tools*.

Strom, K. B., and Papanicolaou, A. N. (2006) Toward prediction of the spatial distribution of clusters in a watershed via geomorphic and hydraulic methods. In G. Parker and M. H. Garcia (Eds.), Paper presented at 4th IAHR symposium on river coastal and estuarine morphodynamics RCEM 2005 (pp. 119–129). Urbana, IL: Taylor and Francis.

Strom, M. A., Pasternack, G. B., and Wyrick, J. R. (2016) Reenvisioning velocity reversal as a diversity of hydraulic patch behaviours. *Hydrological Processes, 30*(13), 2348-2365. doi:10.1002/hyp.10797

Tan, L., and Curran, J. C. (2012) Comparison of Turbulent Flows over Clusters of Varying Density. *Journal of Hydraulic Engineering, 138*(12), 1031-1044. doi:doi:10.1061/(ASCE)HY.1943-7900.0000635

Thompson, C. J., Croke, J., Ogden, R., and Wallbrink, P. (2006) A morpho-statistical classification of mountain stream reach types in southeastern Australia. *Geomorphology, 81*(1), 43-65. doi:https://doi.org/10.1016/j.geomorph.2006.03.007

Valle, B. L., and Pasternack, G. B. (2006) Field mapping and digital elevation modelling of submerged and unsubmerged hydraulic jump regions in a bedrock step-pool channel. *Earth Surface Processes and Landforms, 31*(6), 646-664. doi:10.1002/esp.1293

van der Mark, C. F., Blom, A., and Hulscher, S. J. M. H. (2008) Quantification of variability in bedform geometry. *Journal of Geophysical Research: Earth Surface, 113*(F3). doi:10.1029/2007jf000940

Venditti, J.G., Nelson, P.A., Bradley, R.W., Haught, D., and Gitto, A.B. (2017). Bedforms, Structures, Patches, and Sediment Supply in Gravel-Bed Rivers. In Gravel-Bed Rivers (eds D. Tsutsumi and J.B. Laronne). https://doi.org/10.1002/9781118971437.ch16

Wiener, J. S., and Pasternack, G. B. (2019) Diversity and organization of mountain river morphological units challenge conceptions of riffle-pool, step-pool, and cascade channel types. Abstract EP51E-2129 presented at 2019 Fall Meeting, AGU, San Francisco, CA, 9-13 Dec.

Wiener, J. S., and Pasternack, G. B. (2022) Scale dependent spatial structuring of mountain river large bed elements maximizes flow resistance. *Geomorphology, 416*(1). doi:https://doi.org/10.1016/j.geomorph.2022.108431

Wittenberg, L., and Newson, M. D. (2005) Particle clusters in gravel-bed rivers: an experimental morphological approach to bed material transport and stability concepts. *Earth Surface Processes and Landforms, 30*(11), 1351-1368. doi:10.1002/esp.1184

Wohl, E., and Merritt, D. M. (2008) Reach-scale channel geometry of mountain streams. *Geomorphology, 93*(3), 168-185. doi:https://doi.org/10.1016/j.geomorph.2007.02.014

Wolman, M. G. (1954) A method of sampling coarse river-bed material. *Eos, Transactions American Geophysical Union, 35*(6), 951-956. doi:https://doi.org/10.1029/TR035i006p00951

Wyrick, J. R., and Pasternack, G. B. (2014) Geospatial organization of fluvial landforms in a gravel–cobble river: Beyond the riffle–pool couplet. Geomorphology, 213(Supplement C), 48-65. doi:https://doi.org/10.1016/j.geomorph.2013.12.040

Yager, E. M., Kirchner, J. W., and Dietrich, W. E. (2007) Calculating bed load transport in steep boulder bed channels. *Water Resources Research, 43*(7). doi:10.1029/2006wr005432

Yen, B. C. (2002) Open channel flow resistance. Journal of hydraulic engineering, 128(1), 20-39. doi: 10.1061/(ASCE)0733-9429(2002)128:1(20)

Yuba County Water Agency (YCWA) (2013) *Technncal Memorandum 1-1. Channel Morphology Upstream of Englebright Reservoir. Yuba River Development Project FERC Project No. 2246.* Retrieved from http://www.ycwa-relicensing.com/Technical%20Memoranda/Forms/AllItems.aspx

Yochum, S. E., Bledsoe, B. P., David, G. C. L., and Wohl, E. (2012) Velocity prediction in high-gradient channels. *Journal of Hydrology, 424-425*, 84-98. doi:https://doi.org/10.1016/j.jhydrol.2011.12.031

Yochum, S. E., Bledsoe, B. P., Wohl, E., and David, G. C. L. (2014) Spatial characterization of roughness elements in high-gradient channels of the Fraser Experimental Forest, Colorado, USA, *Water Resour. Res.*, 50, doi:10.1002/2014WR015587.

9 Supplementary Materials File

Supporting Information for
‘Process-based similarity’ revealed by discharge-dependent relative submergence dynamics of thousands of large bed elements

Contents of this file

Text S1 to S6

Figures S1 to S13

Tables S1 and S5

This document provide supplemental materials and it is organized using the same headings as the main article to help make it easier for readers to find what they are interested in knowing more about. Subject headings followed by the word “none” indicate no supplemental information is provided for that section.

1 Introduction

1.1 Bed roughness, flow resistance, and relative submergence

In reviewing the scientific literature, we found that it is very common that authors refer to a diameter when presenting the formal definition of relative submergence, but then if the objects they are investigating are not individual particles, then they substitute another metric in for diameter. Another interesting example is the case of the classic study of Judd and Peterson (1969) in which they define a large bed element “k” value as “roughness or bed element height or diameter”. This approach to the definition creates flexibility so that one can decide which is the appropriate length scale depending on the nature of the object. In other articles, we found that people used a variety of height scales, such as average particle-cluster height and bedform amplitude as the denominator in the relative submergence equation, so not strictly using an individual particle diameter (e.g., Strom &Papanicolaou, 2006; Wohl & Merritt, 2008). In studies of alluvial sediment, even boulders, when talking about the relative submergence of an entire bed, the characteristic metric was D_{84}. Overall, people can use a variety of terminology ranging from directly defining submergence with a specific length scale or providing a textbook definition of the variable using D_c and then defining some metric as counting as D_c. Both ways are in the literature. We chose to follow those who do it the latter way, which seems acceptable and standard.

1.2 LBE submergence effects

None.

2 Styles of LBE relative submergence response to discharge

As stated in the article, the evolution of river channel h/D_c distributions from one discharge to another involves: (i) depth changes at previously wetted LBEs result in a new distribution of h/D_c values at just these LBEs; and (ii) new LBEs become wetted along the expanding channel margin (i.e. the incremental inundation corridor [IIC]) and their distribution is convolved with the new distribution of previously wetted LBEs. The assumption for this study is that h/D_c values at newly wetted LBEs would be relatively low compared to the set of previously wetted LBE and depth at most previously wetted LBEs would increase with increasing discharge. Both assumptions are realistic for partly-confined to confined rivers, but may not always be the case. For each change in discharge the two processes described above occur in tandem to form each unique set of discharged-dependent h/D_c values. Examples of how these processes could result in the conceptualized Style 2 and Style 3 conditions are described in the article and graphically depicted in Figure S1.

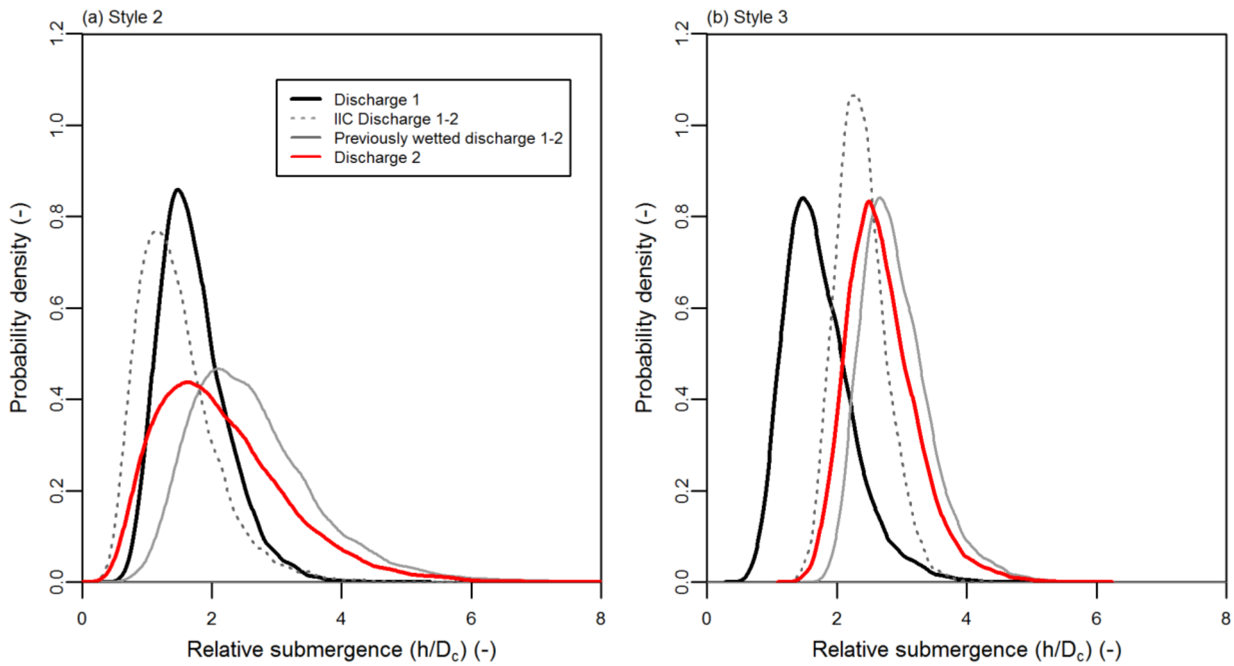

Figure S1. Conceptual illustration showing how a h/D_c distribution at an initial discharge (solid dark line) can evolve to a new h/D_c distribution at a second discharge (solid red line) through combination of the new h/D_c distribution of previously wetted LBEs (solid gray line) and the incremental inundation corridor h/D_c distribution (dashed gray line) that result in conditions conceptualized in (a) Style 2 and (b) Style (3).

3 Study river segment

The longitudinal profile of the river is shown in Figure S2. When delineating reaches in a steep mountain river on the basis of bed slope, the exact slope break position is complicated by the presence of tall steps that can create an apparent reach break, but we do not consider a step itself to be a slope break- a step is usually internal to a reach, especially when the reach has many steps. Care was used to factor in the effects of the exact relative longitudinal position of each potential slope break along the continuum of pool trough to riffle crest on the piecewise bed-elevation regression lines. It is important to start and end the reach at the same relative position along a periodic low-frequency, high-amplitude undulation, but in some cases with steps it can be impossible to achieve that ideal.

Another critical factor to be aware of in deciding where to put a slope break is the difference between (a) the general downstream decrease in gradient typical of a concave up mountain-scale river bed longitudinal profile and (b) a non-trending, low-frequency, high-amplitude bed undulation. For the former phenomenon, there is no objective way to decide where to put a slope break along a curve and how many to use. We chose to be parsimonious with fewer breaks, such as in reach 4 where a different expert could have chosen two reaches with slopes of 1.8 and 2.6% instead of a single reach with 2.3%. A factor in our decision at this location is that the apparent position of the additional slope break was located at the tail of a large pool, which made it seem more of a local phenomenon driving an apparent change than a wise place for a slope break at the scale of the mountain's concave up profile, but another expert could view it differently.

For the latter phenomenon (b), some people may choose to break a low-frequency, high-amplitude bed undulation into several discrete pieces on the interpretation that each section of the periodic pattern is caused by a different mechanism. Others may view the whole of it as a single periodic undulation functioning as one coherent unit. For the purposes of this study, we wanted to have a parsimonious set of reaches, so we chose the latter way of thinking, thereby not breaking a single low-frequency undulation into several shorter intervals. For example, we interpreted reach 2 as a single high-amplitude bed undulation on the basis of visualizing the detrended longitudinal profile and inspecting the aerial imagery. Others could choose to break it up into 3 or 4 discrete reaches. We saw no morphodynamic or other process-based reason to do that, rather viewing the reach as a continuous low-frequency, high-amplitude bed undulation.

Procedurally, the easiest-to-delineate breaks along the mountain's concave-up gradient were set first. Then, more difficult ones in low-frequency, high-amplitude bed undulations were evaluated, as well considering the effect of tall steps. Many potential slope breaks were checked by making regression lines to see how they would affect the outcome. As a final check, the detrended longitudinal profile was created and inspected, and the relative amplitude of bed undulation between two adjacent reaches was used to help decide if a given slope break position was in the best position. We view the final set of six reaches as serving the main purpose of this study, which is to have areas with significantly contrasting geomorphic settings within which to evaluate the study hypotheses and see if outcomes differ.

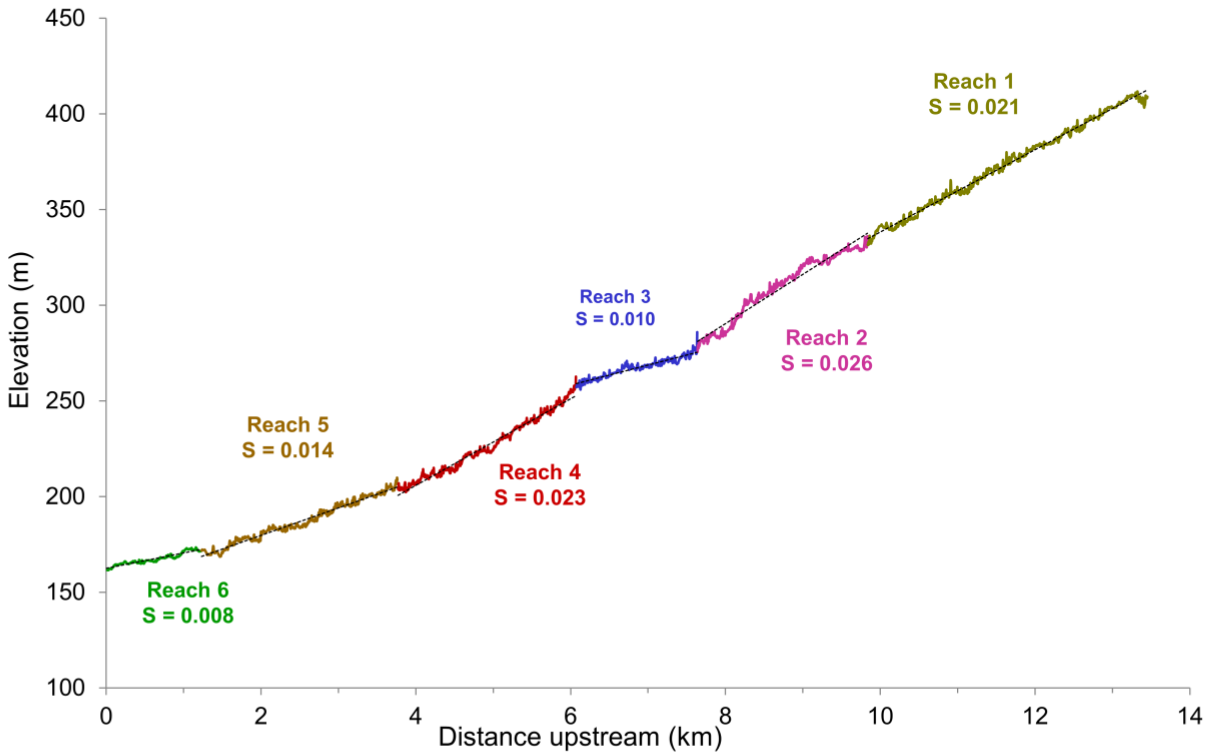

Figure S2. Longitudinal profile showing the extent and slope (m/m) of geomorphic reaches

4 Methods

4.1 Topo-bathymetric and LBE mapping

Between September 27-29, 2014 Airborne Light Detection and Ranging (LiDAR) data were collected within the study segment by a professional surveying firm (Quantum Spatial, https://www.quantumspatial.com/) using a Riegl VQ-820-G bathymetric sensor system and a Leica ALS50 Phase II system (near infrared) mounted in a Cessna Grand Caravan.

The LBE mapping of Wiener and Pasternack (2022) does not differentiate boulders from bedrock outcrops or fully decouple individual boulders from boulder clusters. Therefore, at times, clusters are represented as individual polygons. Performance assessment by Wiener and

Pasternack (2022) using four performance metrics common to classification (producers accuracy, producers overlap, a modified Jaccard similarity index and missed-to-excess ratio) found LBE mapping performance comparable to or better than forestry benchmarks for mapping tree crowns, the best available proxy.

4.2 Two-dimensional hydrodynamic modeling

The decision to use 2D modeling represented a compromise between performance and accuracy compared to simpler 1D models and more complex 3D modeling (Benjankar et al., 2015). Depth predictions were assessed using two tests and a suite of standard model performance metrics (Pasternack, 2011; Moriasi et al., 2007). First, deviations between observed and predicted water-surface elevations (WSEs) were assessed at 147,644 discrete point locations distributed throughout the 13.2-km domain. Observed WSE measurements were obtained as part of LiDAR data collection. Discharge during the period of LiDAR collection was estimated at 1.19 m^3/s. Simulation of this discharge was used to generate the set of predicted WSE values at the observation locations. Mean absolute deviation between LiDAR-measured and model-predicted WSE was 0.162 m. Second, depth measurements made at 61 independent locations with a standard wading rod during a period of discharge of 3.51 m^3/s were compared to collocated model predictions for this same flow. Among hydrologist-preferred metrics, depth predictions significantly outperformed standards for Nash-Sutcliffe efficiency, percent bias, and the root mean square error-observations standard deviation ratio. Overall, the 2D model met relevant modeling standards and performed comparably to similar models from published articles (Lisle et al., 2000; Pasternack et al., 2006).

4.3 Relative submergence calculations

Choice of maximum height as a metric for Dc

Our approach to identifying a D_c metric was to use the maximum RSM height of each LBE, per Figure 5 of the article. Use of the term D_c is for consistency with existing studies with acknowledgement that max RSM values and field measured D_c values at LBEs are likely to differ. Uncertainty in D_c estimates was not explicitly quantified, but is assumed to be of the same order of uncertainty inherent in all methods for quantifying bed roughness, especially those reliant on remotely sensed data (Bunte & Abt, 2001; Aberle & Smart, 2003; Hodge & Hoey, 2016).

Interestingly, upon conducting a literature review specifically on this point, we found that Judd and Peterson (1969) used the same definition, including finding the maximum height of an LBE and using that as the roughness height (k), as shown below in the partial clip of Figure 2 of Judd and Peterson (1969):

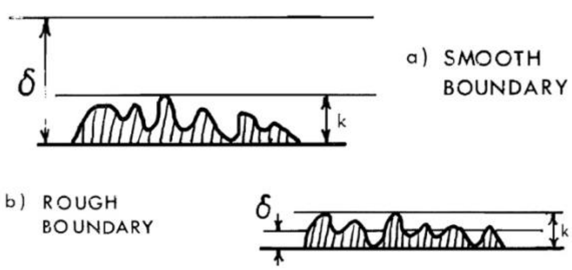

If you think about it, for a single sphere sitting on a table, the diameter is by definition the maximum height of the sphere. In this sense, the two concepts perfectly match. Further, studies that compute the relative submergence of bedforms were found to use the amplitude from trough to crest, which is also the maximum possible height. As another thought exercise, if you seek to measure your own height as a human being, height is defined as the maximum height. The only time that the maximum possible height is not used in relative submerge literature is when the object is not singular, but is an area, in which case D_{50} or D_{84} of the surficial riverbed sediment grain size distribution are used- for boulder-bedded streams it is usually D_{84}. However, this study is not making an area property, it's identifying the height of individual objects, so maximum object height is its height.

Despite this perspective, in the original submission we did not stop there with this assumption. We went on to run four different relative submergence calculations and do hypothesis testing with a variety of alternatives to see if there would be any effect of choosing a different way of estimating D_c. From those we found that the most conservative alternative (i.e., yielding the lowest D_c and highest h/D_c) involved using the average RSM value within each LBE in place of the maximum value. This value would be lower than a D_{84} area property. We also explained that this could be informative if LBEs have complex shapes that are poorly represented by a single maximum height. When we carried through the hypothesis testing with the alternative relative submergence values, we got the same outcomes, though the exact values of h/D_c were higher due to the presence of smaller D_c values. Thus, the main scientific experimental design and results were resilient to changes in the exact way of obtaining D_c.

Testing of alternative metrics for h/D_c

In physical experiments and natural environments, the manner in which h and D_c are estimated varies widely, often involving spatial averaging or back-calculation of depths (Bathurst, 1985; Ferguson et al., 2017) and uncertainty about the bed-level datum from which to measure D_c (Aberle & Smart, 2003). The calculations described in the main article provide reasonable proxies for field-based measurements of h and D_c that would otherwise be impossible to obtain under the range of simulated conditions for the number of LBEs considered in this study. Relative submergence calculations are not without potential issues and uncertainty, thus one alternative method for calculating h as well as an alternative method for D_c at each LBE were explored.

The alternative h metric, $\hat{h}$, was calculated as the maximum depth near each LBE according to:

$$\hat{h} = \max\{(h_i + RSM_i), (h_j + RSM_j)\} \in i\,\{1{:}\,q\}, j\{1{:}\,r\} \qquad \text{(EQ.1)}$$

The alternate to D_c was to use the average RSM value within each LBE ($\bar{D}$).

The alternative grain size metric, $\bar{D}$, could be informative if LBEs have complex shapes that are poorly represented by a single maximum height. For reference, a perfect hemisphere would have $\bar{D} = \frac{2}{3} D_c$. If area was held equal, a wider spheroid would have a $\bar{D}$ that was a larger percentage of D_c, a taller spheroid would have a $\bar{D}$ that was a smaller percentage of D_c, and a cube or rectangle would have $\bar{D} = D_c$. Most of the predicted LBEs, resembled hemispherical to hemispheroidal objects such that 71 percent were in the range of $0.25D_c < \bar{D} < 0.75D_c$ (Wiener & Pasternack, 2022). Therefore, $\bar{D}$ is generally less than D_c for LBEs in the study segment. The alternative depth metric, $\hat{h}$, is always less than or equal to h. Using the two particle size metrics (D_c and $\bar{D}$) and two measures for depth (h and $\hat{h}$), four relative submergence values were calculated for each LBE for each discharge reflecting sensible upper and lower bounds for each LBE for comparison.

4.4 LBE relative submergence general hypothesis testing

To spatially stratify LBEs within multiple discharge-dependent portions of the river corridor, LBE data were subset into five groups comprising the set of LBE polygons that intersected with each simulated discharge's wetted area polygon. LBE polygons that only partially intersected a wetted area polygon or only intersected the wetted area along their border were included in a group's set of LBEs. This allowed bank attached LBEs to be included in each subset as long as they were partially inundated. These subsets are referred to as 'discharge-dependent LBEs'. In this manner, discharge served to hierarchically nest spatial domains, because lower discharge wetted areas were always located within higher discharge wetted areas. Thus, discharge is often used in the context of a spatial reference throughout this study.

Answering study questions required obtaining 39 h/D_c distributions to represent different spatial domains for a range of discharges. The first 35 consisted of seven spatial domains (entire river segment plus the six reaches), each spatially mapped using the 2D model's wetted area, and this was done for five specified discharges. An additional four segment-scale datasets were generated for LBEs within the portions of the channel that became inundated between discharges, (i.e., incremental inundation corridor) (Figure 6 in the article). Incremental inundation corridor polygons are made by erasing a lower discharge's wetted area from the next higher discharge's wetted area (Wiener & Pasternack, 2022). This domain isolates analysis to the series of nested, non-overlapping portions of the river corridor that become successively inundated and geomorphically active with increasing discharge, and addresses how h/D_c distributions vary among just these discharge-dependent river margins.

Statistical properties of all 39 h/D_c distributions were calculated using the R programming language and included the arithmetic mean [$\bar{x}$], standard deviation [σ], mode [φ], coefficient of skewness [g], and coefficient of kurtosis [β_2] (R Core Team, 2021). Both g and β_2 were calculated using the 'EnvStat' package (Millard, 2013**)**. Modal values were calculated from frequency histograms using the midpoint of the bin with the highest count. The number of bins for each dataset followed the approach of Freedman and Diaconis, (1981) (Table S1).

Table S1. Segment- and reach-scale h/D_c histogram bin-widths (m) used for modal calculations.

Discharge (m^3/s)	Spatial Domain						
	Segment	Reach 1	Reach 2	Reach 3	Reach 4	Reach 5	Reach 6
1.54	0.05	0.1	0.05	0.1	0.05	0.05	0.1
10.73	0.05	0.1	0.1	0.1	0.1	0.1	0.1
82.12	0.1	0.2	0.2	0.5	0.2	0.2	0.5
343.6	0.2	0.5	0.5	0.5	0.5	0.5	0.5
1184.6	0.5	1	1	1	0.5	1	1

4.5 LBE discharge-dependent style hypothesis testing

Six conceptual discharge-dependent h/D_c distribution behavior styles were presented in the article (Section 1.2), additional details on hypothesis testing for Styles 2-4 not described in the article are presented below.

As discussed in the article an initial requirement of all hypothesized Styles was that h/Dc distributions were from the same distribution type. Thus, in the first step toward h/D_c distribution Style hypothesis testing, data were fit with several parametric distributions (i.e. Normal, Log-normal, Weibull, Exponential, and Gamma) using maximum likelihood and method of moment estimators. All fitting was conducted using the 'fitdistrplus' R package (Delignette-Muller & Dutang, 2015). These distributions are common amongst natural phenomena and have been found to accurately describe the size, shape, or spacing of sedimentological and morphological attributes of fluvial bedforms (Van der Mark et al., 2008; Singh et al., 2012), submarine turbidites (Rothman et al., 1994), and other Earth surface landforms (Ely et al., 2018).

Fitted h/D_c distributions were evaluated on the basis of whether they were best fit by the same type of distribution within (i.e. between discharge-dependent datasets in the same domain) and between spatial domains. Fits were compared using negative, log-likelihood values to select the best-fitting distribution for each dataset. Selected distributions were then evaluated with non-parametric or distribution-appropriate parametric goodness-of-fit tests (i.e. Anderson-Darling, Kolmogorov-Smirnov, and/or Shapiro-Wilk tests).

All distribution goodness-of-fit testing was done in R code using a permutation based approach, whereby a random set of 500 values was selected from each dataset for use in each test. This process was repeated 500 time for each test. Fit was considered good if the arithmetic mean of p values from the set of 500 tests was > 0.05. The corrected Anderson-Darling test was performed using the 'ad.test' function from the Goftest package (Faraway et al., 2019**)**. Additional test results not reported directly in the article are presented below.

If distributions in a given segment- and/or reach-scale domain were all of the same type, h/D_c behavior was tested relative to hypothesized Styles. As discussed in the article, statistical properties of h/D_c data (e.g. $\bar{x}$, σ, φ, g, and β_2) were compared within domains either qualitatively, or using non-parametric or appropriate parametric statistical tests. Comparison of φ, g, and, β_2 values was done qualitatively, simply comparing relative magnitudes and trends of how values changed between datasets. Comparison of $\bar{x}$ and σ values between datasets was done using Welch's t-test and F-test, respectively, for normally distributed h/D_c datasets and with the

Mann-Whitney U and Levene's tests, respectively, for non-normally distributed h/D_c datasets (R Core Team, 2021; Fox & Weisberg, 2019). Normality was assessed based on the best fitting distribution for each dataset. The above analyses were extended to multiple spatial domains for each of those best fit by the same distribution type, whereby fitting parameters and statistical properties were compared between all relevant datasets.

Acceptance of the Style 1 hypothesis required statistical equivalency of all discharge-dependent h/D_c dataset properties within a given domain (i.e. distribution type, fitting parameters, and statistical properties), thus indicting that mechanisms, such as those hypothesized in Section 2 of the article that conserve h/D_c distribution scaling were present. Presence of statistical self-similarity across multiple domains would support even greater invariance of h/D_c distributions in the study segment. Acceptance of Style 2 in a given domain was based on central tendency being statistically equivalent between all discharge-dependent datasets and having to reject that variances were equal. Contrarily, Style 2 was rejected if central tendencies were not statistically equivalent between discharge-dependent datasets or any variances were statistically equivalent between datasets. Acceptance of Style 3 required variance to be statistically equivalent and rejecting that central tendencies were equal between datasets in a given domain. Style 3 was rejected if either of these criteria were not upheld.

Unlike Styles 1, 2, and 3, acceptance of Style 4 was based on statistical similarity in how discharge-dependent h/D_c distributions changed between domains. Style 4 testing first required that both central tendency and variance were not equivalent between discharge-dependent h/D_c datasets within compared domains (i.e. rejection of all previous Styles). To determine the rate that parametric and statistical properties changed between discharges statistical models were fit for each domain using discharge as a dependent variable and h/D_c dataset properties (i.e. $\bar{x}$, σ, φ, g, β_2, and Θ values, where Θ is a placeholder for distribution parameters) as independent variables. A positive test for Style 4 was based on two criteria: (i) data were reasonably fit (F-test, $p<0.05$) by the same type of model (e.g. linear, power-law, etc.); and (ii) statistical equivalency of modeled slopes between domains. Slope comparison was conducted using the approach of Paternoster et al. (1998) by employing a test statistic computed according to their equation 4 as follows:

$$Z = \frac{b_1 - b_2}{\sqrt{SEb_1^2 + SEb_2^2}} \qquad \text{(EQ. S2)}$$

where b_1 and b_2 are regression slopes for the models being compared, SEb_1 and SEb_2 are standard errors of the regression slopes from the respective models, and Z is a test statistic that follows a *t*-distribution with degrees of freedom $(n_1 + n_2 - 4)$ with n_1 and n_2 equal to the number of samples in each dataset.

Notably, while comparing the rate of change of all dataset properties could be of general interest, the expectation that all properties would evolve at similar rates is not necessarily appropriate. For example, let us presume h/D_c distributions are positively skewed and leptokurtic, and thus may be reasonably modeled as having log-normal distributions. Applying the following system of discharge-specific linear scaling relationships:

$$\begin{aligned} F\left(\frac{h}{D_{c_{i+1,j}}}\right) &= \lambda_i \cdot F\left(\frac{h}{D_{c_{i,j}}}\right) + C_i \\ F\left(\frac{h}{D_{c_{i+1,j+1}}}\right) &= \lambda_i \cdot F\left(\frac{h}{D_{c_{i,j+1}}}\right) + C_i \end{aligned} \qquad \text{(EQ.S3)}$$

where F() is the frequency distribution of h/D_c values, *i* is and index for discharge, *j* is an index for domain, λ is a unique scalar for each discharge, and C is a unique constant for each discharge by definition only $\bar{x}$, σ, μ, and σ_{ln} would have equivalent discharge-dependent slopes between domains, where μ and σ_{ln} are the first and second parameters of the log-normal distribution estimated according to maximum likelihood, respectively. Values for *g*, and β_2 would be constant across discharges (i.e. zero slope for all domains) and non-linear scaling of φ values result in non-equivalent slopes between domains. While these between domain variable relationships are specific for log-normally distributed data, they remain true for several other distributions including Gamma distributed data. Scaling relationship in EQ. 3 are much simpler than the complex convolution of previously wetted and newly wetted LBE h/D_c values that occur between discharges, but provide a basis for the Style 4 acceptance criteria that only $\bar{x}$, σ, and distribution parameters would have equivalent discharge-dependent slopes between domains.

5 Results

5.1 Hypothesis 1 and 2 results

Table S2. Segment- and reach-scale h/D_c dataset statistical properties.

Discharge (m^3/s)	Spatial Domain							Reach-scale CV†
	Segment	Reach 1	Reach 2	Reach 3	Reach 4	Reach 5	Reach 6	
$\bar{x}$ (-)								
1.54	0.73	0.82	0.68	0.75	0.70	0.70	0.67	0.08
10.73	1.02	1.18	0.96	1.04	0.95	0.96	0.89	0.10
82.12	1.97	2.22	1.85	2.09	1.79	1.94	1.69	0.10
343.6	3.63	4.00	3.37	3.90	3.26	3.71	3.48	0.08
1184.6	6.78	7.17	6.33	7.06	6.22	6.93	7.99	0.09
s (-)								
1.54	0.53	0.69	0.44	0.58	0.44	0.44	0.29	0.29

Discharge (m^3/s)	Spatial Domain							Reach-scale CV†
	Segment	Reach 1	Reach 2	Reach 3	Reach 4	Reach 5	Reach 6	
10.73	0.81	1.04	0.71	0.84	0.67	0.65	0.41	0.29
82.12	1.67	1.99	1.58	1.76	1.41	1.55	1.03	0.21
343.6	3.15	3.54	3.01	3.49	2.63	3.16	2.11	0.18
1184.6	5.66	6.27	5.46	6.18	4.88	5.93	4.64	0.12
φ (-)								
1.54	0.53	0.55	0.53	0.55	0.53	0.73	0.75	0.17
10.73	0.68	0.55	0.65	0.45	0.65	0.75	0.85	0.22
82.12	0.85	0.70	0.70	0.75	0.70	0.70	0.75	0.04
343.6	0.70	0.75	0.75	0.75	0.75	0.75	3.25	0.87
1184.6	0.75	1.50	1.50	1.50	0.75	0.50	5.50	0.98
g (-)								
1.54	3.98	3.94	2.39	4.08	2.90	3.30	2.84	0.20
10.73	2.85	2.62	2.18	2.84	2.71	2.27	2.62	0.10
82.12	1.73	1.62	1.75	1.67	1.70	1.38	1.08	0.17
343.6	1.39	1.30	1.54	1.38	1.31	1.16	0.65	0.25
1184.6	1.24	1.22	1.37	1.40	1.07	1.13	0.26	0.39
β_2 (-)								
1.54	37.52	33.18	14.29	33.30	21.76	27.31	25.69	0.28
10.73	18.74	15.27	10.90	17.81	17.42	14.14	22.98	0.25
82.12	7.30	6.39	6.98	7.06	7.47	5.23	5.71	0.13
343.6	5.15	4.59	5.76	5.12	4.96	3.99	3.42	0.18
1184.6	1.50	1.16	2.02	2.14	0.96	0.80	-0.47	0.86
α (-)								
1.54	2.53	2.05	2.75	2.30	2.93	2.92	5.75	0.43
10.73	2.05	1.65	2.09	1.95	2.52	2.33	4.72	0.44
82.12	1.53	1.33	1.55	1.48	1.77	1.58	2.51	0.25
343.6	1.31	1.22	1.31	1.21	1.50	1.28	2.16	0.25
1184.6	1.32	1.21	1.33	1.30	1.49	1.24	2.58	0.34
β (-)								
1.54	3.45	2.49	4.02	3.08	4.19	4.19	8.56	0.48
10.73	2.00	1.39	2.18	1.87	2.66	2.44	5.29	0.52
82.12	0.78	0.60	0.84	0.71	0.99	0.81	1.48	0.34
343.6	0.36	0.30	0.39	0.31	0.46	0.34	0.62	0.30
1184.6	0.19	0.17	0.21	0.18	0.24	0.18	0.32	0.26

†Coefficient of variation (CV) calculated as ratio of standard deviation and mean of reach-scale values.

Table S3. Incremental inundation corridor h/D_c dataset statistics.

Discharge (m^3/s)	Value
$\bar{x}$ (-)	
1.54-10.73	0.75
10.73-82.12	1.14
82.12-343.6	1.55
343.6-1184.6	2.28
σ (-)	
1.54-10.73	0.33
10.73-82.12	0.70
82.12-343.6	1.14
343.6-1184.6	2.07
φ (-)	
1.54-10.73	0.63
10.73-82.12	0.75
82.12-343.6	0.75
343.6-1184.6	0.90
g (-)	
1.54-10.73	1.45
10.73-82.12	1.84
82.12-343.6	1.84
343.6-1184.6	1.64
β_2 (-)	
1.54-10.73	3.86
10.73-82.12	4.54
82.12-343.6	4.22
343.6-1184.6	2.79
μ (-)	
1.54-10.73	-0.26
10.73-82.12	-0.37
82.12-343.6	-0.03
343.6-1184.6	0.22
σ_{ln} (-)	
1.54-10.73	0.48
10.73-82.12	0.42
82.12-343.6	0.55
343.6-1184.6	0.64

5.2 Hypothesis 3 results

Goodness-of-fit testing

As discussed in section 5.2 of the article, distribution fitting found four of five segment-scale h/D_c datasets to be best fit by two-parameter Gamma distributions, and one best fit by a Weibull distribution (LBEs associated with the 1184.6 m^3/s wetted area). This was supported by the Anderson-Darling goodness-of-fit test applied with Braun's (1980) correction to account for parameters being estimated from the data (Faraway et al., 2019), which concluded it was not possible to reject that the 1.54-343.6 m^3/s datasets were drawn from Gamma distributions and the 1184.6 m^3/s dataset from a Weibull distribution at the 95% confidence level (p >>0.05). This test also supported that it was not possible to reject that the 1184.6 m^3/s dataset could be drawn from a Gamma distribution.

As discussed in the article, 24 of 30 reach-scale datasets were best fit by two-parameter Gamma distributions, and six were best fit by Weibull distributions (Figure S3). Goodness-of-fit testing confirmed it was not possible to reject these data were drawn from the aforementioned distributions above the 95% confidence level (corrected Anderson-Darling test; p >>0.05) and also supported it was not possible to reject that all datasets could be drawn from Gamma distributions at the 95% confidence level.

Notably, the two-parameter Gamma distribution is parameterized by a shape parameter (α) and an inverse scale or rate (β) parameter with probability density function for random variable x:

$$f(x;\alpha,\beta) = \frac{\beta^\alpha}{\Gamma(\alpha)} x^{\alpha-1} e^{-\beta x} \quad for\ x > 0 \mid \alpha,\beta > 0 \qquad \text{(EQ. S4)}$$

where Γ() is the Gamma function. Equivalent α values but different β's correspond to distributions with similar overall shapes that scale such that the ratio of variances (σ^2) are roughly proportional to the ratio of squared β values ($\frac{\sigma_1^2}{\sigma_2^2} \approx \frac{\beta_1^2}{\beta_2^2}$) and the ratio of mean ($\overline{x}$) and modal (φ) values are roughly proportional to the ratio of β values. Thus, α's being equal, lower β values result in similarly shaped distributions with larger variance and increasing central tendency and *vice versa* for larger β values. Alternately, when β is constant and α varies, distributions take different shapes and ratios of means and variances scale proportionally to the ratio of α values ($\frac{\sigma_1^2}{\sigma_2^2} \approx \frac{\alpha_1}{\alpha_2} \approx \frac{\bar{x}_1}{\bar{x}_2}$).

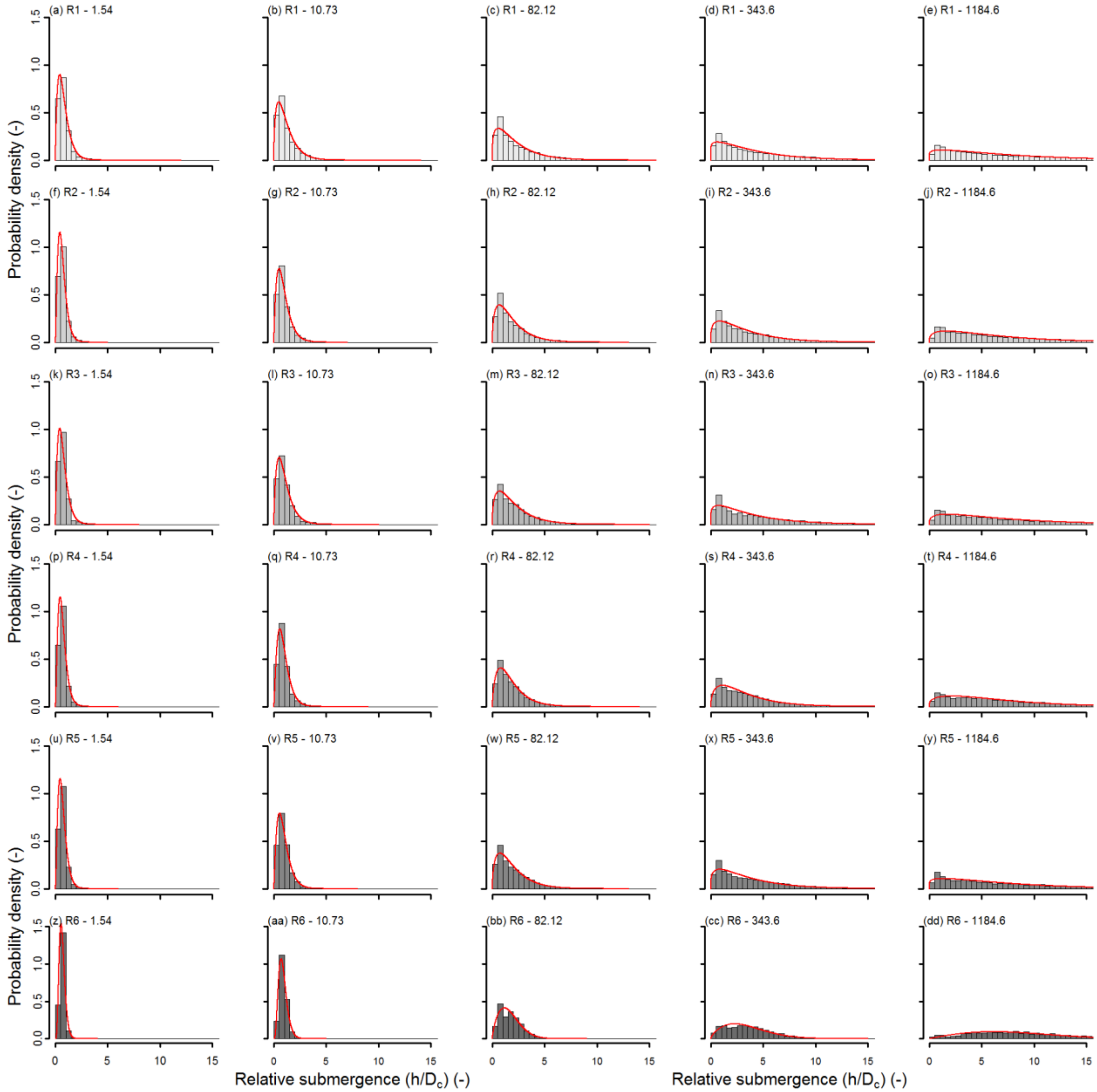

Figure S3. Histograms of reach-scale discharge-dependent *h/Dc* probability densities (bars) overlain with best fitting distribution (red lines) (a-dd). The 'R' in plot titles denotes reach and the number next to R is the reach number. The next number in the plot titles is discharge in m^3/s. Panels are organized such that each row is a different geomorphic reach and each column is a different discharge.

Parameter and statistical testing

Comparison of between segment- and reach-scale domain h/D_c dataset properties for the purpose of determining if statistical self-similarity existed across multiple domains had mixed results. For comparing fitted α and β values the likelihood-ratio-test of Krishnamoorthy et al. (2015) returns two test statistics representing *p* values for each dataset for each individual test. If both test statistics were > 0.05 then equality of parameters was rejected above a 95% confidence level. Only 19 of 150 possible between segment and reach domain α value comparisons could not be rejected as being equal above a 95% confidence level, and equality of β values was rejected for all comparisons (Figure S4a). Overall, 8 of 19 datasets with equivalent α values occurred for LBEs associated with the same discharge. Comparison of reach-scale α and β values between reaches found only 36 α and 12 β values of the 425 possible pair-wise combinations for each variable could not be rejected as being equal (Figure S4b and Figure S4c). No segment-to-reach or reach-to-reach pairs had similar parameters across all discharge-dependent datasets.

Figure S5 depicts network graphs showing positive results (i.e. fail to reject null hypothesis) of the between segment- and reach-scale domain Mann-Whitney U and Levene's testing ($p > 0.05$). Only 12 and 5 of 150 between segment and reach datasets had positive Mann-Whitney U and Levene's tests, respectively. Of the 425 possible tests, between reach datasets had 24 and 13 positive Mann-Whitney U and Levene's tests, respectively. All but three of these between reach tests occurred at the same discharge. These results indicate h/D_c statistical self-similarity did not exist between spatial domains.

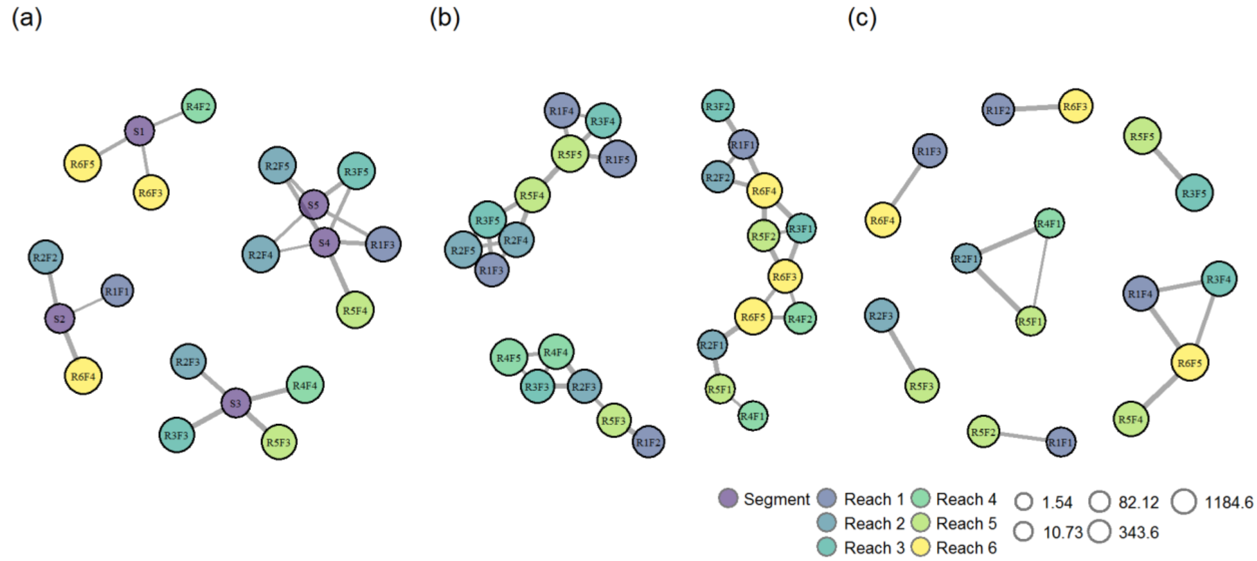

Figure S4. Network graphs of spatial domains as nodes (colored circles) with links (lines) to other domains indicating equivalency between (a) segment- and reach-scale α values, (b) between reach-scale α values, and (c) between reach-scale β values. Nodes are colored by domain and sized by discharge. ‘S’ and ‘R’ are shorthand for segment and reach, respectively. The number next to R is the reach number. The number next to F is the discharge: 1 – 1.54; 2 – 1.73; 3 – 81.12; 4 – 343.6; and 5 – 1184.6 m^3/s. Domains or links that are absent did not have equivalent properties. Link line thicknesses are weighted by *p* values.

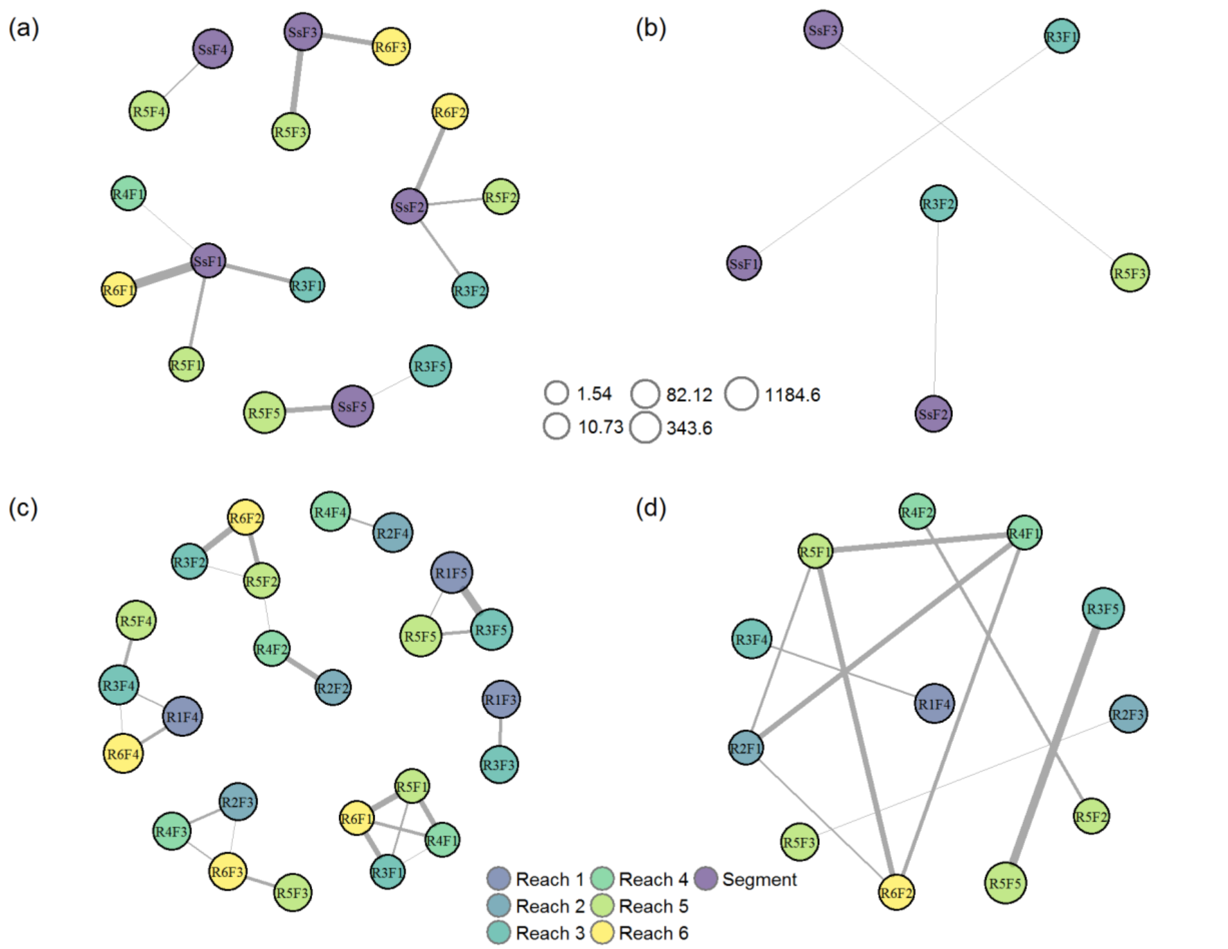

Figure S5. Network graphs of (a) Mann-Whitney U and (b) Levene's tests between segment-scale and reach datasets and (c) Mann-Whitney U and (d) Levene's tests between reach-scale datasets. Nodes are colored by domain and sized by discharge. 'S' and 'R' are shorthand for segment and reach, respectively. The number next to R is the reach number. The number next to F is the discharge: 1 – 1.54; 2 – 1.73; 3 – 81.12; 4 – 343.6; and 5 – 1184.6 m^3/s. Domains or links that are absent did not have equivalent properties. Link line thicknesses are weighted by *p* values.

In terms of detailed testing of the potential for the study segment to fit Style 4, the study investigated the degree to which the scatter data of h/D_c dataset properties versus discharge fit the power function with a high coefficient of determination and high statistical confidence (section 4.5). This analysis found that there was a mutualistic and predictable nature to how values changed between Q's, with the caveat that analysis was based on only five data points

(Figure S6a). The same pattern was observed in each reach independently, but only partially when looking at all reaches together, as Reach 6 had somewhat distinct parameter values (Figure S6b). A strong linear correspondence was also present across Q's between h/D_c $\bar{x}$ and σ values, showing a connection between increasing spread and central tendency (Figure S6c-d).

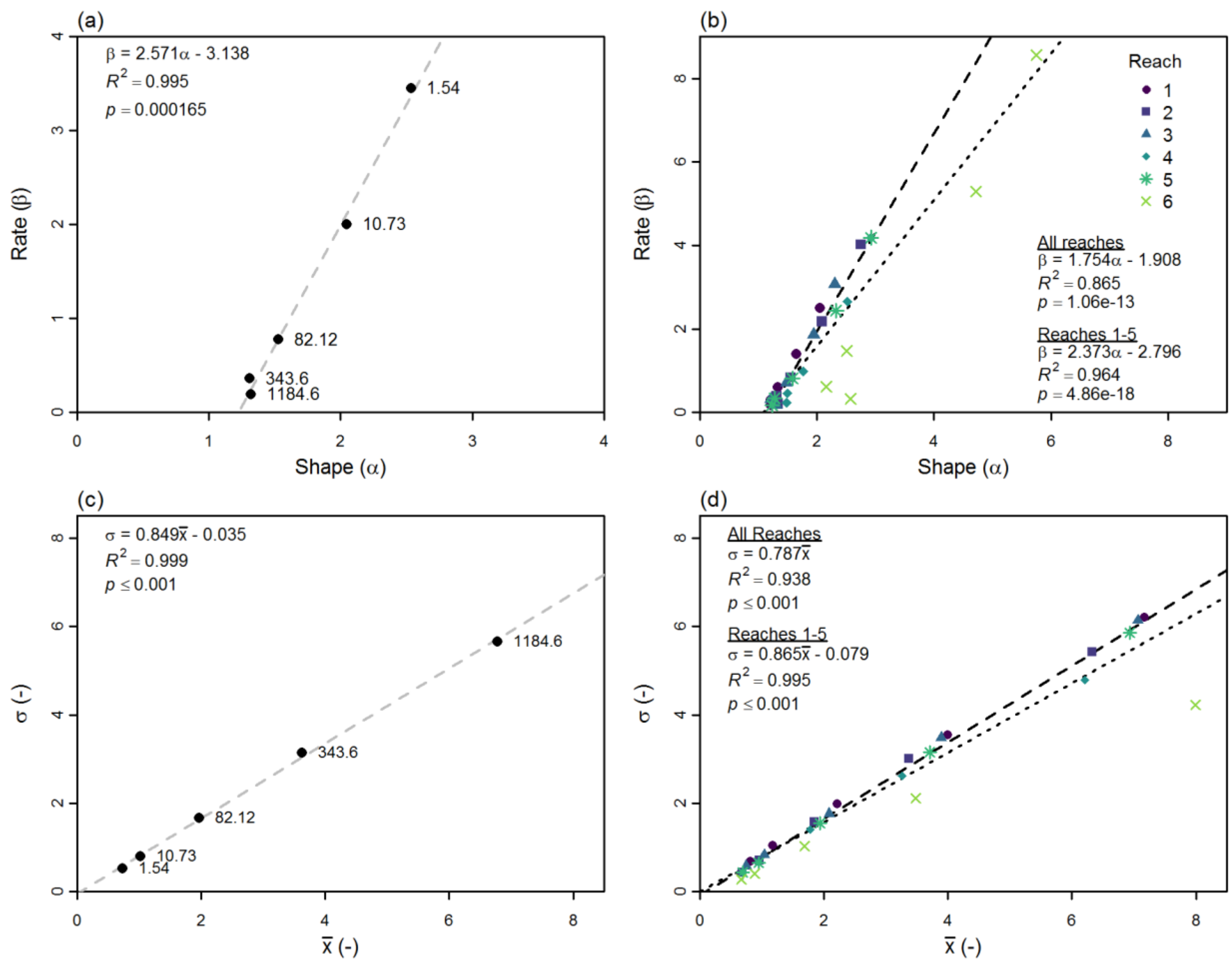

Figure S6. Scatter plots of (a) segment and (b) reach scale fitted Gamma distribution parameters (β vs α) for discharge-dependent *h/D*$_c$ distributions and (c) segment and (d) reach scale standard deviation (σ) versus mean ($\bar{x}$) discharge-dependent *h/D*$_c$ values. Gray dashed line in panels (a) and (c) are lines of best fit for segment data. Regression equations and statistics are shown in the upper left corners. Short and long dashed lines in (b) and (d) are lines of best fit for all reaches and for data from only reaches 1-5, respectively. Numbers next to segment points are discharge in m^3/s associated with the data point. Discharge decreases from top-right to bottom-left in (b) and from bottom-left to top-right in (d).

5.3 Processed-based similarity

Relationships between parametric and statistical properties versus discharge and associated power-law models are shown in Figure S7. Details of the models, including model coefficients, adjusted-R^2 values, and F-test p-values are provided in Table S4. Of the 23 rejected slope comparisons five were comparing the φ model of Reach 5 to Reaches 1, 2, 3, 4, and 5; five were comparing the *g* model of Reach 6 to the Segment and to Reaches 1, 3, 4, and 5; six were comparing the *g* model of Reach 2 to the Segment and to Reaches 1, 3, 4, 5, and 6; six were comparing the β_2 model of Reach 2 to the Segment and to Reaches 1, 3, 4, 5, and 6; and one was comparing the α model of Reach 1 to Reach 5.

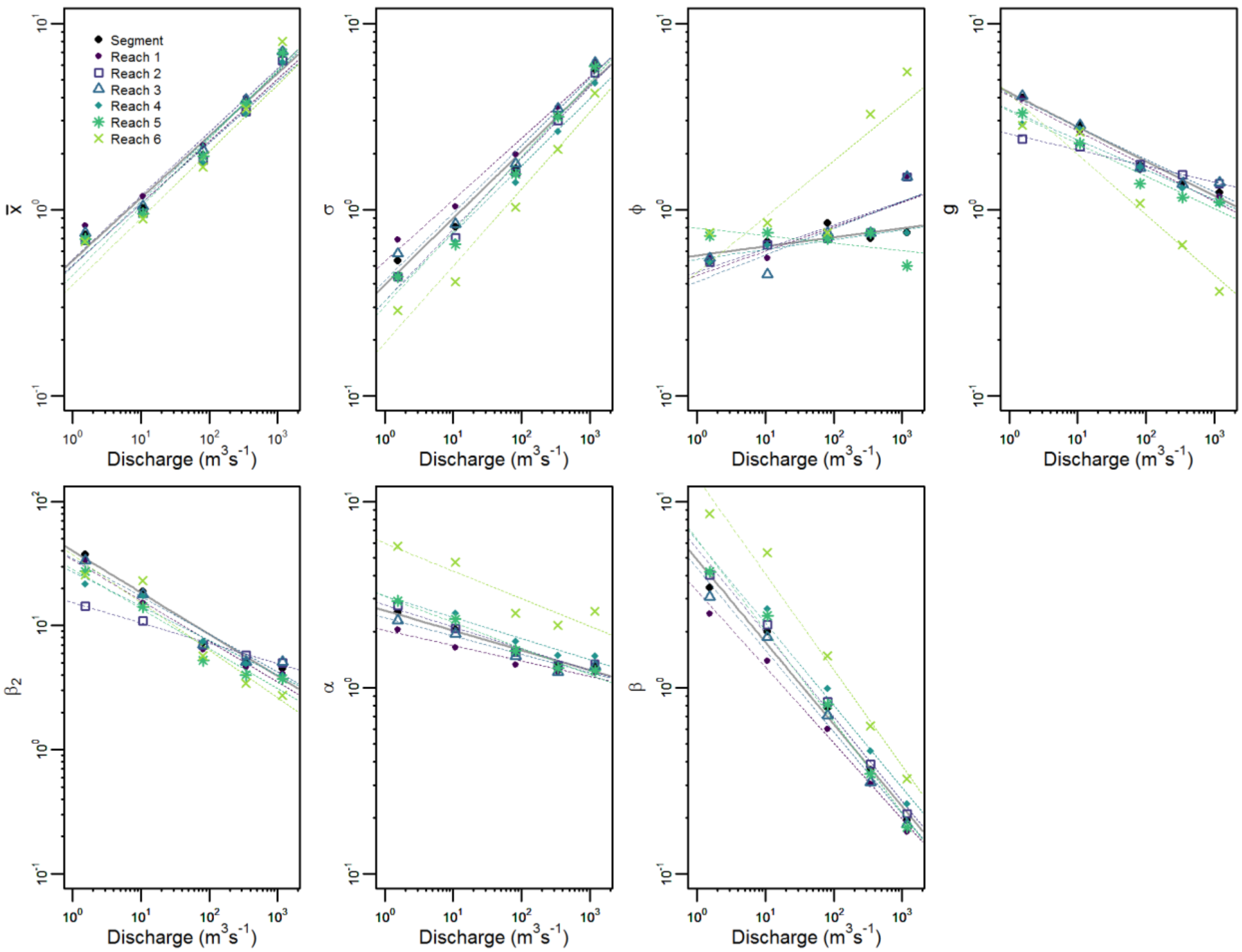

Figure S7. Log-log plot of statistical and parametric properties ($\bar{x}$, σ, φ, g, β_2, α, and β values) versus discharge (points) and fitted power law models (dashed lines). Spatial domains are differentiated using point shape and color.

Table S4. Summary of discharge (Q) vs *h/D_c* dataset property (Φ) power-law models of the form $\Phi = a'(Q)^b$ including model parameters (a',b), adjusted-R^2, and F-test p-values.

Spatial Domain	a'	b	adjusted-R^2	F-test p-value
$\bar{x}$ (-)				
Segment	0.53	0.3351	0.96	0.003
R1	0.61	0.3259	0.96	0.002
R2	0.50	0.3347	0.96	0.003
R3	0.54	0.3410	0.96	0.002
R4	0.50	0.3280	0.95	0.003
R5	0.49	0.3490	0.95	0.003
R6	0.44	0.3671	0.91	0.007
σ (-)				
Segment	0.39	0.36	0.97	0.001
R1	0.53	0.33	0.97	0.001
R2	0.32	0.38	0.98	0.001
R3	0.42	0.36	0.97	0.002
R4	0.32	0.36	0.97	0.001
R5	0.30	0.40	0.97	0.001
R6	0.19	0.41	0.96	0.002
φ (-)				
Segment	0.57	0.05	0.38	0.162
R1	0.44	0.13	0.62	0.070
R2	0.46	0.13	0.64	0.066
R3	0.41	0.14	0.60	0.077
R4	0.54	0.05	0.86	0.015
R5	0.80	-0.04	0.18	0.263
R6	0.46	0.30	0.62	0.070
g (-)				
Segment	4.25	-0.18	0.98	0.001
R1	4.08	-0.19	0.97	0.001
R2	2.56	-0.09	0.98	0.001
R3	4.17	-0.17	0.92	0.006
R4	3.44	-0.16	0.94	0.004
R5	3.39	-0.17	0.95	0.003
R6	4.18	-0.32	0.92	0.006
β_2 (-)				
Segment	40.10	-0.34	0.96	0.002
R1	33.98	-0.33	0.95	0.003

R2	15.37	-0.16	0.98	0.001
R3	34.80	-0.30	0.93	0.005
R4	27.26	-0.28	0.96	0.002
R5	28.60	-0.32	0.93	0.005
R6	37.16	-0.38	0.91	0.007
α (-)				
Segment	2.59	-0.11	0.95	0.004
R1	2.04	-0.08	0.93	0.005
R2	2.77	-0.12	0.94	0.004
R3	2.38	-0.10	0.90	0.009
R4	3.11	-0.11	0.94	0.004
R5	3.10	-0.14	0.97	0.002
R6	5.96	-0.15	0.78	0.031
β (-)				
Segment	4.87	-0.44	0.98	0.001
R1	3.32	-0.41	0.99	0.000
R2	5.56	-0.45	0.99	0.000
R3	4.38	-0.44	0.98	0.001
R4	6.16	-0.44	0.97	0.001
R5	6.27	-0.49	0.98	0.001
R6	13.40	-0.52	0.97	0.001

5.4 Incremental inundation corridor relative submergence

All four incremental inundation corridor h/D_c datasets were best fit by log-normal distributions, which was supported at the 95% confidence level by the corrected Anderson-Darling test (section S5.2). This finding was only corroborated for the 1.54-10.73 m^3/s corridor data when applying the Shapiro-Wilk test (Millard, 2013), which is considered a relatively powerful test for normally distributed data.

As discussed in the article, comparison of D_c values within each incremental inundation corridor were found to have greater similarity than h values across the four corridors (Figure S8).

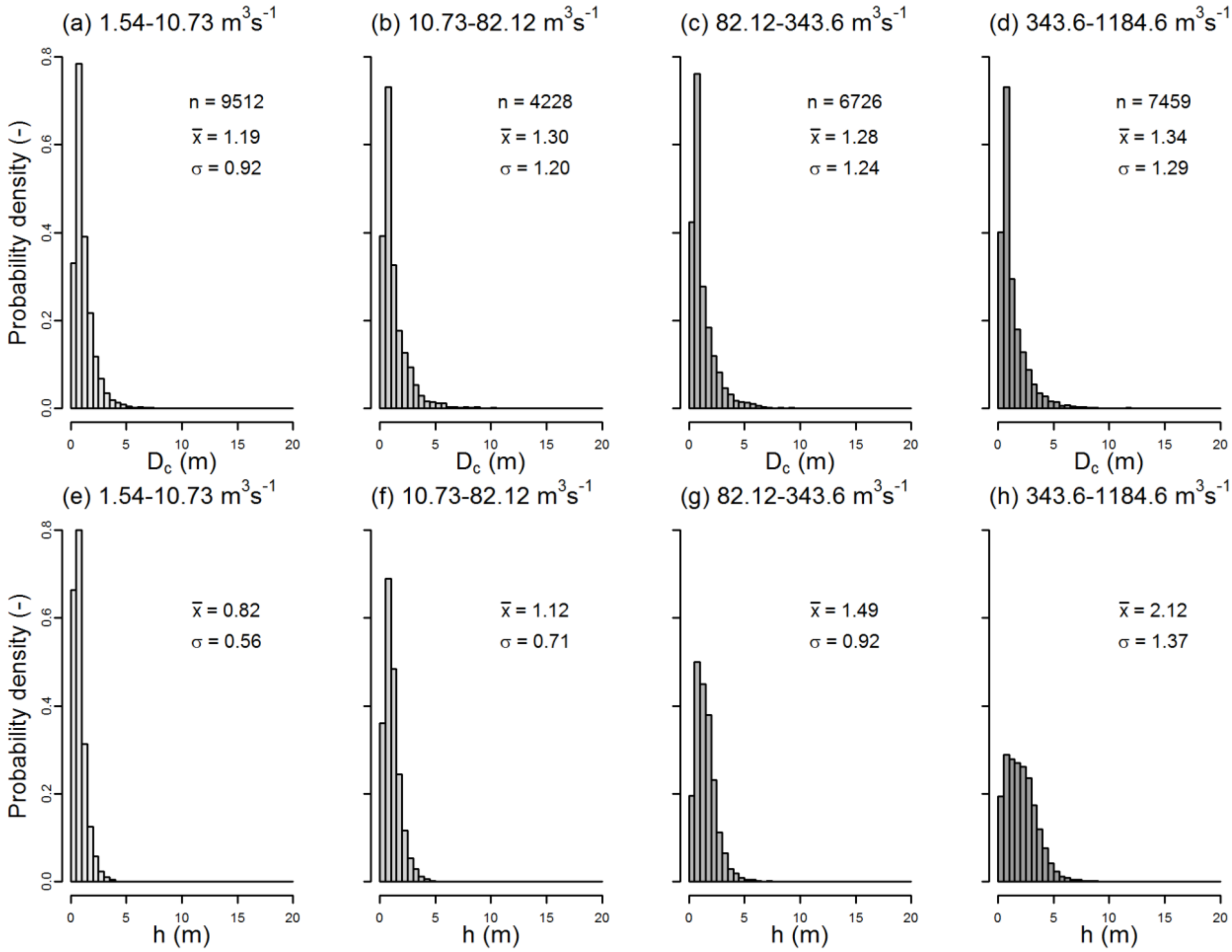

Figure S8. Histograms of (a-d) D_c values and (e-h) h values at LBEs within each incremental inundation corridor. Note greater similarity of D_c values between datasets compared to h values.

5.5 Submergence trends

To isolate sets of h/D_c values at newly wetted LBEs between discharges, only those LBEs that were not wetted at lower discharges were included (e.g. for 10.73-82.12 m^3/s dataset only LBEs not wetted at 10.73 m^3/s considered). In order to isolate how depths changed at previously wetted LBEs between discharges, differences in h/D_c values between successive discharges (e.g. h/D_c at 10.73 m^3/s minus h/D_c at 1.54 m^3/s) were calculated for each LBE. From these data only those LBEs that were wetted at lower discharges were included (e.g. for 10.73-82.12 m^3/s dataset only LBEs wetted at 10.73 m^3/s considered), essentially the opposite of the incremental inundation corridor and the set of newly wetted LBE.

Differences in h/D_c dataset means resulting solely from the addition of newly wetted LBEs ($\Delta\bar{x}_n$) were calculated for each change in discharge by subtracting the mean of the set of h/D_c values resulting from combining h/D_c values at newly wetted LBEs with h/D_c values of previously wetted LBEs from the prior discharge (e.g. for 10.73-82.12 m^3/s this comprised combining h/D_c values from the 82.12 m^3/s dataset for LBEs that were not wetted at 10.73 m^3/s and h/D_c values from the 10.73 m^3/s dataset) from the mean of the complete h/D_c dataset of the higher discharge (e.g. using the same example, the 82.12 m^3/s dataset). Differences in h/D_c dataset means due solely to depth changes at previously wetted LBEs ($\Delta\bar{x}_p$) were calculated for each change in discharge by subtracting the mean of h/D_c values from each subsequently higher discharge for the set of LBEs that were wetted at the prior discharge (e.g. for 10.73-82.12 m^3/s h/D_c values came from the higher discharge but were limited to the set of LBEs that were wetted at 10.73 m^3/s) from the mean of the complete h/D_c dataset.

As discussed in the article, comparison of segment-scale (Figure S9) and reach-scale (Figure S10) discharge-dependent D_c values were found to be visually similar within each spatial domain, independently, especially compared to distributions of h values. Overlap index values from comparing all possible reach-scale D_c datasets within each independent reach varied between 0.69-0.98 versus between 0.07-0.73 for h comparisons (Pastore & Calcagni, 209).

As discussed in the article, LBE submergence did not occur equally within each laterally nested discharge-dependent portion of the river corridor, such that LBEs located in the baseflow channel were often more submerged at any given discharges relative to LBEs in other portions of the river corridor. The percent of LBEs intersecting each wetted area that exceeded relevant h/D_c thresholds at each higher discharge are presented in Table S5.

As discussed in the article discharge-dependent distributions of relative submergence were consistent in their shape and how they changed between datasets regardless of method for calculating h and D_c. For instance, segment-scale distributions of h/D_c, $h/\overline{D}$, $\hat{h}/D_c$, and $\hat{h}/\overline{D}$ were all positively skewed and predominantly leptokurtic (Figure S11). The majority of datasets (8 of 15) were best fit by Gamma distributions with the rest best fit by Weibull distributions. Calculations using h/D_c had the lowest average values as $D_c>\overline{D}$ and $h<\hat{h}$. Alternately, $\hat{h}/\overline{D}$ had the highest average values.

Compared to the alternative methods for calculating h and D_c, the preferred metric, h/D_c, yielded the lowest values, and thus may have a tendency for underestimation. Potential underestimation is expected to be relatively minimal as values across methods were comparable in magnitude. Regressing h/D_c values against the calculation method with the highest values, $\hat{h}/\overline{D}$, found a scaling factor of 1.38 minimized error between estimates, which serves as an expected value for the magnitude of uncertainty. Comparisons of h/D_c values with the other two calculation methods, $\hat{h}/D_c$ and $h/\overline{D}$, returned scaling factors of 1.09 and 1.26, respectively. Regardless of calculation method, discharge-dependent distributions of relative submergence were consistent in their shape and how they changed between datasets (Figure S8). Ultimately, the h/D_c calculation method allowed reasonable approximation of relative submergence values for thousands of macroroughness features over 13 km of river spanning a range of discharges, for which there is scientific as well as practical value, such as mapping submerged hazards (Strom et al., 2017).

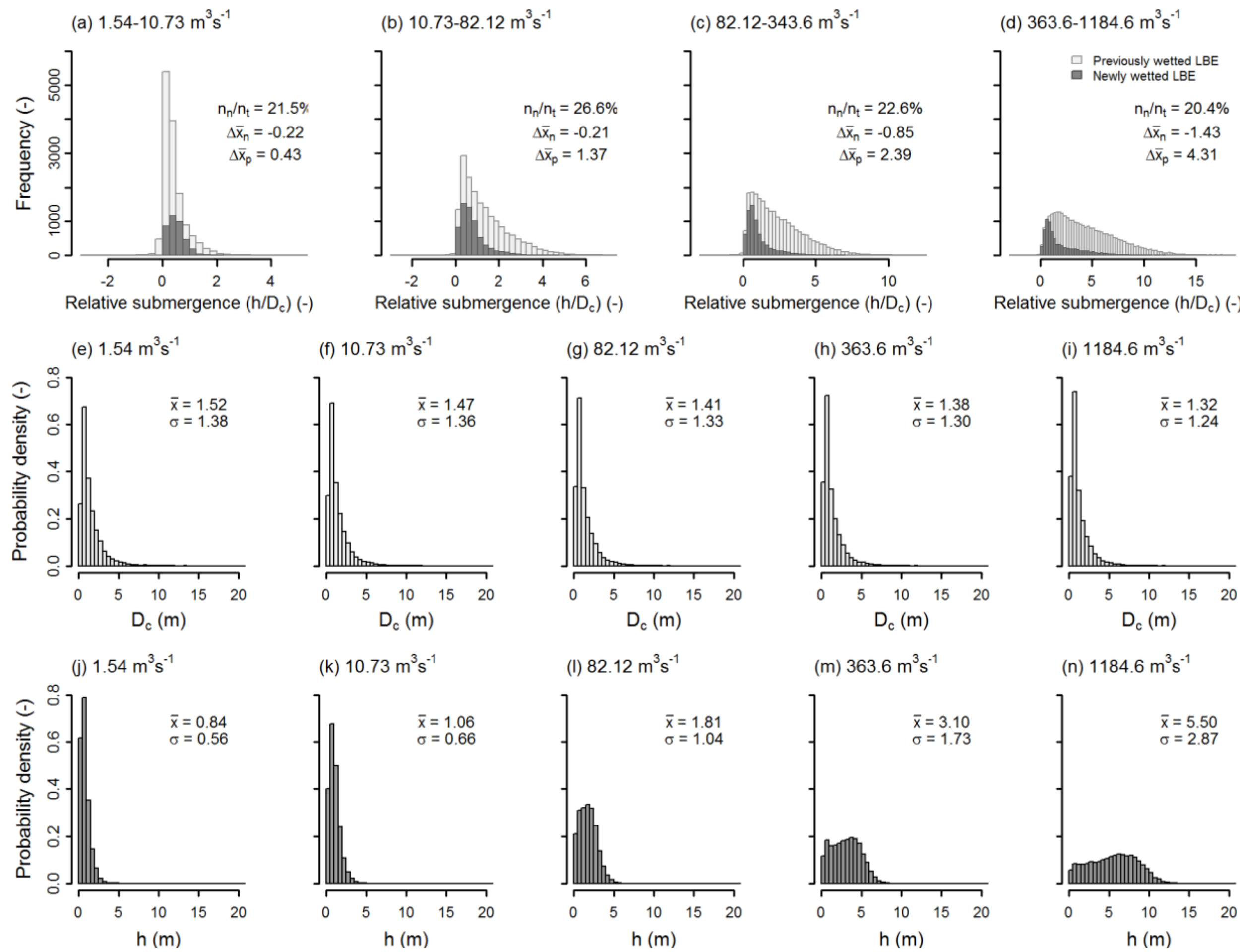

Figure S9. Frequency histograms of (a-d) segment-scale h/D_c values at LBEs that become newly wetted between each successive Q (dark gray bars) superimposed with histograms of changes to h/D_c values that occurred at previously wetted LBEs between each Q (light gray bars) and probability density histograms of (e-i) D_c values and (j-n) h values at LBEs within each segment-scale, discharge-dependent LBE dataset. The percentage of newly wetted LBEs (n_n) relative to the total number of LBEs (n_t) at each ending Q (second number in header) are shown in (a). Differences in mean h/D_c dataset values due solely to the addition of newly wetted LBEs ($\Delta\bar{x}_n$) and those due solely to changes in h at previously wetted LBEs ($\Delta\bar{x}_p$) are also shown in (a). For (e-n) note greater similarity of D_c values between datasets compared to h values.

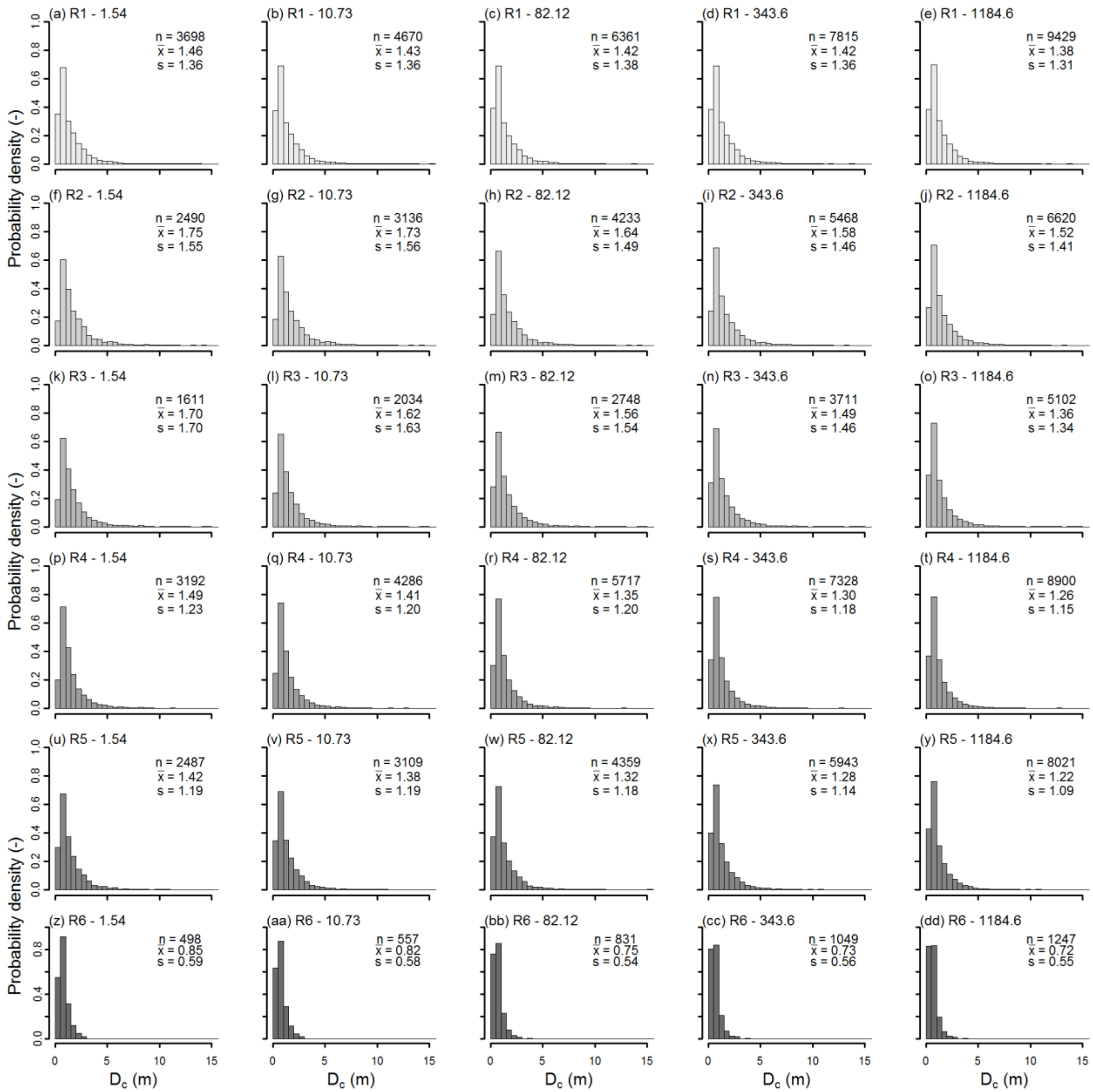

Figure S10. Histograms of LBE heights (D_c) for reach-scale discharge-dependent LBEs (a-dd). Panels are organized such that each row is a different geomorphic reach and each column is a different discharge.

Table S5. Percentage of segment-scale h/D_c values for just those LBEs within each discharges wetted area exceeding certain thresholds at each higher discharge.

Simulated Discharge (m^3/s)	Threshold					
	1	2	3	3.5	4	10
LBEs in 1.54 m^3/s wetted area						
10.73	45.9	11.8	3.8	2.2	1.3	0.0
82.12	81.4	52.7	31.0	23.6	17.9	0.4
343.6	94.6	79.8	64.8	57.6	51.3	9.3
1184.6	98.6	93.4	86.0	81.4	76.9	35.9
LBEs in 10.73 m^3/s wetted area						
82.12	77.8	48.9	27.9	20.9	15.5	0.3
343.6	93.5	78.4	63.7	56.8	50.6	8.4
1184.6	98.5	92.8	85.5	81.1	76.8	36.7
LBEs in 82.12 m^3/s wetted area						
343.6	90.0	73.3	58.3	51.5	45.3	6.4
1184.6	98.0	91.3	83.6	79.3	75.1	35.3
LBEs in 343.6 m^3/s wetted area						
1184.6	96.7	88.0	79.5	75.0	70.6	30.3

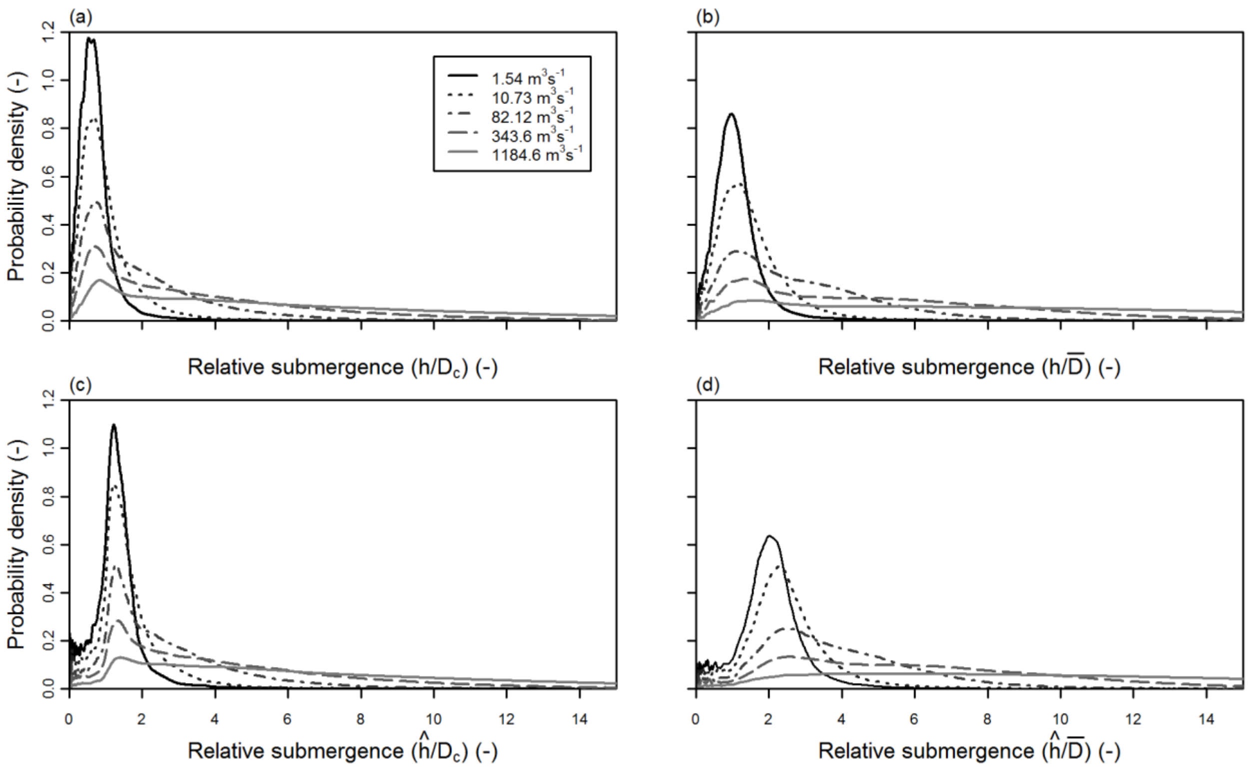

Figure S11. Overlain kernel densities of segment-scale relative submergence probability densities for all five discharge-dependent LBE datasets based on relative submergence calculated according to (a) h/D_c, (b) $h/\bar{D}$, (c) $\hat{h}/D_c$, and (d) $\hat{h}/\bar{\mathbf{D}}$.

6 Discussion

6.1 LBE h/D_c distributions and styles

As discussed in section 6.1 of the article, a near-universal takeaway of this study was that distributions of h/D_c values were leptokurtic and positively skewed. We are not aware of h/D_c datasets for comparison, however, Hodge et al. (2009) found distributions of surface elevations in two gravel-cobble-bed English rivers were positively skewed. Additionally, Day (1976), Gomez (1993), and Aberle and Nikora (2006) independently found roughness heights to evolve toward skewed and leptokurtic distributions during armoring in gravel-bedded flumes, and several workers document heights of finer-grained bedforms such as dunes to follow distributions with similar characteristics (Van der Mark et al., 2008; Singh et al., 2012).

Coarse-bedded ($D_{50} \geq 5$ mm) rivers generally display skewed, often lognormal grain-size distributions (GSDs) (Bunte & Abt, 2001). Relationships between surface GSDs and roughness height distributions typically don't exhibit 1:1 correspondence as they are influenced by several factors such as imbalances in sediment supply-to-transport ratios that promote fining and development of planar beds or from heterogeneous packing, spacing, and clustering of grains (Kirchner et al., 1990; Gomez, 1993). Nonetheless, for armored beds, it is reasonable that roughness height distributions would follow the general form of surface GSDs as large particles protrude further into the flow (Kirchner et al., 1990; Gomez, 1993).

Similarity in the magnitude of reach-scale h/D_c dataset properties at the same Q can also be used to make inference about channel adjustment (Wohl & Merritt, 2008; Schneider et al., 2015). For instance, the coefficient of variation (CV) of mean reach-scale h/D_c values ($\bar{x}$) were less than 10% at each distinct Q (Table S2). Using the logic at the beginning of the preceding paragraph and substituting $\bar{x}$ values in place of R/D_{84}, first-order estimates of the Darcy-Weisbach friction factor in each reach at each Q can be made using the unbiased and widely used variable-power resistance equation of Ferguson (2007) (see Text S6.4 for equation). For the calculations, the assumption that $h{\sim}R$ is applied, which is simplifying, but not uncommon in practice (Bathurst, 1985), and reasonable given the comparative nature of the exercise. The CV of these resistance estimates do not exceed 16% between reaches for any given Q. This is phenomenologically similar to the findings of Wohl and Merritt (2008), who found the range of bankfull flow resistance values (f) to be constant between geographically distributed mountainous steam reaches with different channel morphologies. They concluded such uniformity was consistent with the extremal hypotheses that channels were adjusted to maximize resistance.

6.2 Evolution toward steady-state relative submergence

None.

6.3 Resistance trends and fixed roughness coefficients

None.

6.4 Implications of relative submergence distributions

A universal trend for skewed roughness height distributions has implications for random-field based approaches to roughness approximation. These methods generally rely on the assumption that bed elevations are homogenous and Gaussian distributed (Nikora et al., 1998), otherwise requiring higher-order structure functions when beds are anisotropic and non-Gaussian (i.e. skewed and leptokurtic) (Aberle & Nikora, 2006).

A fundamental limiting assumption of most reach-averaged resistance equations is that for a given Δ value, a 1:1 relation exists between mean depth and mean velocity (Ferguson, 2007). Attempts to reduce scatter between observed and predicted resistance have typically involved the addition of variables (e.g. slope and LBE concentration) into resistance equations (Nitsche et al., 2012), the use dimensionless variables (Ferguson, 2007; Rickenmann & Recking, 2011), or partitioning approaches (David et al., 2011). David et al. (2011), for example, employed a drag force approach to estimate grain resistance by summing drag contributions from all individual large grains present in their study reach. These resistance estimates were always higher than those from typical resistance equations, but were still considered to underestimate grain resistance at low flows. The linearity assumption of such additive approaches is complicated by wake interactions that result in non-linear relations between LBE concentrations and resistance (e.g., Wiener & Pasternack, 2022).

Conceptually, the inclusion of multiple roughness length scales (Ferguson et al., 2019) or methods that better characterize bed roughness and depth heterogeneity, such as the discharge-dependent relative-submergence distributions presented in this study, could address the equifinality issues described above (Ferguson, 2007). To this end, a simple numerical example is introduced to demonstrate one way h/D_c distributions may be used to estimate resistance. For the example, four resistance equations were selected and solved traditionally, and with a h/D_c distribution-based approach. Specifically, the resistance equations of Bathurst (1985), Ferguson (2007), Katul et al. (2002), and Thompson & Campbell (1979) were used to estimate reach-scale flow resistance using a traditional single h/D_{84} value approach and with a distribution-based approach involving numerical integration of each reach-scale h/D_c dataset as input for h/D_{84}:

Bathurst (1985):

$$\sqrt{\frac{8}{f}} = 4 + 5.62\log\left(\frac{h}{D_{84}}\right) \quad \text{(EQ. S5)}$$

Ferguson (2007):

$$\sqrt{\frac{8}{f}} = \frac{a_1 a_2\left(\frac{h}{D_{84}}\right)}{\sqrt{a_1^2 + a_2^2\left(\frac{h}{D_{84}}\right)^{5/3}}} \quad \text{(EQ. S6)}$$

Katul et al. (2002) [from Ferguson, 2007]:

$$\sqrt{\frac{8}{f}} = 1 + \frac{k}{h}\log\left[0.65\cosh\left(\frac{h}{k} - 1\right)\right] \qquad \text{(EQ. S7)}$$

Thompson & Campbell (1979) [from Ferguson, 2007]:

$$\sqrt{\frac{8}{f}} = 2.5\left(1 - \frac{0.1k}{R}\right)\ln\left(\frac{12R}{k}\right) \qquad \text{(EQ. S8)}$$

Equation (7) of Katul et al. (2002) is the result of integration of a mixing layer type equation with a vertical velocity profile represented by a hyperbolic tangent function and mixing layer thickness *k*. When solving (7), *k* was set equal to $1 \cdot D_{84}$ as recommended by Ferguson (2007). In Thompson and Campbell's (1979) modified Keulegan equation (8), *k* was set equal to $2.37 \cdot D_{84}$. In Ferguson's (2007) variable-power equation (6) values for a_1 and a_2 were set equal to 6.5 and 2.5, respectively as recommended by Rickenmann and Recking (2011). For all calculations, the assumption that h~R was applied.

We focus on these four equations as they are widely referenced, apply to and provide unbiased solutions for coarse-bedded rivers with low submergence, provide solutions for the same common resistance coefficient (*f*), and beyond empirical coefficients only require input of h/D_{84} (i.e. h~R). Each equation uses D_{84} to parameterize $\varDelta$, consistent with the view that large particles dominate flow resistance. While effectiveness of D_{84} and characteristic particle sizes in general in estimating resistance are the subject of controversy (Yochum et al., 2012), alternatives (e.g. σ_z most commonly) are not without drawbacks and have not always outperformed particle-size approaches in application (Schneider et al., 2015).

When computing resistance using the distribution-based approach we began with the definition for the expected value of a continuous random variable x:

$$E[x] = \int_{-\infty}^{\infty} x \cdot f(x)dx \qquad \text{(EQ. S9)}$$

which can be discretized into *i* bins and solved with numerical integration as:

$$E[x] = \sum_i x_i \cdot p(x_i) \qquad \text{(EQ. S10)}$$

where x_i is a discrete value of x with probability $p(x_i)$. Thus, substituting (10) into (5) for instance, with x = h/D_c yields:

$$\sqrt{\frac{8}{f}} = \sum_i p(\frac{h}{D_{c_i}})\left(4 + 5.62\log\left(\frac{h}{D_{c_i}}\right)\right) \qquad \text{(EQ. S11)}$$

Solving (11) for *f*, using each reach-scale h/D_c dataset yields the 'integrated-*f*' values described in the article. Substituting (10) into equations 5-8, and solving for *f* using each reach-scale h/D_c dataset was done to obtain integrated-*f* values for these equations. The number of bins used for numerical integration were defined for each dataset following the approach of Freedman and Diaconis, (1981).

For the traditional approach each equation was solved for each reach at each simulated discharge using a single h/D_{84} value, as intended by their original formulation. Estimates of *h* were made by averaging model predicted depths over each reach. A constant D_{84} of 0.512 m obtained from previous sampling (YCWA, 2013) was used for all calculations. These were used to solve each equation for *f*, and are referred to as 'traditional–*f*' values. Next, the same resistance equations were solved for *f*, but this time numerically integrating over each reach-scale h/D_c dataset as input for h/D_{84}. These are referred to as 'integrated–*f*' values.

Comparison found integrated–*f* values were on average ~6.8 times larger than traditional–*f* values, which is not surprising given the range of lower submergence values present in the former (Figure S12a). Differences varied by equation, as integrated–*f* values computed using the Bathurst equation were on average ~16.1 times larger than traditional–*f* values, whereas integrated–*f* values were only ~3.1-4.3 times larger for the other three equations. Several workers have demonstrated popular resistance equations, including those referenced above, tend to underestimate resistance coefficients (*n* and *f*) in course-bedded rivers at low flows, resulting in velocity overestimation and shear-stress underestimation (e.g. Yochum et al., 2012; Ferguson et al., 2017). Notably, error trends are not universal, and a tendency for resistance under-prediction at lower relative submergence and over-prediction at higher relative submergence is well documented (Rickenmann & Recking, 2011).

At this time, it remains unclear if resistances calculated using the integrated approach actually outperformed traditional estimates. However, the integrated approach does provide more complete representation of bed-surface heterogeneity and the joint-distribution of local flow depths. The approach also allows unique resistance value to be estimated for any given discharge and spatial domain and we believe it has potential for improving resistance estimation despite the greater input data requirements. For instance, for a given reach and given discharge, the integration approach provided a marginal degree of similarly collapse between equations as the CV of integrated–*f* values were reduced by ~2.9% compared to traditional–*f* CV values, which we interpret as a positive outcome. Additional analysis on these fronts is beyond the scope of this study, but could be an area of future research, especially given availability of improved methods for remotely-sensed depth measurements (Legleiter & Harrison, 2019).

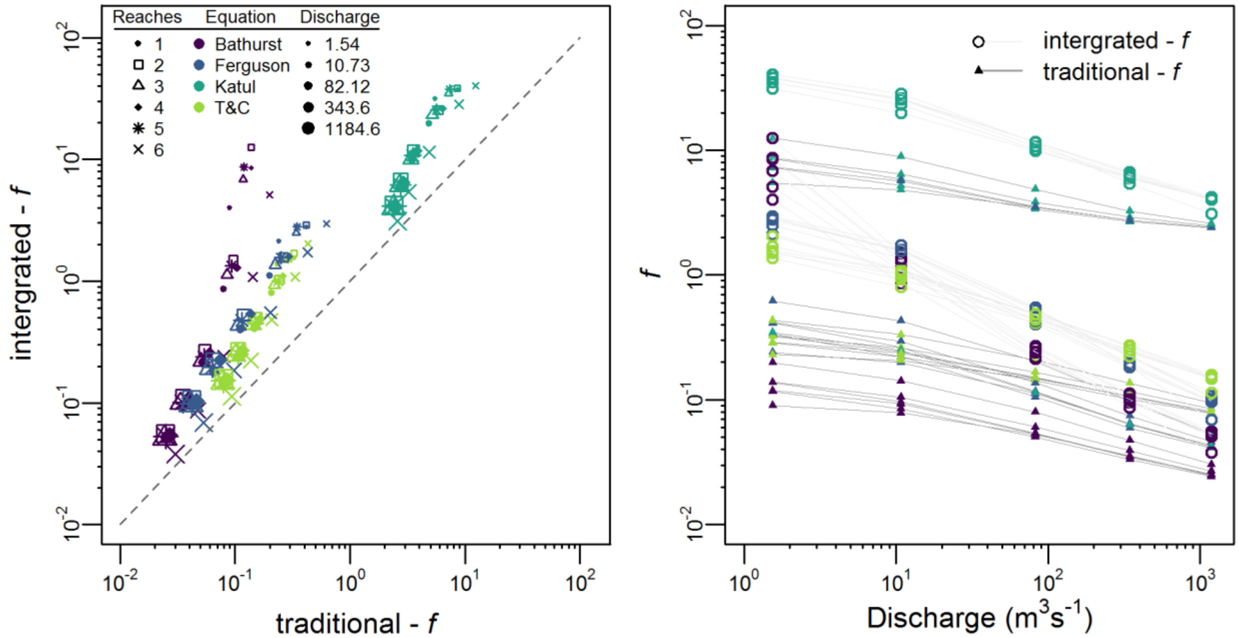

Figure S12. (a) Comparison of reach-scale Darcy-Weisbach friction factor (*f*) estimates made using *h*/D_{84} – *f* and *h*/D_c integrated– *f* calculation methods; and (b) calculated *f* versus discharge for all reaches. In (a) data from each reach are represented by unique symbols. Symbols are colored according to resistance equation and sized according to corresponding discharge simulation. Dashed gray line is the 1:1 line. In (b) symbols correspond to the method used to calculate *f* and are colored according to resistance equation.

6.5 Dynamism of local relative submergence

As stated by Groom and Friedrich (2019), "Understanding the spatial patterns and structure of flow properties across a bed has fundamental implications for geomorphic processes and local ecology." Thus far we have focused on LBE relative submergence conditions aggregated at segment and reach scales, however element-explicit h/D_c values produced by the methods presented herein can be used to study submergence patterns and dynamics at many spatial scales, such as at individual LBE or clusters of elements. For discussion purposes, an example using element-explicit h/D_c values for more local-scale analysis is presented below. The example focuses on documenting h/D_c conditions that would be encountered by an arbitrary object traveling along a portion of the river's thalweg under different discharge conditions. While highly simplified, the object could be representative of a particle or organism, such as a fish or macroinvertebrate, moving along this dominate flowline. An arbitrary 520-m (~20 channel widths) portion of Reach 1 was selected as the domain of interest. Within the domain, the object's path was set as the baseflow thalweg and LBEs within 1 m of the thalweg were identified and assigned a longitudinal position along the thalweg, assuming these represent LBEs that interact with the object or visa-versa. Discharge-dependent h/D_c values at these LBEs were recorded and plotted longitudinally (Figure S13).

First, it can be observed that numerous LBEs with variable h/D_c conditions would be encountered along the object's journey. If relevant h/D_c values are known (e.g. a range of h/D_c values that provide physical habitat for an aquatic organism of interest), inference may be drawn from the sets of encountered conditions. For instance, from the perspective of bedload particles traveling along the specified route, at discharges at or below 10.73 m^3/s, nearly all LBEs were in the LRS regime ($h/D_c<3.5$). This condition is associated with enhanced deposition of mobile bedload upstream of LBEs (Monsalve & Yager, 2017; Papanicolaou & Tsakiris, 2017). Thus, it may be inferred that there would be many opportunities for deposition and intermittent storage upstream of these LBEs. Monsalve & Yager (2017) also found LRS regime bedload deposition promoted cluster formation and increased stability of stoss-side sediment patches with little effect on wake GSD or bed elevations (see also Wittenberg & Newson, 2005). At higher discharges (≥82.12 m^3/s), most encountered LBEs were in the HRS regime ($h/D_c<3.5$), which is associated with increased probability for mobile particle deposition in LBE wakes (Papanicolaou

& Tsakiris, 2017). Notably, higher transport capacities and associated selective entrainment or equal mobility of the bed and increased potential for cluster destabilization and LBE mobilization during these higher discharges may limit depositional processes (Wittenberg & Newson, 2005). Patch stability at a given LBE, a feature of interest in river management (Kondolf et al., 1996), is likely enhanced by persistence of LRS or HRS regime conditions across a wide range of discharges that would be easy to track from the data. In the example, the few LBEs remaining in the LRS regime at high discharges may, for instance, harbor sediment patches and provide shelter from surrounding higher velocities and turbulent intensities important to aquatic organisms (Crowder & Diplas, 2006; Lacey & Roy, 2008). Lastly, while no attempt is made to track time and flow-dependent particle movements, as discharge cycles between periods of baseflow and flood the transition of LBEs between LRS and HRS regimes provide a plausible mechanism for intermittent, localized storage and transport as bedload particles hop-scotch downriver between locations that favor deposition. This stage-dependent LBE morphodynamic control may mediate sediment yield and facilitate observed long term storage (>10^3 of years) of theoretically highly mobile grains in mountain rivers (Faustini & Jones, 2003; Sutfin & Wohl, 2019).

Despite its simplicity, the example above yields high-level incite regarding how LBE relative submergence dynamics can lead to unique patterns for sediment storage and transport through mountain river systems and provide crucial environmental conditions for aquatic biota. It is acknowledged we have barely broached the surface of how element-explicit h/D_c values may be used in river science and management, but the hope is presenting these concepts can stimulate further research.

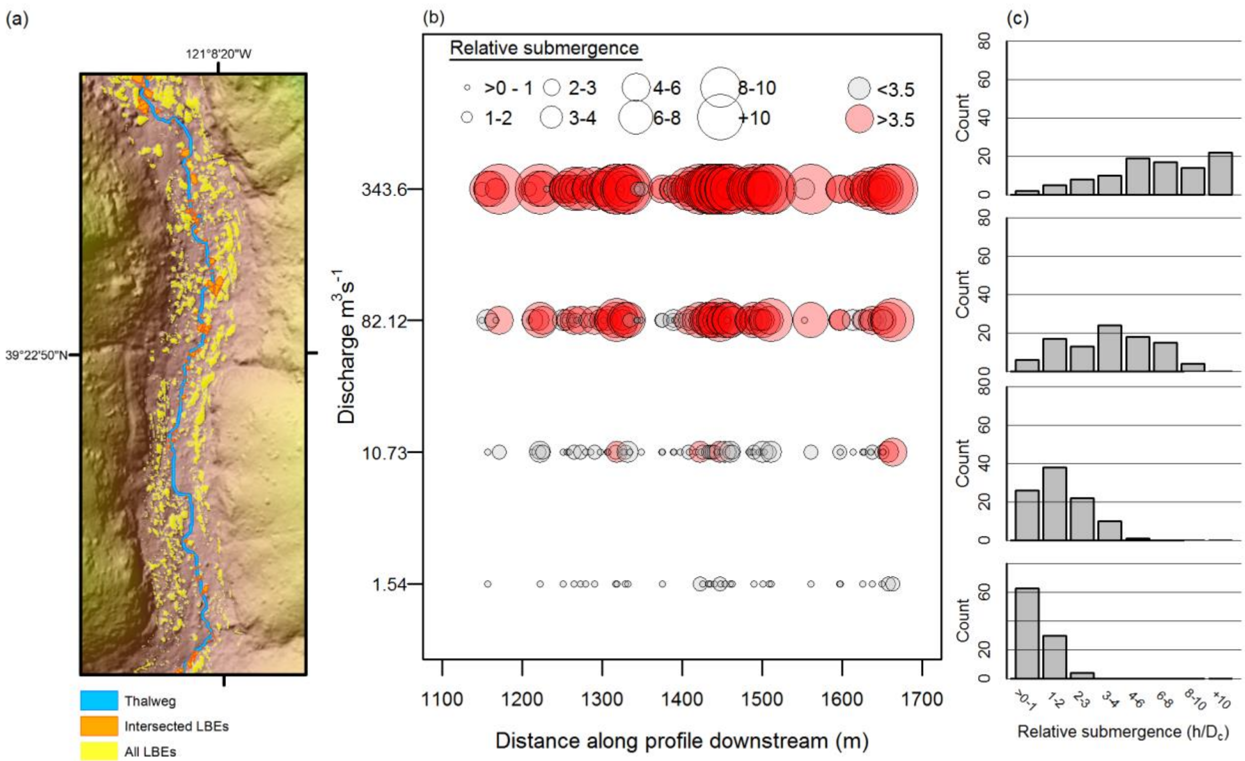

Figure S13. (a) Selected 520 m portion of Reach 1 used to illustrate discharge-dependent h/D_c conditions at each LBE encountered by object moving along the baseflow thalweg. (b) Longitudinal plots of LBE locations (circles) along the thalweg scaled (circle size) based on relative submergence and color coded as being in the LRS (gray) or HRS (red) regimes. Each row in (b) depicts h/D_c conditions at the same set of LBEs for the discharge depicted on the vertical axis. (c) Histograms of h/D_c values for each discharge, also stacked following the same order as in panel (b). Flow in (a) is from top to bottom. The object encounters 678 LBEs.

7 Conclusions

None.

8 References

Aberle, J., and Nikora, V. (2006) Statistical properties of armored gravel bed surfaces. *Water Resources Research, 42*(11). doi:10.1029/2005WR004674

Aberle, J., and Smart, G. M. (2003) The influence of roughness structure on flow resistance on steep slopes. *Journal of Hydraulic Research*, *41*(3), 259-269. doi:10.1080/00221680309499971

Bathurst, J. C. (1985). Flow Resistance Estimation in Mountain Rivers. *Journal of Hydraulic Engineering*, *111*(4), 625-643. doi:doi:10.1061/(ASCE)0733-9429(1985)111:4(625)

Benjankar, R., Tonina, D., and McKean, J. (2015) One-dimensional and two-dimensional hydrodynamic modeling derived flow properties: impacts on aquatic habitat quality predictions. *Earth Surface Processes and Landforms*, *40*(3), 340-356. doi:10.1002/esp.3637

Braun, H. (1980) A Simple Method for Testing Goodness of Fit in the Presence of Nuisance Parameters. *Journal of the Royal Statistical Society. Series B (Methodological)*, *42*(1), 53-63.

Bunte, K., and Abt, S.R., (2001) Sampling surface and subsurface particle-size distributions in wadable gravel-and cobble-bed streams for analyses in sediment transport, hydraulics, and streambed monitoring. Gen. Tech. Rep. RMRS-GTR-74. Fort Collins,CO: U.S. Department of Agriculture, Forest Service, Rocky Mountain Research Station. 428 p.

Crowder, D. W., and Diplas, P. (2006) Applying spatial hydraulic principles to quantify stream habitat. *River Research and Applications*, *22*(1), 79-89. doi:10.1002/rra.893

David, G. C. L., Wohl, E., Yochum, S. E., and Bledsoe, B. P. (2011) Comparative analysis of bed resistance partitioning inhigh-gradient streams, *Water Resour. Res.*, 47, W07507, doi:10.1029/2010WR009540

Day, T. J., (1976) Preliminary results of flume studies into the armouring of a coarse sediment mixture, Pap. 76-1C, pp. 277-287, Can. Geol. Surv., Ottawa.

Delignette-Muller, M. L., and Dutang, C. (2015) fitdistrplus: An R Package for Fitting Distributions. *2015, 64*(4), 34. doi:10.18637/jss.v064.i04

Ely, J. C., Clark, C. D., Spagnolo, M., Hughes, A. L. C., and Stokes, C. R. (2018) Using the size and position of drumlins to understand how they grow, interact and evolve. *Earth Surface Processes and Landforms, 43*(5), 1073-1087. doi:10.1002/esp.4241

Faraway, J., Marsaglia, G., Marsaglia, J., & Baddeley, A., (2019). goftest: Classical Goodness-of-Fit Tests for Univariate Distributions. R package version 1.2-2. https://CRAN.R-project.org/package=goftest

Faustini, J. M., and Jones, J. A. (2003) Influence of large woody debris on channel morphology and dynamics in steep, boulder-rich mountain streams, western Cascades, Oregon. *Geomorphology, 51*(1), 187-205. doi:https://doi.org/10.1016/S0169-555X(02)00336-7

Ferguson, R. (2007). Flow resistance equations for gravel- and boulder-bed streams. *Water Resources Research, 43*(5). doi:10.1029/2006wr005422

Ferguson, R. I., Hardy, R. J., and Hodge, R. A. (2019) Flow resistance and hydraulic geometry in bedrock rivers with multiple roughness length scales. *Earth Surface Processes and Landforms, 44*(12), 2437-2449. doi:10.1002/esp.4673

Ferguson, R. I., Sharma, B. P., Hardy, R. J., Hodge, R. A., and Warburton, J. (2017) Flow resistance and hydraulic geometry in contrasting reaches of a bedrock channel. *Water Resources Research*, *53*(3), 2278-2293. doi:10.1002/2016WR020233

Fox, J., & Weisberg, S. (2019). An R Companion to Applied Regression, Third edition. Sage, Thousand Oaks CA. https://socialsciences.mcmaster.ca/jfox/Books/Companion/.

Freedman, D., & Diaconis, P. (1981). On the histogram as a density estimator:L_2 theory. Z. *Wahrscheinlichkeitstheorie verw Gebiete* 57, 453–476. https://doi.org/10.1007/BF01025868

Gomez, B. (1993) Roughness of stable, armored gravel beds. *Water Resources Research*, *29*(11), 3631-3642. doi:10.1029/93wr01490

Groom, J., and Friedrich, H. (2019) Spatial structure of near-bed flow properties at the grain scale. *Geomorphology, 327*, 14-27. doi:https://doi.org/10.1016/j.geomorph.2018.10.013

Hodge, R., Brasington, J., and Richards, K. (2009) Analysing laser-scanned digital terrain models of gravel bed surfaces: linking morphology to sediment transport processes and hydraulics. *Sedimentology*, *56*(7), 2024-2043. doi:10.1111/j.1365-3091.2009.01068.x

Hodge, R. A., and Hoey, T. B. (2016) A Froude-scaled model of a bedrock-alluvial channel reach: 1. Hydraulics. *Journal of Geophysical Research: Earth Surface, 121*(9), 1578-1596. doi:https://doi.org/10.1002/2015JF003706

Judd, H. E., and Peterson, D. F. (1969) Hydraulics of large bed element channels. Utah Water Research Laboratory Reports, Paper 285. https://digitalcommons.usu.edu/water_rep/285

Katul, G., Wiberg, P., Albertson, J., & Hornberger, G. (2002). A mixing layer theory for flow resistance in shallow streams. *Water Resources Research, 38*(11), 32-31-32-38. doi:https://doi.org/10.1029/2001WR000817

Kirchner, J. W., Dietrich, W. E., Iseya, F., and Ikeda, H. (1990) The variability of critical shear stress, friction angle, and grain protrusion in water-worked sediments. *Sedimentology, 37*(4), 647-672. doi:10.1111/j.1365-3091.1990.tb00627.x

Kondolf, G. M., Vick, J. C., and Ramirez, T. M. (1996) Salmon Spawning Habitat Rehabilitation on the Merced River, California: An Evaluation of Project Planning and Performance. *Transactions of the American Fisheries Society, 125*(6), 899-912. doi:10.1577/1548-8659(1996)125<0899:SSHROT>2.3.CO;2

Krishnamoorthy, K., Lee, M., & Xiao, W. (2015). Likelihood ratio tests for comparing several gamma distributions. *Environmetrics, 26*(8), 571-583. doi:10.1002/env.2357

Lacey, R. W. J., and Roy, A. G. (2008) The spatial characterization of turbulence around large roughness elements in a gravel-bed river. *Geomorphology, 102*(3), 542-553. doi:https://doi.org/10.1016/j.geomorph.2008.05.045

Legleiter, C. J., and Harrison, L. R. (2019) Remote Sensing of River Bathymetry: Evaluating a Range of Sensors, Platforms, and Algorithms on the Upper Sacramento River, California, USA. *Water Resources Research, 55*(3), 2142-2169. doi:https://doi.org/10.1029/2018WR023586

Lisle, T. E., Nelson, J. M., Pitlick, J., Madej, M. A., and Barkett, B. L. (2000) Variability of bed mobility in natural, gravel-bed channels and adjustments to sediment load at local and reach scales. *Water Resources Research, 36*(12), 3743-3755. doi:10.1029/2000wr900238

Millard, S. P. (2014). EnvStats, an R Package for Environmental Statistics *Wiley StatsRef: Statistics Reference Online*.

Monsalve, A., and Yager, E. M. (2017) Bed Surface Adjustments to Spatially Variable Flow in Low Relative Submergence Regimes. *Water Resources Research, 53*(11), 9350-9367. doi:https://doi.org/10.1002/2017WR020845

Moriasi, D. N., Arnold, J. G., Van Liew, M. W., Bingner, R. L., Harmel, R. D., and Veith, T. L. (2007) Model Evaluation Guidelines for Systematic Quantification of Accuracy in Watershed Simulations. *Transactions of the ASABE, 50*(3), 885. doi:https://doi.org/10.13031/2013.23153

Nikora, V. I., Goring, D. G., and Biggs, B. J. F. (1998) On gravel-bed roughness characterization. *Water Resources Research*, *34*(3), 517-527. doi:10.1029/97wr02886

Papanicolaou, A. N., and Tsakiris, A. G. (2017) Boulder Effects on Turbulence and Bedload Transport. In D. T. a. J. B. Laronne (Ed.), *Gravel-Bed Rivers*.

Pasternack, G. B., Ellis, C. R., Leier, K. A., Vallé, B. L., and Marr, J. D. (2006) Convergent hydraulics at horseshoe steps in bedrock rivers. *Geomorphology*, *82*(1), 126-145. doi:https://doi.org/10.1016/j.geomorph.2005.08.022

Pastore, M., and Calcagnì, A. (2019) Measuring Distribution Similarities Between Samples: A Distribution-Free Overlapping Index. *Front. Psychol*. 10:1089. doi: 10.3389/fpsyg.2019.01089

Paternoster, R. Brame, R. Mazerolle, P, & Piquero A. (1998). Using the correct statistical test for the equality of regression coefficients. *Criminology*, *36*(4), 859-866. doi:https://doi.org/10.1111/j.1745-9125.1998.tb01268.x

R Core Team (2021). R: A language and environment for statistical computing. R Foundation for Statistical Computing, Vienna, Austria. URL https://www.R-project.org/.

Rickenmann, D., & Recking, A. (2011). Evaluation of flow resistance in gravel-bed rivers through a large field data set. *Water Resources Research*, *47*(7). doi:10.1029/2010wr009793

Rothman, D. H., Grotzinger, J. P., and Flemings, P. (1994) Scaling in turbidite deposition. *Journal of Sedimentary Research*, *64*(1a), 59-67. doi:10.1306/d4267d07-2b26-11d7-8648000102c1865d

Schneider, J. M., Rickenmann, D., Turowski, J. M., and Kirchner, J. W. (2015) Self-adjustment of stream bed roughness and flow velocity in a steep mountain channel. *Water Resources Research*, *51*(10), 7838-7859. doi:10.1002/2015wr016934

Singh, A., Guala, M., Lanzoni, S., and Foufoula-Georgiou, E. (2012) Bedform effect on the reorganization of surface and subsurface grain size distribution in gravel bedded channels. *Acta Geophysica, 60*(6), 1607-1638. doi:10.2478/s11600-012-0075-z

Strom, K. B., and Papanicolaou, A. N. (2006) Toward prediction of the spatial distribution of clusters in a watershed via geomorphic and hydraulic methods. In G. Parker and M. H. Garcia (Eds.), Paper presented at 4th IAHR symposium on river coastal and estuarine morphodynamics RCEM 2005 (pp. 119–129). Urbana, IL: Taylor and Francis.

Strom, M. A., Pasternack, G. B., Burman, S. G., Dahlke, H. E., and Sandoval-Solis, S. (2017) Hydraulic hazard exposure of humans swept away in a whitewater river. *Natural Hazards, 88*(1), 473-502. doi:10.1007/s11069-017-2875-6

Sutfin, N. A., and Wohl, E. (2019) Elevational differences in hydrogeomorphic disturbance regime influence sediment residence times within mountain river corridors. *Nature Communications, 10*(1), 2221. doi:10.1038/s41467-019-09864-w

Thompson, S. M., & Campbell, P. L. (1979). Hydraulic of a large channel paved with boulders. *Journal of Hydraulic Research, 17*(4), 341-354. doi:10.1080/00221687909499577

van der Mark, C. F., Blom, A., and Hulscher, S. J. M. H. (2008) Quantification of variability in bedform geometry. *Journal of Geophysical Research: Earth Surface, 113*(F3). doi:10.1029/2007jf000940

Wiener, J. S., & Pasternack, G. B. (2022). Scale dependent spatial structuring of mountain river large bed elements maximizes flow resistance. *Geomorphology, 416*(1). doi:https://doi.org/10.1016/j.geomorph.2022.108431

Wittenberg, L., and Newson, M. D. (2005) Particle clusters in gravel-bed rivers: an experimental morphological approach to bed material transport and stability concepts. *Earth Surface Processes and Landforms, 30*(11), 1351-1368. doi:10.1002/esp.1184

Wohl, E., and Merritt, D. M. (2008) Reach-scale channel geometry of mountain streams. *Geomorphology, 93*(3), 168-185. doi:https://doi.org/10.1016/j.geomorph.2007.02.014

Yuba County Water Agency (YCWA) (2013) *Technncal Memorandum 1-1. Channel Morphology Upstream of Englebright Reservoir*. *Yuba River Development Project FERC Project No. 2246.* Retrieved from http://www.ycwa-relicensing.com/Technical%20Memoranda/Forms/AllItems.aspx

Yochum, S. E., Bledsoe, B. P., David, G. C. L., and Wohl, E. (2012) Velocity prediction in high-gradient channels. *Journal of Hydrology, 424-425*, 84-98. doi:https://doi.org/10.1016/j.jhydrol.2011.12.031